Supporting Information for

In-depth Structural Analysis of Lanthanoid Coordination Networks Based on a Flexible Tripodal Zwitterionic Isonicotinate Ligand

Antti Tiihonen,[a] and **Manu Lahtinen**[a*]

[a] *Department of Chemistry, P.O.Box 35, FI-40014 , University of Jyväskylä, Finland*

E-mail address: manu.k.lahtinen@jyu.fi

CONTENTS

S1 Preface 4

S2 Experimental 4

S2.1 Materials and methods 4

S2.2 Preparation of $H_{2.5}$TTTPC 5

S2.3 $H_{2.5}$TTTPC nitrate exchange, and syntheses of TTTPC $La(NO_3)_3$, TTTPC $Nd(NO_3)_3$ and TTTPC $Y(NO_3)_3$ .. 5

S2.4 Syntheses of network solids with other metals and anions 5

S2.4.1 TTTPC $YbBr_3$ 5

S2.4.2 TTTPC $LaBr_2OTf$ 5

S2.4.3 TTTPC $SmBr_2OTf$, TTTPC $SmBr(OTf)_2$ and $TTTPC_2$ $Sm_2(OTf)_6$ 6

S2.4.4 TTTPC $EuBr_2OTf$ and TTTPC $EuBr(OTf)_2$ 6

S2.4.5 TTTPC $GdBr_2OTf$ 6

S2.4.6 TTTPC $TbBr_2OTf$ and TTTPC $TbBr(OTf)_2$ 6

S2.4.7 TTTPC $YbOTf_3$ 6

S2.5 Theoretical yield calculations of main text compounds 7

S3 Crystallographic results of network solids 8

S3.1 TTTPC $LnBr_3$ additional images and tables 8

S3.1.1 TTTPC $NdBr_3$ (CSD ref. 1833442) 9

S3.1.2 TTTPC $YbBr_3$ (CSD ref. 1833439) 10

S3.2 TTTPC $LnBr_2OTf$ additional images and tables 11

S3.2.1 TTTPC $NdBr_2OTf$ (CSD ref. 1833432) 13

S3.2.2 TTTPC $LaBr_2OTf$ (CSD ref. 1833430) 14

S3.2.3 TTTPC $SmBr_2OTf$ (CSD ref. 1833436) 14

S3.2.4 TTTPC $EuBr_2OTf$ (CSD ref. 1833428) 15

S3.2.5 TTTPC $GdBr_2OTf$ (CSD ref. 1833429) 15

S3.2.6 TTTPC $TbBr_2OTf$ (CSD ref. 1833438) 16

S3.3 TTTPC $LnBr(OTf)_2$ additional images and tables 17

S3.3.1 TTTPC $NdBr(OTf)_2$ (CSD ref. 1833434) 18

S3.3.2 TTTPC $SmBr(OTf)_2$ (CSD ref. 1833437) 19

S3.3.3 TTTPC $EuBr(OTf)_2$ (CSD ref. 1833445) 20

S3.3.4 TTTPC $TbBr(OTf)_2$ (CSD ref. 1833443) 20

S3.4 TTTPC $Ln(OTf)_3$ additional images and tables 21

S3.4.1 TTTPC $Nd(OTf)_3$ (CSD ref. 1833435) 22

S3.4.2 TTTPC $Yb(OTf)_3$ (CSD ref. 1833440) 23

S3.5 $TTTPC_2$ $Sm_2(OTf)_6$ (CSD ref. 1833446) 24

S3.6 TTTPC $NdBr_2OAc$ (CSD ref. 1833431) additional images and tables 26

S3.7 TTTPC $NdBr_2OTf$ (vac) (CSD ref. 1842357) additional images and tables 27
S3.8 TTTPC $NdBr_2OAc$ (dry) (CSD ref. 1894870) additional images and tables 29
S3.9 TTTPC $Ln(NO_3)_3$ 31
S3.9.1 TTTPC $Nd(NO_3)_3$ (CSD ref. 1842358) 32
S3.9.2 TTTPC $La(NO_3)_3$ (CSD ref. 1833441) 33
S3.9.3 TTTPC $Y(NO_3)_3$ (CSD ref. 1833444) 33
S3.10 Other supporting figures 35
S4 Visual decomposition studies of network solids 38
S5 Thermal analysis results of network solids 38
S5.1 TTTPC $NdBr_3$ 40
S5.2 TTTPC $NdBr_2OTf$ 41
S5.3 TTTPC NdBrOTfMix 42
S5.4 TTTPC $NdBr_2OAc$ 42
S6 Elemental Analysis results of network solids 43
S6.1 TTTPC $NdBr_3$ 43
S6.2 TTTPC $NdBr_2OTf$ 43
S6.3 TTTPC NdBrOTfMix 43
S6.4 TTTPC $NdBr_2OAc$ 43
S7 IR spectra of network solids 44
S8 X-ray powder diffraction patterns of network solids and discussion 46
S9 SEM Imaging and EDX analyses of network solids and discussion 50
S10 Solid State UV-vis spectra of network solids and discussion 53
S11 BET surface area analysis results and discussion 54
S12 Characterization results of $H_{2.5}$TTTPC 55
S12.1 NMR and CHN characterization of $H_{2.5}$TTTPC ethyl ester 55
S12.2 NMR and CHN characterization of $H_{2.5}$TTTPC 56
S12.3 Crystallography of $H_{2.5}$TTTPC (CSD ref. 1833433) 57
S12.4 Previously reported crystal structure, CSD ref. ENIVUT 60
S12.5 Thermal analysis of $H_{2.5}$TTTPC 61
References 61

S1 PREFACE

In the paper, only neodymium is presented as an archetype for the different networks. The other metals are presented here in the ESI as they form nearly isostructural systems with only some individual quirks.

There seems to be some indication that light and middle lanthanoids prefer to crystallize in a certain system whereas the heaviest element, Yb in our case, forms slightly different crystals with the same conditions. In an experiment where triflate and bromide were both present in a way that neither was dominating the other (Br^- to OTf^- ratio 1:1), only bromide was found associated with Yb in **TTTPC $YbBr_3$**, whereas the other metals formed bromide-triflate systems (**TTTPC $LnBr_2OTf$)** in similar conditions. Several crystals were screened and the crystallization experiment with Yb was repeated twice with identical results. Also, when triflate was heavily dominating the bromide by the addition of KOTf (Br^- to OTf^- ratio 1:3), a **TTTPC $Yb(OTf)_3$** system was preferably formed (with no indication of **TTTPC $YbBr(OTf)_2$** type). The tri-triflate system was essentially the same as with the lighter elements, but the metal had only two water molecules in its coordination sphere, instead of the conventional three. Also the anion disorder tendencies presented in the main text are perhaps due to the effect of the particular metal used. All in all, whether these effects are only due to the lanthanoid contraction, definite answer cannot be given, but the difference in ionic radii of the heavy and light lanthanoids seems to be at least a slightly exploitable property in engineering systems presented here.

We also experimented briefly using only nitrate in the system, first by performing a ligand anion exchange from bromide to nitrate via complete silver bromide precipitation in slightly acidic conditions, separating the precipitate by centrifugation, adding metal nitrate and finally by crystallizing MOFs from this homoanionic solution. The ligand was not acquired as a solid product between anion exchange and MOF crystallization, but the clear supernatant was tested for bromide by adding some $AgNO_3$ solution (with a negative result). The concentration of the solution was not kept constant due to the addition of aqueous $AgNO_3$, and due to some loss of product during centrifugation of the precipitated (unwashed) solid. Amounts of the dissolved ligand species and addition of the metal salt were therefore somewhat crude approximations, but close to ligand-metal ratio 1:1. The end result was single crystals that are relatable with the homoanionic bromide system, and it seemed appropriate to conclude that the nitrate itself doesn't induce a change in network topology. Initially we used lanthanum and yttrium nitrate in our experiment, and because primary results from the nitrate experiments didn't significantly expand the horizons in the overall studies of this paper, no further studies were carried out. Upon approaching the completion of the studies, however, **TTTPC $Ln(NO_3)_3$** synthesis also with Nd was conducted, and its structure was determined to better relate to the other structures presented in the main text.

S2 EXPERIMENTAL

S2.1 Materials and methods

Commercial lanthanum nitrate hexahydrate (≥ 99 %, Merck), neodymium nitrate hexahydrate (≥ 99 %, Aldrich) and yttrium nitrate pentahydrate (≥ 99 %, Merck) were used without further purification.

1.0 M and 0.1 M silver nitrate solutions were prepared fresh by dissolving respectively 16.99 g and 1.69 g of solid $AgNO_3$ salt (≥ 99.5 %, VWR) into 100 ml of deionized water. Solutions were not standardized.

TTTPC ligand and intermediate purities were checked using NMR and CHN elemental analysis. NMR equipment used was Bruker Avance III HD Nanobay 300 MHz with 5 mm BBFO autotune probe, and for CHN analysis an Elementar Vario EL III with thermal conductivity detector was used. Before CHN analysis, all samples were dried by keeping them under medium vacuum for three consecutive days in 1×10^{-6} bar pressure. Furthermore, bulk network solid samples presented in the main text were analysed using a Bruker Alpha FT-IR spectrometer, and they were also subjected to CHN analysis.

Two laboratory scales were used for weighing reagents in bulk (Texas Instruments APX-200, d = 0.1 mg and Precisa 310 C, d = 0.01 g) and one for reagents and products in mg quantities (Mettler Toledo MT5, d = 0.001mg). Stuart SMP3 melting point apparatus was used to visually study the compounds' decomposition.

S2.2 Preparation of $H_{2.5}$TTTPC

2,4,6-tris(bromomethyl)mesitylene (1.79 g, 4.5 mmol) was dissolved in 100 ml of warm acetonitrile in a two-necked round-bottom flask with a magnetic stirrer, and ethyl isonicotinate (2.50 ml, 2.52 g, 16.7 mmol) was added after no solids remained. The mixture was refluxed at 81 °C for a total of 24 h, but already after 30 min from the addition of ethyl isonicotinate, a solid yellow precipitate started to form. After reflux, the system was cooled to room temperature and the product was filtered, washed twice with acetonitrile and vacuum dried overnight. Yield was 3.65 g (95.1 %) of pure ester intermediate product. De-esterification was conducted by dissolving the intermediate in a round-bottomed flask to a mixture of 15 ml of 62 % HBr and 35 ml of deionized water, and stirring the solution at 80 °C for 20 h. After this, the solution was evaporated on a hot plate until solid products started to appear, and was left to cool. Crude product was collected from the cool acidic solution by filtration and was vacuum dried overnight. Recrystallization from water yielded 2.28 g (overall 66.3 %) of colorless crystals of $H_5TTTPC_2Br_5 \cdot 4H_2O$ proper, or $H_{2.5}TTTPCBr_{2.5} \cdot 2H_2O$ (**$H_{2.5}$TTTPC**) with respect to the stoichiometry per one equivalent of the ligand.

S2.3 $H_{2.5}$TTTPC nitrate exchange, and syntheses of TTTPC $La(NO_3)_3$, TTTPC $Nd(NO_3)_3$ and TTTPC $Y(NO_3)_3$

52.5 mg (68.7 µmol) of **$H_{2.5}$TTTPC** was dissolved in 5 ml of deionized water and divided into two 2.5 ml aliquots in small test tubes (34.4 µmol of **TTTPC** per tube). 110 µl of 1 M $AgNO_3$ solution was added into both test tubes, forming a yellowish precipitate of silver bromide. The tubes were centrifuged for 5 min in 2500 rpm. Clear supernatants were tested for bromide by adding a drop of 0.1 M $AgNO_3$ solution, which didn't produce more precipitate. Supernatants were carefully pipetted into 4 ml glass vials into which 15.1 mg (34.9 µmol) of $La(NO_3)_3 \cdot 6H_2O$ and 12.5 mg (34.2 µmol) of $Y(NO_3)_3 \cdot 5H_2O$ were weighed. The salts were dissolved into the solution, and the vessels were left to crystallize for two weeks under acetone vapor diffusion. Colorless crystals suitable for single crystal experiments were then harvested. Yields were not calculated.

50.1 mg (65.6 µmol) of **$H_{2.5}$TTTPC** was dissolved in 5 ml of deionized water and 210 µl of 1 M $AgNO_3$ solution was added forming a precipitate, which was separated as described above. Clear solution was checked for bromide with a negative result. 28.1 mg (64.1 µmol) of $Nd(NO_3)_3 \cdot 6H_2O$ was weighed and dissolved into the ligand solution, and the solution was transferred to a 20 ml glass jar to crystallize for two weeks under acetone vapor diffusion. Light purple blocks (colorless under fluorescent light) were harvested with a yield of 46.1 mg (71.9 %, calculated as hexahydrate from X-ray data) after drying with acetone and keeping in a desiccator overnight.

S2.4 Syntheses of network solids with other metals and anions

Yields for the unoptimized crystallizations presented here in the ESI were not calculated. Main goal was to get suitable crystals for single crystal experiments. Some of the initial 50 mg crystallization experiments were very crude, but eventually produced proper crystals.

S2.4.1 TTTPC $YbBr_3$

8.76 mg (11.5 µmol) of **$H_{2.5}$TTTPC** and 7.12 mg (11.5 µmol) of $Yb(OTf)_3$ were dissolved in 0.5 ml of deionized H_2O in a 2 ml borosilicate vessel and were left to crystallize under acetone vapor diffusion for four days. Irregular colorless blocks suitable for single crystal experiments were harvested.

S2.4.2 TTTPC $LaBr_2OTf$

10.39 mg (13.6 µmol) of **$H_{2.5}$TTTPC** and 7.97 mg (13.6 µmol) of $La(OTf)_3$ were dissolved in 0.5 ml of deionized H_2O in a 2 ml borosilicate vessel and were left to crystallize under acetone vapor diffusion for four days. Large colorless shards were harvested and a piece was cut for a single crystal experiment.

S2.4.3 TTTPC $SmBr_2OTf$, TTTPC $SmBr(OTf)_2$ and $TTTPC_2$ $Sm_2(OTf)_6$

50.0 mg (65.5 µmol) of **$H_{2.5}$TTTPC** and 60.0 mg (100.4 µmol) of $Sm(OTf)_3$ were mixed in 3.0 ml of deionized H_2O in a 10 ml borosilicate jar, and the undissolved solids were filtered off. The clear solution was left to crystallize under acetone vapor diffusion for a few weeks. Due to a serendipitous find, an exceptional rather good quality crystal was found from this batch. This structure corresponded to **$TTTPC_2$ $Sm_2(OTf)_6$**. At first we believed this to be the bulk material representative structure, but instead it was an aberration. A new experiment with the same rationale as with the other metals was conducted later:

9.87 mg (12.9 µmol) of **$H_{2.5}$TTTPC** and 7.72 mg (12.9 µmol) of $Sm(OTf)_3$ were dissolved in 0.5 ml of deionized H_2O in a 2 ml borosilicate vessel and were left to crystallize under acetone vapor diffusion overnight. Thin colorless planks were collected, and a suitable piece for the single crystal experiments was used. These turned out to be **TTTPC $SmBr_2OTf$**. Another experiment was still made later, in search of the $Br(OTf)_2$ type:

30.1 mg (39.4 µmol, 1.00 eqv) of **$H_{2.5}$TTTPC** and 24.70 mg (41.3 µmol, 1.05 eqv) of $Sm(OTf)_3$ and 45.14 mg (239.9 µmol, 6.09 eqv) were dissolved in 3.5 ml of deionized H_2O in a 10 ml borosilicate jar and were left to crystallize under acetone vapor diffusion for two weeks. Colorless needles, blocks and interpenetrated thin plates were harvested, and the plate-like structure was determined to be **TTTPC $SmBr(OTf)_2$**.

S2.4.4 TTTPC $EuBr_2OTf$ and TTTPC $EuBr(OTf)_2$

7.68 mg (10.1 µmol) of **$H_{2.5}$TTTPC** and 6.02 mg (10.0 µmol) of $Eu(OTf)_3$ were dissolved in 0.5 ml of deionized H_2O in a 2 ml borosilicate vessel and were left to crystallize under acetone vapor diffusion overnight. Very small colorless shards and blocks of **TTTPC $EuBr_2OTf$** were collected and a block was used for diffraction experiments.

50.0 mg (65.5 µmol) of **$H_{2.5}$TTTPC** and 60.0 mg (100.1 µmol) of $Eu(OTf)_3$ were mixed in 3.0 ml of deionized H_2O in a 10 ml borosilicate jar, and the undissolved solids were filtered off. The clear solution was left to crystallize under acetone vapor diffusion for a few weeks. Colorless miscellaneous crystals were harvested and a piece of a thin plate was selected for diffraction experiments. Structure corresponded to **TTTPC $EuBr(OTf)_2$**.

S2.4.5 TTTPC $GdBr_2OTf$

7.84 mg (10.3 µmol) of **$H_{2.5}$TTTPC** and 6.21 mg (10.3 µmol) of $Gd(OTf)_3$ were dissolved in 0.5 ml of deionized H_2O in a 2 ml borosilicate vessel and were left to crystallize under acetone vapor diffusion overnight. Mediocre sized colorless shards, planks and blocks were collected, and a suitable piece was used for diffraction experiments.

S2.4.6 TTTPC $TbBr_2OTf$ and TTTPC $TbBr(OTf)_2$

12.98 mg (17.0 µmol) of **$H_{2.5}$TTTPC** and 10.29 mg (17.0 µmol) of $Tb(OTf)_3$ were dissolved in 0.5 ml of deionized H_2O in a 2 ml borosilicate vessel and were left to crystallize under acetone vapor diffusion for four days. Large colorless shards and planks were collected and a piece was cut for diffraction experiments. Structure corresponded to **TTTPC $TbBr_2OTf$**.

50.0 mg (65.5 µmol) of **$H_{2.5}$TTTPC** and 60.0 mg (99.0 µmol) of $Tb(OTf)_3$ were mixed in 3.0 ml of deionized H_2O in a 10 ml borosilicate jar, and the undissolved solids were filtered off. The clear solution was left to crystallize under acetone vapor diffusion for several weeks. Colorless miscellaneous crystals were harvested and a piece of a large plate was selected for diffraction experiments. Structure corresponded to **TTTPC $TbBr(OTf)_2$**.

S2.4.7 TTTPC $YbOTf_3$

30.1 mg (39.4 µmol, 1.00 eqv) of **$H_{2.5}$TTTPC** and 24.89 mg (40.1 µmol, 1.02 eqv) of $Yb(OTf)_3$ and 45.14 mg (239.9 µmol, 6.09 eqv) were dissolved in 3.5 ml of deionized H_2O in a 10 ml borosilicate jar and were left to crystallize under acetone vapor diffusion for two weeks. Colorless blocks and planks were harvested, and despite screening more than one crystal, only single structure was encountered. That was **TTTPC $Yb(OTf)_3$**.

S2.5 Theoretical yield calculations of main text compounds

Theoretical yields of network solids presented in the main text experimental sections are based on M_r of the solvent-impregnated products when prepared fresh (with additional coordinated and non-coordinated solvent water molecules included from the crystallographic data, see Table 1). Theoretical yields can be calculated from the evacuated samples as well, assuming only metal coordinated water molecules stay in the structure, and diffuse water is removed by the evacuation process (or in the case of **TTTPC $NdBr_2OAc$ (dry)** the structure has no coordinated water, but rather discrete "water of crystallization"). In these scenarios, theoretical and experimental yields can be calculated as follows:

TTTPC $NdBr_3$

350.7 mg, 87.0 %, M_r = 1071.66 g/mol, two coordinated and seven additional non-coordinated H_2O

309.5 mg, 98.6 %, M_r = 945.52 g/mol, only coordinated water included

TTTPC $NdBr_2OAc$

374.4 mg, 74.9 %, M_r = 1122.85 g/mol, two coordinated and eleven additional non-coordinated H_2O

338.3 mg, 82.9 %, Mr = 1014.76 g/mol, seven non-coordinated H_2O

296.3 mg, 94.6 %, M_r = 888.66 g/mol, completely devoid of water

However, since the samples were held in a desiccator overnight for a rather ambiguous amount of time before recording the yield, the proper amount of diffuse water is most likely somewhere between the estimated maximum and minimum, and thus realistic theoretical yields fall between the values above. These amounts of water are challenging to determine quantitatively due to uncertainties in the intermediate hydrated structures, and thus the lowest estimated yield is used in the main text. In future experiments, a controlled bulk drying process in suitable elevated temperature according to results from thermogravimetric analyses is most likely the best method to ascertain the amount of dry final product, but this was unfortunately beyond this paper.

Theoretical yields for the **TTTPC $NdBr_2OTf$** and **TTTPC NdBrOTfMix** products were not calculated due to the mixture nature and unknown amounts of individual products in the bulk.

S3 CRYSTALLOGRAPHIC RESULTS OF NETWORK SOLIDS

Table S1. Figure 1 Symmetry labels

a) $NdBr_3$	**b) $NdBr_2OTf$**	**c) $NdBr(OTf)_2$**	**d) $NdBr(OTf)_3$**	**e) $NdBr_2OAc$**
i -X,1-Y,-Z	i -X,-Y,1-Z	i -1+X,+Y,-1+Z	i 1-X,1-Y,1-Z	i 1+X,+Y,1+Z
ii -X,-Y,-Z	ii 1-X,1-Y,2-Z	ii -1+X,3/2-Y,-1/2+Z	ii 1-X,-Y,-Z	ii 2-X,2-Y,1-Z
iii 1-X,1-Y,1-Z	iii 1-X,-Y,2-Z	iii 2-X,-1/2+Y,1/2-Z	iii 1+X,+Y,1+Z	iii 1-X,1-Y,-Z
iv +X,1+Y,1+Z	iv +X,+Y,-1+Z	iv +X,3/2-Y,-1/2+Z	iv 1-X,-Y,1-Z	iv +X,1+Y,1+Z
v +X,+Y,1+Z	v +X,-1+Y,-1+Z	v 2-X,2-Y,-Z		v 1-X,2-Y,1-Z

S3.1 TTTPC $LnBr_3$ additional images and tables

Table S2. Crystal structure and refinement data for **TTTPC $NdBr_3$** and **TTTPC $YbBr_3$**

Name	**TTTPC $NdBr_3$**	**TTTPC $YbBr_3$**
Empirical formula	$C_{30}H_{45}Br_3N_3NdO_{15}$	$C_{30}H_{45}Br_3N_3O_{15}Yb$
Formula weight	1071.66	1100.46
Temperature / K	120.01(10)	120.00(10)
Crystal system	triclinic	triclinic
Space group	*P*-1	*P*-1
a / Å	9.4378(3)	9.2767(3)
b / Å	12.3546(3)	13.0591(5)
c / Å	18.8810(4)	18.3855(8)
α / °	104.683(2)	107.284(4)
β / °	98.809(2)	98.961(3)
γ / °	99.428(2)	94.147(3)
Volume / Å^3	2056.71(10)	2084.10(14)
Z	2	2
ρ_{calc} / g/cm^3	1.73	1.754
μ / mm^{-1}	13.614	8.081
F(000)	1062	1082
Crystal size / mm^3	0.231 × 0.123 × 0.073	0.089 × 0.077 × 0.023
Radiation	CuKα (λ = 1.54184)	CuKα (λ = 1.54184)
2Θ range for data collection / °	7.57 to 135.984	7.146 to 135.988
Index ranges	$-11 \leq h \leq 10$, $-14 \leq k \leq 14$, $-22 \leq l \leq 21$	$-11 \leq h \leq 9$, $-14 \leq k \leq 15$, $-19 \leq l \leq 22$
Reflections collected	12580	12920
Independent reflections	7446 [R_{int} = 0.0275, R_{sigma} = 0.0405]	7538 [R_{int} = 0.0293, R_{sigma} = 0.0418]
Data/restraints/parameters	7446/0/421	7538/0/439
Goodness-of-fit on F^2	1.038	1.034
Final R indexes [$I \geq 2\sigma(I)$]	R_1 = 0.0449, wR_2 = 0.1163	R_1 = 0.0327, wR_2 = 0.0847
Final R indexes [all data]	R_1 = 0.0463, wR_2 = 0.1179	R_1 = 0.0372, wR_2 = 0.0879
Largest diff. peak/hole / e Å^{-3}	1.73/-1.44	1.44/-1.15
CSD reference no.	1833442	1833439

S3.1.1 TTTPC NdBr$_3$ (CSD ref. 1833442)

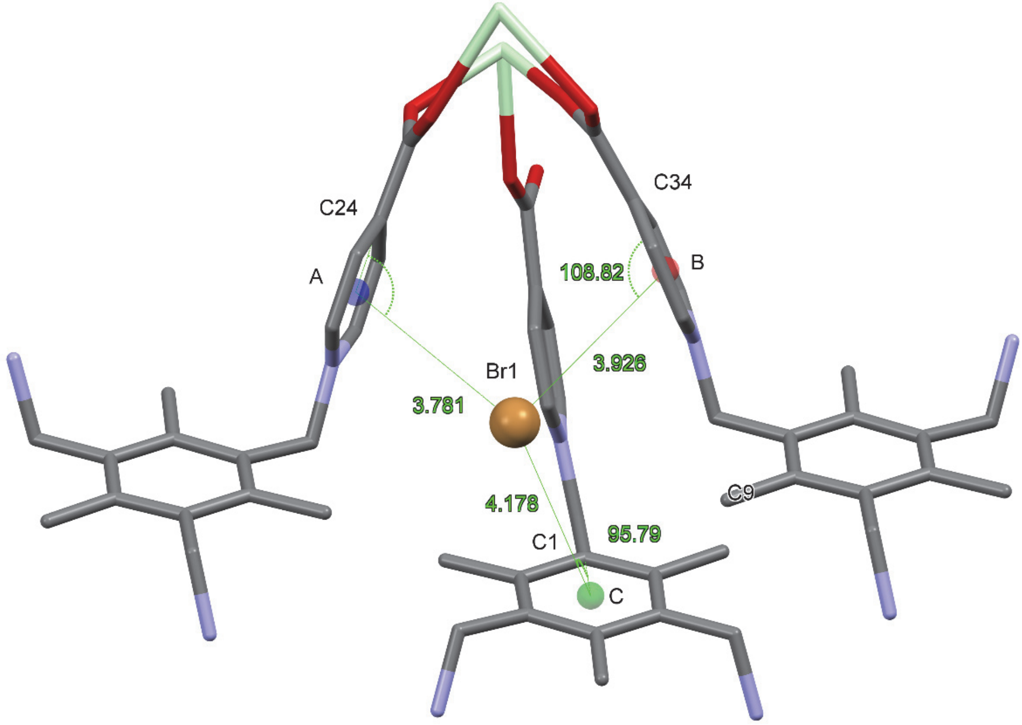

Figure S1. Close-up of the Br1 of **TTTPC NdBr$_3$**. Aromatic centroid distances and angles indicate a possible charge transfer (electrostatic) interaction. Anion-π interaction is doubtful because of the rather long distances and the Br- positioning offset from above the ring centroid.

Table S3. C-H···Br$^-$ interaction (hydrogen bond) distances, angles and types for **TTTPC NdBr$_3$** and **TTTPC YbBr$_3$**

TTTPC NdBr$_3$	**Distance / Å**	**Angle / °**	**Type**
C12-H16···Br1	2.916	171.12	*o-pyr*
C16-H16···Br1	2.941	142.99	*o-pyr*
C22-H22···Br2	2.842	134.24	*o-pyr*
C26-H26···Br2	2.728	168.51	*o-pyr*
C8-H8B···Br3A	2.607	144.36	CH_3
C9-H9C···Br3A	2.693	168.19	CH_3
C32-H32···Br3A	2.623	175.07	*o-pyr*
C35-H35···Br3A	2.620	144.60	*m-pyr*
C8-H8C···Br3B	2.883	170.00	CH_3

TTTPC YbBr$_3$	**Distance / Å**	**Angle / °**	**Type**
C7-H7A···Br1	2.877	162.40	CH_3
C12-H12···Br1	2.735	169.29	*o-pyr*
C15-H15···Br1	2.959	127.46	*µ-pyr*
C16-H16···Br1	2.984	126.73	*µ-pyr*
C7-H7C···Br2	2.980	158.45	CH_3
C22-H22···Br2	2.781	178.05	*o-pyr*
C26-H22···Br2	2.775	136.85	*o-pyr*
C8-H8A···Br3A	2.999	147.42	CH_3
C32-H36•••Br3A	2.898	131.30	*o-pyr*
C36-H36•••Br3A	2.784	135.38	*o-pyr*

S3.1.2 TTTPC $YbBr_3$ (CSD ref. 1833439)

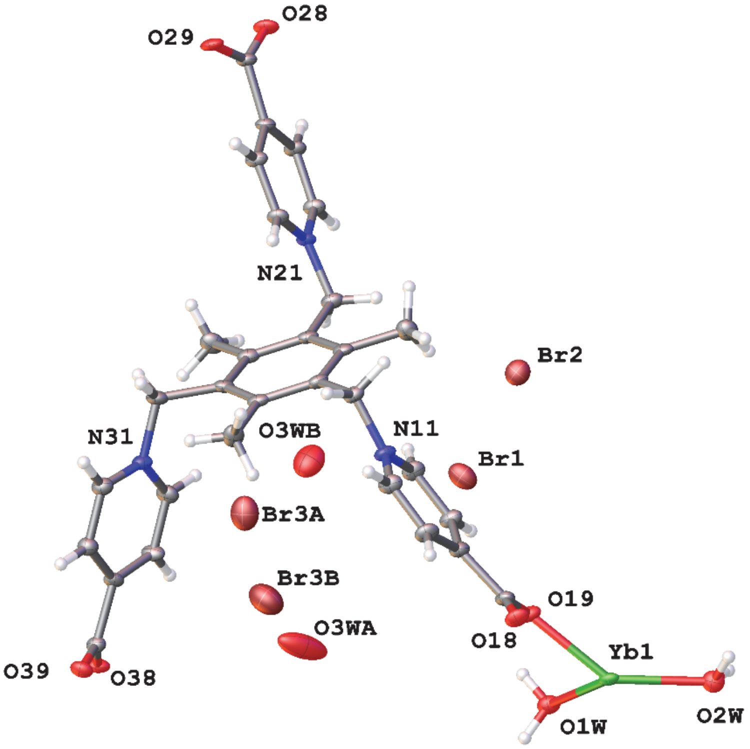

Figure S2. Asymmetric unit contents of **TTTPC $YbBr_3$**. Two water molecules (O3WA and O3WB) have been assigned additionally due to remaining electron density that the OLEX[2] solvent mask procedure couldn't remove. Occupancies approximately O3WA: 75 % and O3WB: 25 %. Thermal ellipsoids are presented at 50 % probability level here, and in the following pictures, where applicable.

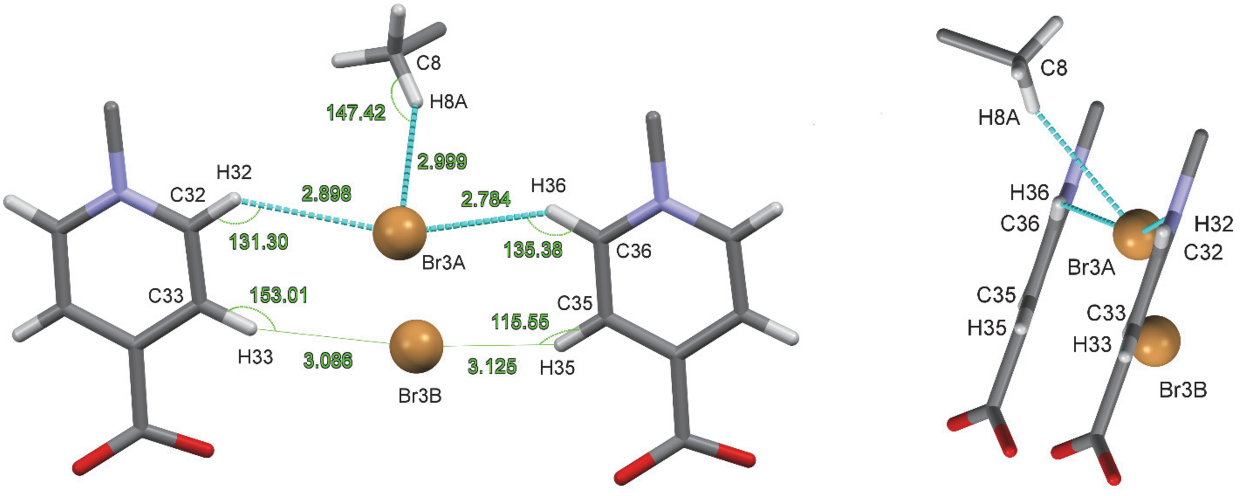

Figure S3. **TTTPC YbBr3** structure close-up of C-H···Br^- interactions of disordered Br3A and Br3B. Bromide is disordered next to the parallel, offset pyridinium rings (right). C35-H35···Br3B is most likely not a proper interaction due to rather long distance (3.125 Å) and strictly deviating angle (115.55 °), but C33-H33···Br3B is maybe a borderline interaction, although a very weak one. Occupancies (Br3A: 75 % and Br3B: 25%) most likely reflect this.

S3.2 TTTPC LnBr$_2$OTf additional images and tables

Table S4. Crystal structure and refinement data for **TTTPC LaBr$_2$OTf**, **NdBr$_2$OTf** and **SmBr$_2$OTf**

Name	**TTTPC LaBr$_2$OTf**	**TTTPC NdBr$_2$OTf**	**TTTPC SmBr$_2$OTf**
Empirical formula	$C_{30.77}H_{51}Br_{2.23}F_{2.29}LaN_3O_{20.3}S_{0.77}$	$C_{30.68}H_{53}Br_{2.31}F_{2.06}N_3NdO_{21.06}S_{0.69}$	$C_{30.83}H_{53}Br_{2.17}F_{2.5}N_3O_{21.5}S_{0.83}Sm$
Formula weight	1173.28	1191.27	1207.41
Temperature / K	120.01(10)	120.01(10)	120.00(10)
Crystal system	triclinic	triclinic	triclinic
Space group	*P*-1	*P*-1	*P*-1
a / Å	9.6013(3)	9.5721(4)	9.5251(3)
b / Å	14.3577(3)	14.4092(6)	14.2183(3)
c / Å	18.7825(5)	18.7321(7)	18.8650(7)
α / °	106.592(2)	106.854(4)	107.596(3)
β / °	102.854(2)	103.019(4)	102.916(3)
γ / °	99.256(2)	99.792(4)	99.489(2)
Volume / Å^3	2348.44(11)	2331.09(18)	2298.27(13)
Z	2	2	2
ρ_{calc} / g/cm^3	1.659	1.697	1.745
μ / mm^{-1}	10.314	11.862	12.952
F(000)	1174	1194	1209
Crystal size / mm^3	0.202 × 0.132 × 0.076	0.145 × 0.095 × 0.063	0.078 × 0.065 × 0.04
Radiation	CuKα (λ = 1.54184)	CuKα (λ = 1.54184)	CuKα (λ = 1.54184)
2Θ range for data collection / °	6.618 to 135.98	5.152 to 135.998	5.136 to 135.994
Index ranges	$-11 \leq h \leq 11$, $-17 \leq k \leq 15$, $-22 \leq l \leq 20$	$-11 \leq h \leq 10$, $-17 \leq k \leq 17$, $-22 \leq l \leq 17$	$-11 \leq h \leq 11$, $-17 \leq k \leq 11$, $-22 \leq l \leq 21$
Reflections collected	14614	14235	13961
Independent reflections	8515 R_{int} = 0.0343, R_{sigma} = 0.0491	8450 R_{int} = 0.0310, R_{sigma} = 0.0477	8320 R_{int} = 0.0346, R_{sigma} = 0.0545
Data/restraints/parameters	8515/6/484	8450/0/484	8320/0/484
Goodness-of-fit on F^2	1.035	1.047	1.060
Final R indexes [I ≥ 2σ (I)]	R_1 = 0.0574, wR_2 = 0.1614	R_1 = 0.0612, wR_2 = 0.1752	R_1 = 0.0606, wR_2 = 0.1672
Final R indexes [all data]	R_1 = 0.0600, wR_2 = 0.1649	R_1 = 0.0642, wR_2 = 0.1788	R_1 = 0.0643, wR_2 = 0.1719
Largest diff. peak/hole / e Å^{-3}	2.42/-2.60	2.89/-2.83	1.97/-2.87
CSD reference no.	1833430	1833432	1833436

Table S5. Crystal structure and refinement data for **TTTPC EuBr$_2$OTf**, **GdBr$_2$OTf** and **TbBr$_2$OTf**

Name	**TTTPC EuBr$_2$OTf**	**TTTPC GdBr$_2$OTf**	**TTTPC TbBr$_2$OTf**
Empirical formula	$C_{30.88}H_{53}Br_{2.13}EuF_{2.62}N_3O_{21.62}S_{0.88}$	$C_{31}H_{51}Br_2F_3GdN_3O_{21}S$	$C_{31}H_{49}Br_2F_3N_3O_{20}STb$
Formula weight	1211.78	1207.88	1191.53
Temperature / K	120.00(10)	120.01(10)	120.00(10)
Crystal system	triclinic	triclinic	triclinic
Space group	*P*-1	*P*-1	*P*-1
a / Å	9.5897(3)	9.5280(4)	9.5114(4)
b / Å	14.3802(7)	14.3123(6)	14.2612(6)
c / Å	18.8257(8)	18.8610(8)	18.8972(6)
α / °	107.624(4)	107.797(4)	108.079(4)
β / °	103.176(3)	103.227(4)	103.298(3)
γ / °	99.794(3)	99.461(3)	99.250(4)
Volume / Å^3	2327.76(18)	2306.53(18)	2295.55(17)
Z	2	2	2
ρ_{calc} / g/cm^3	1.729	1.739	1.724
μ / mm^{-1}	12.942	12.555	10.819
F(000)	1214	1206	1188
Crystal size / mm^3	0.245 × 0.086 × 0.047	0.283 × 0.164 × 0.132	0.127 × 0.076 × 0.048
Radiation	CuKα (λ = 1.54184)	CuKα (λ = 1.54184)	CuKα (λ = 1.54184)
2Θ range for data collection / °	5.16 to 135.996	5.154 to 136	6.736 to 135.99
Index ranges	$-11 \leq h \leq 11$, $-17 \leq k \leq 17$, $-22 \leq l \leq 16$	$-11 \leq h \leq 8$, $-9 \leq k \leq 17$, $-22 \leq l \leq 21$	$-11 \leq h \leq 11$, $-12 \leq k \leq 17$, $-21 \leq l \leq 22$
Reflections collected	14473	14103	13793
Independent reflections	8435 R_{int} = 0.0323, R_{sigma} = 0.0455	8343 R_{int} = 0.0354, R_{sigma} = 0.0508	8301 R_{int} = 0.0278, R_{sigma} = 0.0426
Data/restraints/parameters	8435/0/484	8343/0/484	8301/12/484
Goodness-of-fit on F^2	1.078	1.055	1.049
Final R indexes [I ≥ 2σ (I)]	R_1 = 0.0528, wR_2 = 0.1478	R_1 = 0.0686, wR_2 = 0.1930	R_1 = 0.0688, wR_2 = 0.1859
Final R indexes [all data]	R_1 = 0.0550, wR_2 = 0.1505	R_1 = 0.0724, wR_2 = 0.1984	R_1 = 0.0721, wR_2 = 0.1887
Largest diff. peak/hole / e Å^{-3}	2.21/-1.97	2.86/-1.93	3.16/-2.30
CSD reference no.	1833428	1833429	1833438

S3.2.1 TTTPC NdBr$_2$OTf (CSD ref. 1833432)

Table S6. C-H···Anion interaction (hydrogen bond) distances, angles and types for **TTTPC NdBr$_2$OTf**

TTTPC NdBr$_2$OTf	**Distance / Å**	**Angle / °**	**Type**
C7-H7C···Br1	2.848	142.25	*CH$_3$*
C20-H20A···Br1	2.912	152.63	*μ-pyr-CH$_2$*
C26-H26···Br1	2.665	157.50	*μ-pyr-CH$_2$*
C32-H32···Br2	2.852	131.94	*o-pyr*
C36-H36···Br2	2.840	164.83	*o-pyr*
C12-H12···Br3B	3.108	162.17	*o-pyr*
C16-H16···Br3B	3.017	144.48	*o-pyr*
C15-H15···O2A	2.589	140.58	*μ-pyr*
C16-H16···O3A	2.251	154.59	*μ-pyr*
C10-H10A···O4A	2.658	104.49	*μ-pyr-CH$_2$*
C10-H10B···O4A	2.697	101.94	*μ-pyr-CH$_2$*
C12-H12···O4A	2.261	141.61	*μ-pyr-CH$_2$*
C7-H7A···F6A	2.645	151.08	*CH$_3$*
C8-H8C···F8A	2.620	123.43	*CH$_3$*
C20-H20B···F7A	2.530	129.16	*CH$_2$*

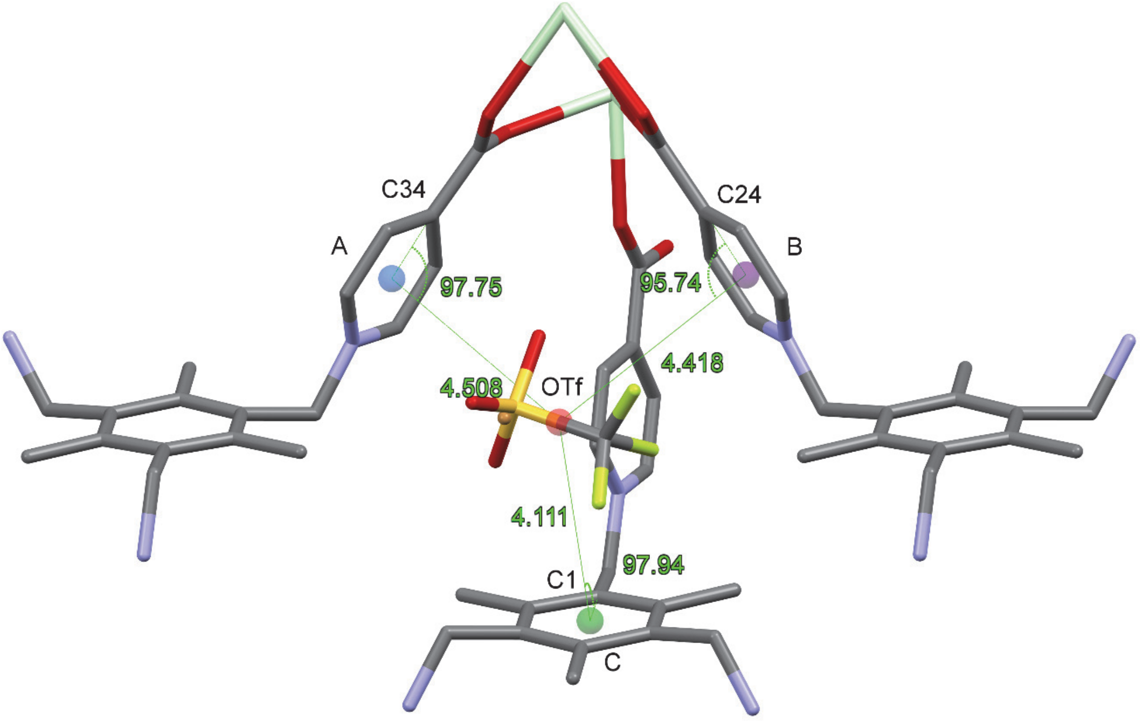

Figure S4. Close-up of the disordered bromide and triflate of **TTTPC NdBr$_2$OTf**. Aromatic centroid distances and angles indicate a possible threefold charge transfer interaction. N11 pyridinium ring (center, back) plane is directed towards the bromide and the sulfonate end of the triflate.

S3.2.2 TTTPC LaBr$_2$OTf (CSD ref. 1833430)

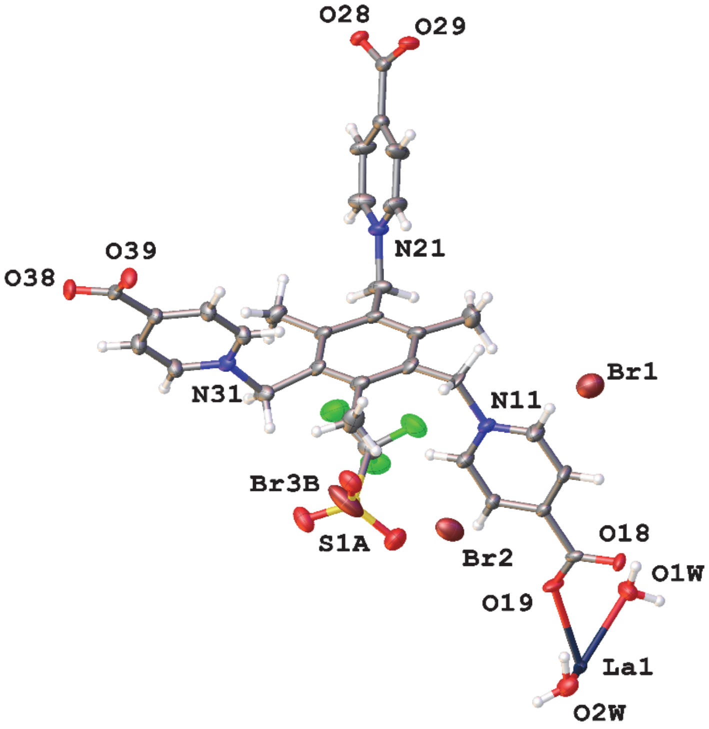

Figure S5. Asymmetric unit contents of **TTTPC LaBr$_2$OTf**.

S3.2.3 TTTPC SmBr$_2$OTf (CSD ref. 1833436)

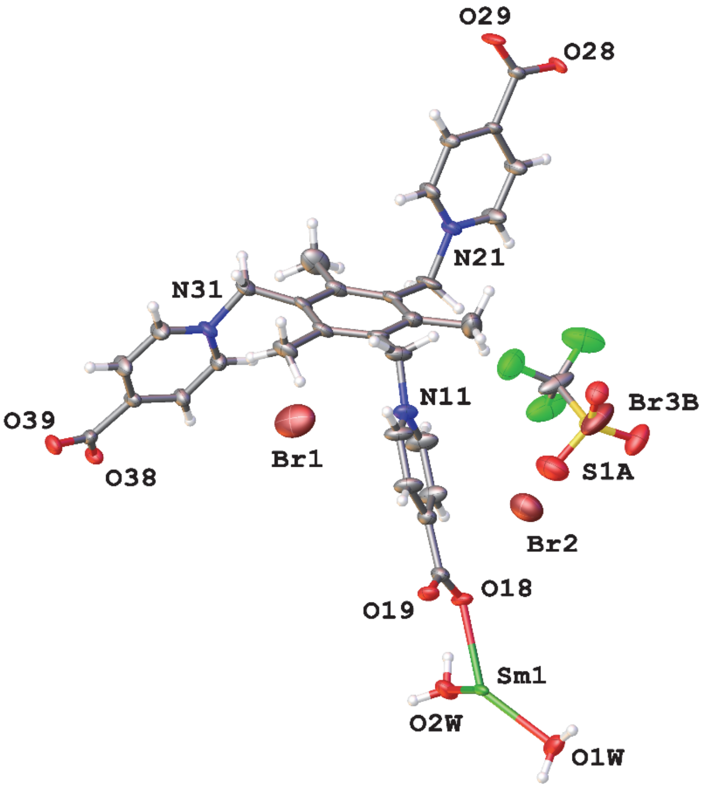

Figure S6. Asymmetric unit contents of **TTTPC SmBr$_2$OTf**.

S3.2.4 TTTPC EuBr$_2$OTf (CSD ref. 1833428)

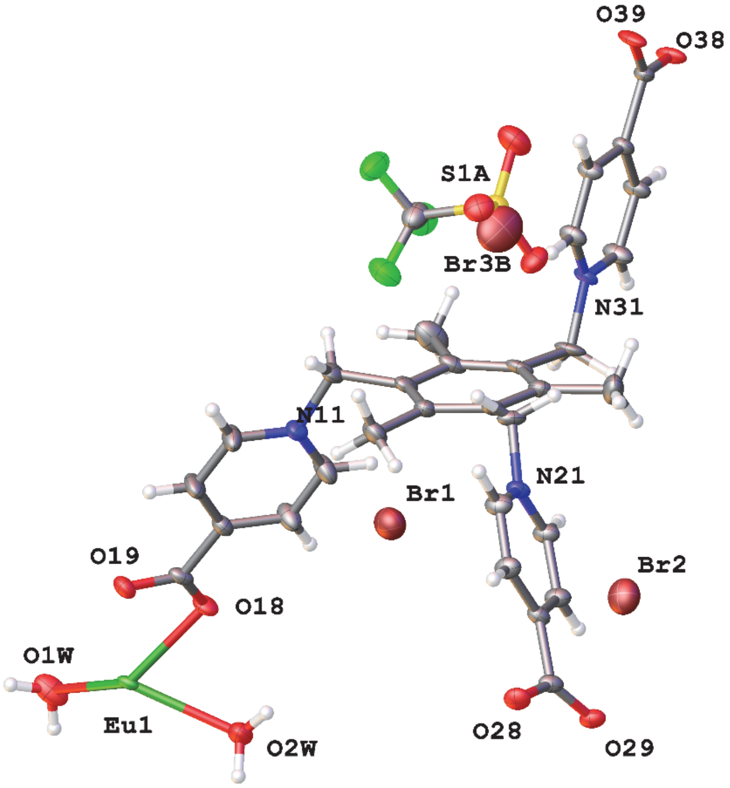

Figure S7. Asymmetric unit contents of **TTTPC EuBr$_2$OTf**.

S3.2.5 TTTPC GdBr$_2$OTf (CSD ref. 1833429)

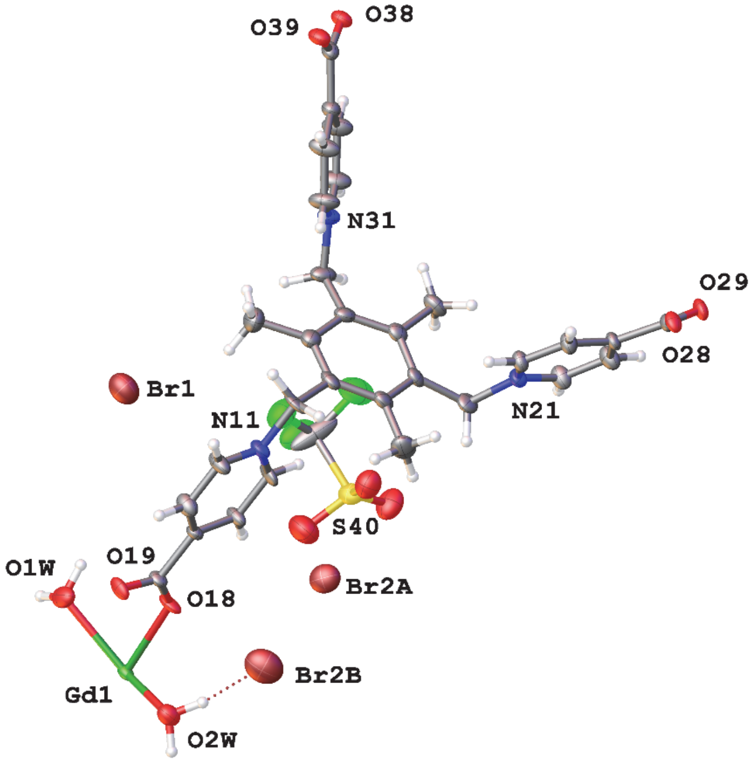

Figure S8. Asymmetric unit contents of **TTTPC GdBr$_2$OTf**.

S3.2.6 TTTPC $TbBr_2OTf$ (CSD ref. 1833438)

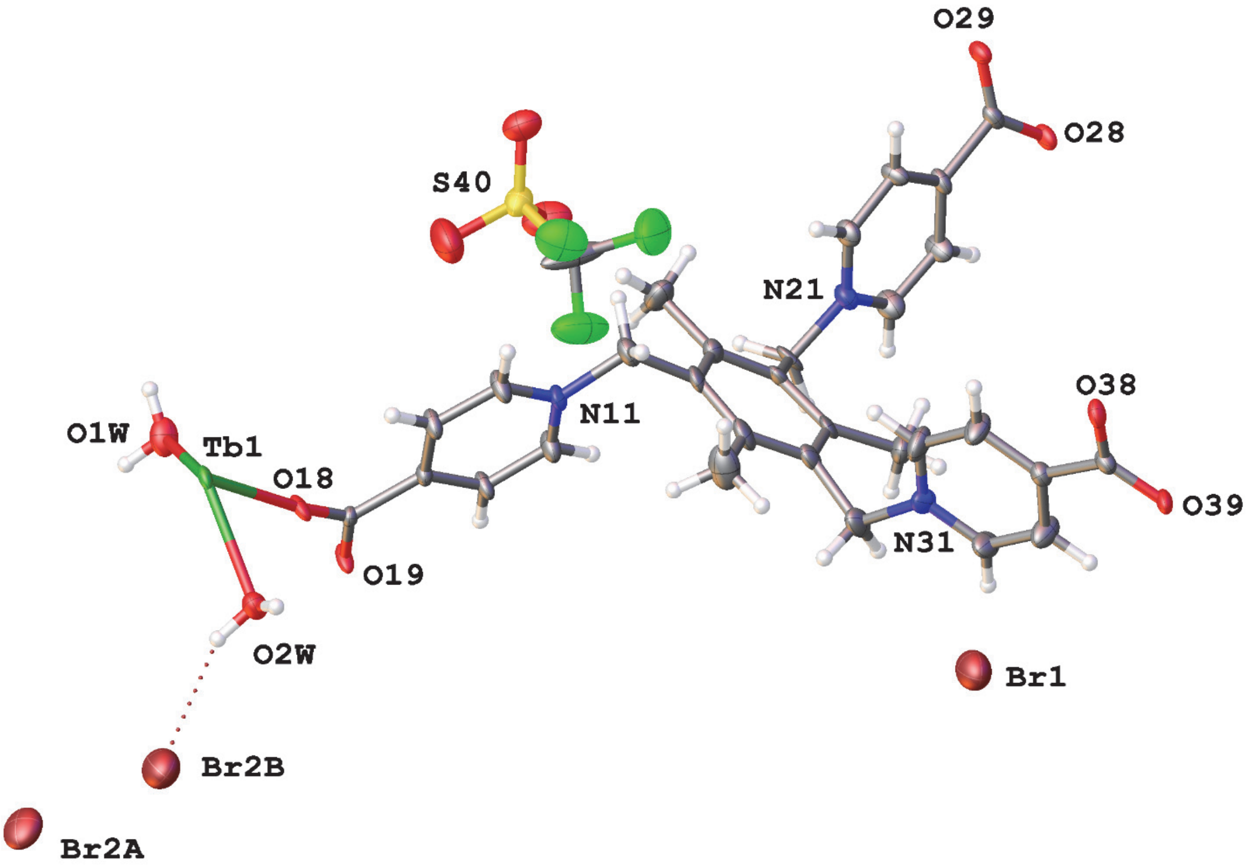

Figure S9. Asymmetric unit contents of **TTTPC $TbBr_2OTf$**.

S3.3 TTTPC LnBr(OTf)$_2$ additional images and tables

Table S7. Crystal structure and refinement data for **TTTPC LnBr(OTf)$_2$**

Name	**TTTPC NdBr(OTf)$_2$**	**TTTPC SmBr(OTf)$_2$**	**TTTPC EuBr(OTf)$_2$**	**TTTPC TbBr(OTf)$_2$**
Empirical formula	$C_{31.65}H_{43}Br_{1.35}F_{4.94}N_3NdO_{19.29}S_{1.65}$	$C_{31.61}H_{47}Br_{1.39}F_{4.84}N_3O_{20.84}S_{1.61}Sm$	$C_{31.55}H_{43}Br_{1.45}EuF_{4.64}N_3O_{19.09}S_{1.55}$	$C_{31.58}H_{47}Br_{1.42}F_{4.73}N_3O_{21.16}S_{1.58}Tb$
Formula weight	1173.14	1207.22	1175.63	1220.21
Temperature / K	120.01(10)	120.01(10)	123.00(10)	123.00(10)
Crystal system	monoclinic	monoclinic	monoclinic	monoclinic
Space group	$P2_1/c$	$P2_1/c$	$P2_1/c$	$P2_1/c$
a / Å	18.7643(2)	18.7334(4)	18.6774(6)	18.5943(2)
b / Å	25.6962(3)	25.6590(5)	25.6718(7)	25.8101(4)
c / Å	9.85675(12)	9.82867(19)	9.7560(3)	9.77200(13)
α / °	90	90	90	90
β / °	102.8557(12)	102.696(2)	102.421(3)	102.3429(13)
γ / °	90	90	90	90
Volume / Å^3	4633.50(10)	4608.92(16)	4568.3(2)	4581.37(11)
Z	4	4	4	4
ρ_{calc} / g/cm^3	1.682	1.74	1.709	1.769
μ / mm^{-1}	11.453	12.543	12.813	10.608
F(000)	2346	2417	2346	2437
Crystal size / mm^3	0.083 × 0.059 × 0.023	0.200 × 0.126 × 0.016	0.168 × 0.161 × 0.014	0.101 × 0.085 × 0.049
Radiation	CuKα (λ = 1.54184)	CuKα (λ = 1.54184)	CuKα (λ = 1.54184)	CuKα (λ = 1.54184)
2Θ range for data collection / °	5.93 to 135.988	5.938 to 135.992	5.944 to 135.996	5.95 to 135.99
Index ranges	$-22 \le h \le 22$, $-22 \le k \le 30$, $-8 \le l \le 11$	$-22 \le h \le 22$, $-30 \le k \le 22$, $-10 \le l \le 11$	$-21 \le h \le 22$, $-30 \le k \le 28$, $-11 \le l \le 10$	$-22 \le h \le 15$, $-22 \le k \le 30$, $-11 \le l \le 11$
Reflections collected	16990	16613	14324	15165
Independent reflections	8412 R_{int} = 0.0245, R_{sigma} = 0.0359	8360 R_{int} = 0.0276, R_{sigma} = 0.0383	8271 R_{int} = 0.0598, R_{sigma} = 0.0870	8286 R_{int} = 0.0391, R_{sigma} = 0.0538
Data/restraints/ parameters	8412/6/556	8360/18/547	8271/7/532	8286/0/556
Goodness-of-fit on F^2	1.068	1.061	1.080	1.040
Final R indexes [I ≥ 2σ (I)]	R_1 = 0.0464, wR_2 = 0.1295	R_1 = 0.0529, wR_2 = 0.1453	R_1 = 0.0835, wR_2 = 0.2359	R_1 = 0.0571, wR_2 = 0.1567
Final R indexes [all data]	R_1 = 0.0552, wR_2 = 0.1363	R_1 = 0.0589, wR_2 = 0.1502	R_1 = 0.0987, wR_2 = 0.2492	R_1 = 0.0637, wR_2 = 0.1651
Largest diff. peak/hole / e Å^{-3}	1.09/-1.91	0.97/-1.83	1.94/-1.60	1.79/-1.70
CSD ref. no.	1833434	1833437	1833445	1833443

S3.3.1 TTTPC NdBr(OTf)$_2$ (CSD ref. 1833434)

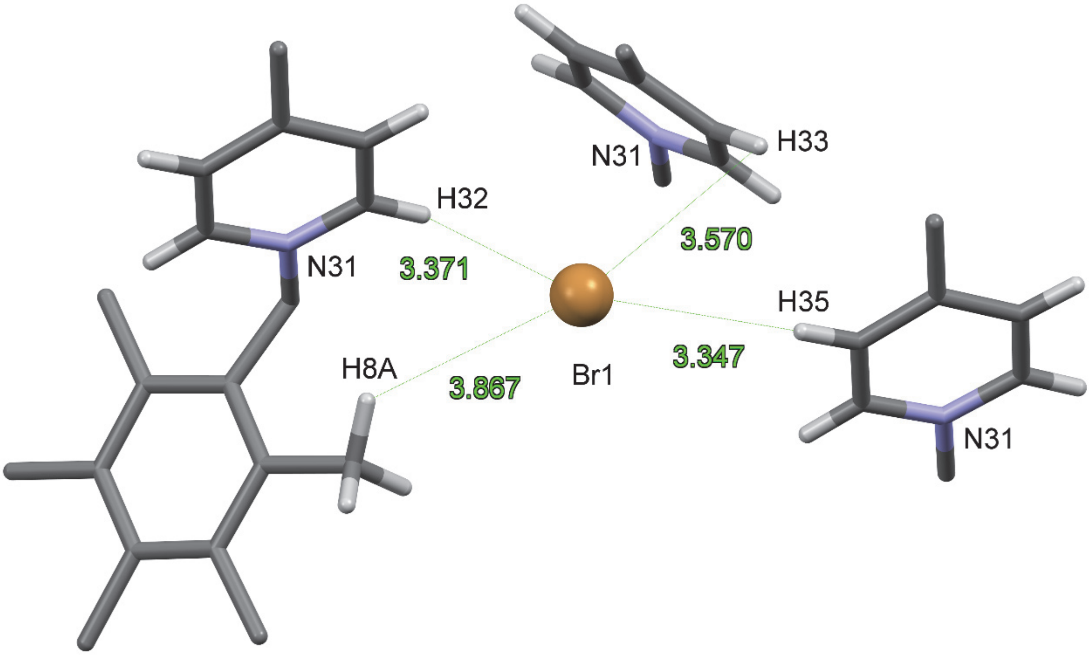

Figure S10. Close-up of Br1 in **TTTPC NdBr(OTf)$_2$** with distant hydrogen bonding donors.

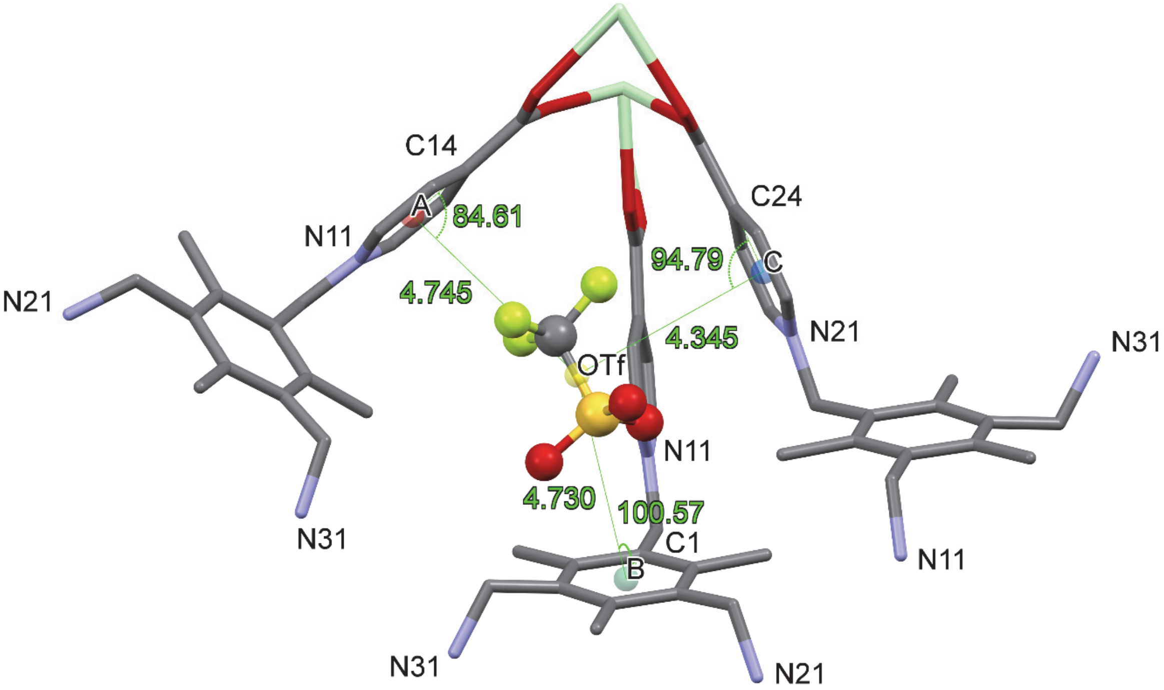

Figure S11. Close-up of the fully occupied triflate of **TTTPC NdBr(OTf)$_2$**. Aromatic centroid distances and angles indicate a possible charge transfer interaction, similar to **TTTPC NdBr$_2$OTf** and **TTTPC NdBr$_3$**.

Table S8. C-H···Anion interaction (hydrogen bond) distances, angles and types for **TTTPC NdBr(OTf)$_2$**

TTTPC NdBr(OTf)$_2$	**Distance / Å**	**Angle / °**	**Type**
C36-H36···O3B	2.453	144.20	*o-pyr*
C10-H10A···O43	2.385	129.43	*μ-pyr-CH*$_2$
C16-H16···O43	2.267	146.79	*μ-pyr-CH*$_2$
C12-H12···O42	2.197	148.55	*o-pyr*
C20-H20B···O42	2.677	133.27	*CH*$_2$
C30-H30A···O41	2.430	124.35	*CH*$_2$
C7-H7C···O43	2.657	122.48	*CH*$_3$
C9-H9C···F47	2.571	161.25	*CH*$_3$
C22-H22···Br2B	3.162	136.03	*o-pyr*
C26-H26···Br2B	3.118	166.00	*o-pyr*
C22-H22···O50A	2.201	150.43	*μ-pyr*
C23-H23···O51A	2.357	135.08	*μ-pyr*
C20-H20A···O49A	2.413	146.68	*μ-pyr-CH*$_2$
C26-H26···O49A	2.070	156.01	*μ-pyr-CH*$_2$
C10-H10B···O50A	2.614	135.06	*CH*$_2$
C7-H7B···O50A	2.286	135.88	*CH*$_3$

S3.3.2 TTTPC SmBr(OTf)$_2$ (CSD ref. 1833437)

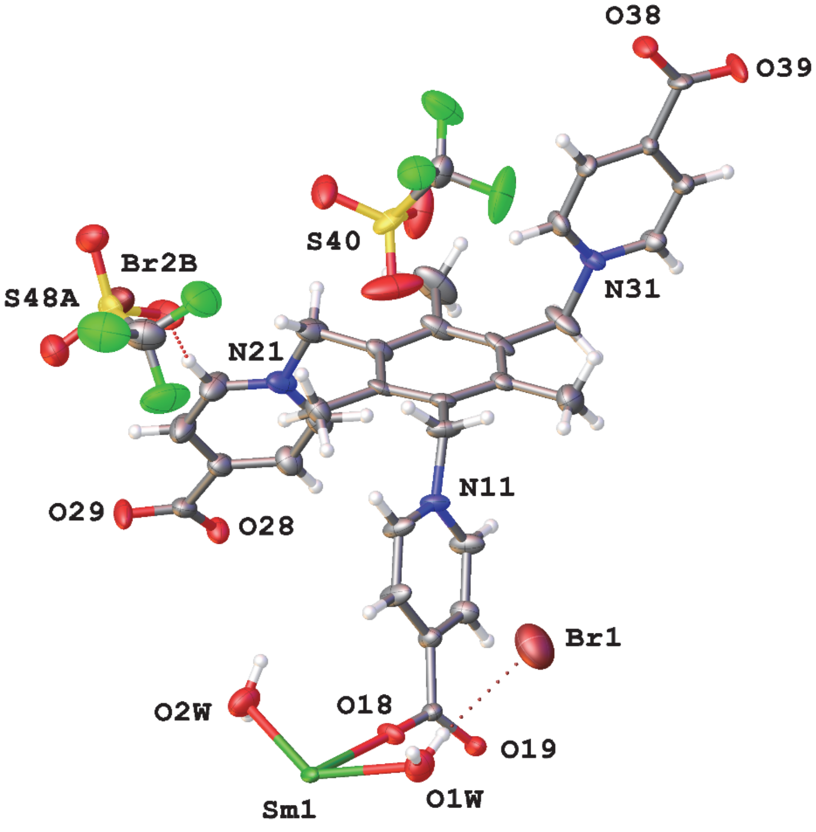

Figure S12. Asymmetric unit contents of **TTTPC SmBr(OTf)$_2$**.

S3.3.3 TTTPC EuBr(OTf)$_2$ (CSD ref. 1833445)

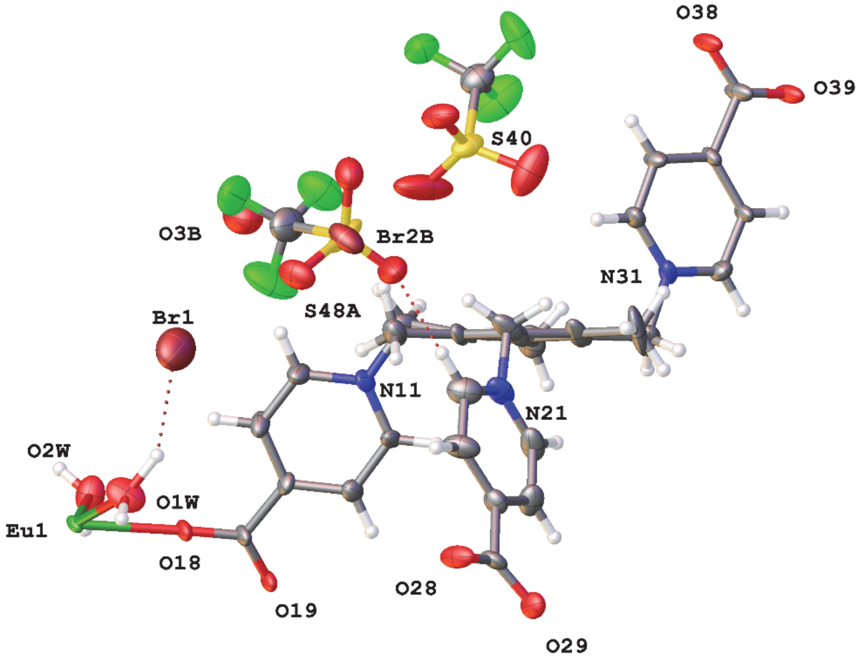

Figure S13. Asymmetric unit contents of **TTTPC EuBr(OTf)$_2$**.

S3.3.4 TTTPC TbBr(OTf)$_2$ (CSD ref. 1833443)

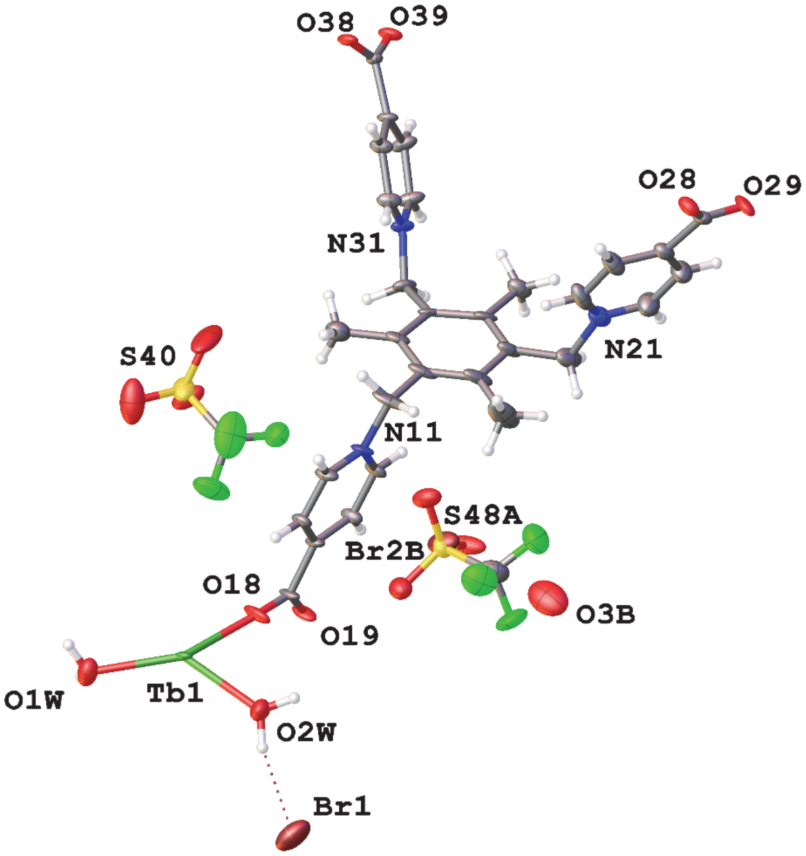

Figure S14. Asymmetric unit contents of **TTTPC TbBr(OTf)$_2$**.

S3.4 TTTPC Ln(OTf)$_3$ additional images and tables

Table S9. Crystal structure and refinement data for **TTTPC Ln(OTf)$_3$**

Name	**TTTPC Nd(OTf)$_3$**	**TTTPC Yb(OTf)$_3$**
Empirical formula	$C_{33}H_{46}F_9N_3NdO_{25}S_3$	$C_{32.9}H_{41}Br_{0.1}F_{8.7}N_3O_{21.7}S_{2.9}Yb$
Formula weight	1296.15	1264.99
Temperature / K	120.00(10)	120.01(10)
Crystal system	triclinic	triclinic
Space group	*P*-1	*P*-1
a / Å	10.1157(3)	10.0256(3)
b / Å	14.2420(4)	14.2571(4)
c / Å	19.1578(7)	18.5311(5)
α / °	110.861(3)	109.018(3)
β / °	101.670(3)	105.086(3)
γ / °	91.706(3)	95.287(2)
Volume / Å^3	2510.09(16)	2372.01(13)
Z	2	2
ρ_{calc} / g/cm^3	1.715	1.771
μ / mm^{-1}	10.144	5.989
F(000)	1308	1262
Crystal size / mm^3	0.148 × 0.051 × 0.042	0.133 × 0.059 × 0.04
Radiation	CuKα (λ = 1.54184)	CuKα (λ = 1.54184)
2Θ range for data collection / °	6.684 to 136	6.856 to 135.99
Index ranges	$-10 \le h \le 12$, $-12 \le k \le 17$, $-23 \le l \le 23$	$-12 \le h \le 11$, $-17 \le k \le 11$, $-22 \le l \le 22$
Reflections collected	15789	14829
Independent reflections	9109 [R_{int} = 0.0595, R_{sigma} = 0.0725]	8573 [R_{int} = 0.0557, R_{sigma} = 0.0577]
Data/restraints/parameters	9109/96/703	8573/222/682
Goodness-of-fit on F^2	1.042	1.184
Final R indexes [I ≥ 2σ (I)]	R_1 = 0.0526, wR_2 = 0.1363	R_1 = 0.0822, wR_2 = 0.2401
Final R indexes [all data]	R_1 = 0.0556, wR_2 = 0.1402	R_1 = 0.0913, wR_2 = 0.2745
Largest diff. peak/hole / e Å^{-3}	2.15/-2.25	3.00/-7.20
CSD reference no.	1833435	1833440

S3.4.1 TTTPC Nd(OTf)$_3$ (CSD ref. 1833435)

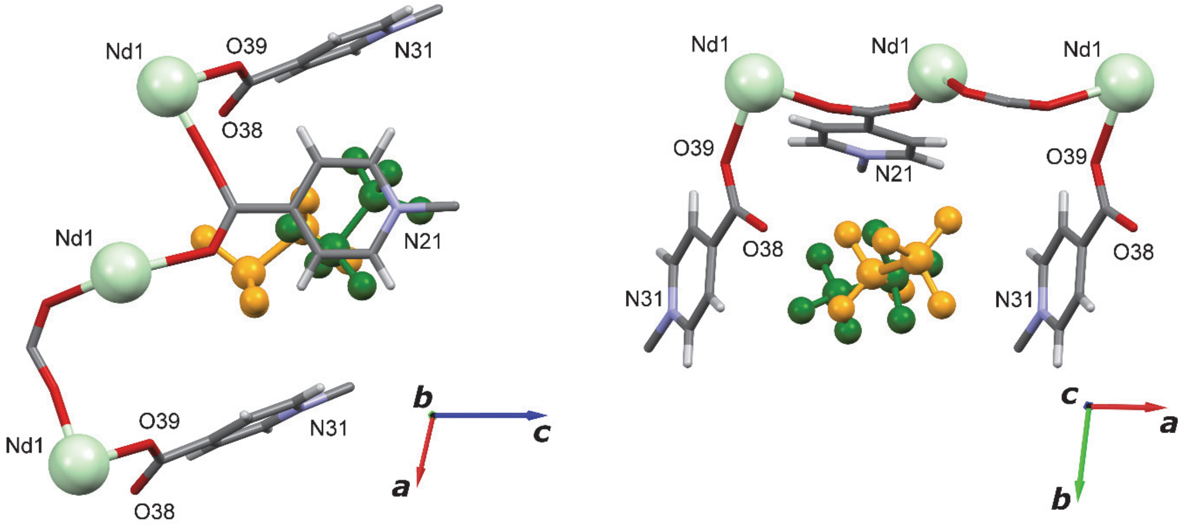

Figure S15. Disordered triflate in **TTTPC Nd(OTf)$_3$** between ligand moieties with possible charge transfer interactions, viewed along *b*-axis (left) and *c*-axis (legend: S56A etc. orange, S56B etc. green).

Table S10. C-H···Anion interaction (hydrogen bond) distances, angles and types for **TTTPC Nd(OTf)$_3$**

TTTPC Nd(OTf)3	**Distance / Å**	**Angle / °**	**Type**
C9-H9B···O59A	2.292	163.32	*CH*$_3$
C8-H8A···O58B	2.510	164.88	*CH*$_3$
C7-H7A···O42	2.359	149.29	*CH*$_3$
C10-H10B···O42	2.562	150.39	*µ-pyr-CH*$_2$
C12-H12···O42	2.248	150.20	*µ-pyr-CH*$_2$
C15-H15···O41	2.508	145.52	*µ-pyr*
C16-H16···O43	2.283	140.09	*µ-pyr*
C22-H22···O50A	2.196	165.93	*o-pyr*
C25-H25···O51	2.652	136.26	*µ-pyr*
C26-H26···O50	2.348	151.30	*µ-pyr*
C35-H35···O51	2.667	114.82	*µ-pyr*
C36-H36···O51	2.330	129.80	*µ-pyr*
C10-H10A···O50	2.517	133.00	*CH*$_2$

S3.4.2 TTTPC Yb(OTf)$_3$ (CSD ref. 1833440)

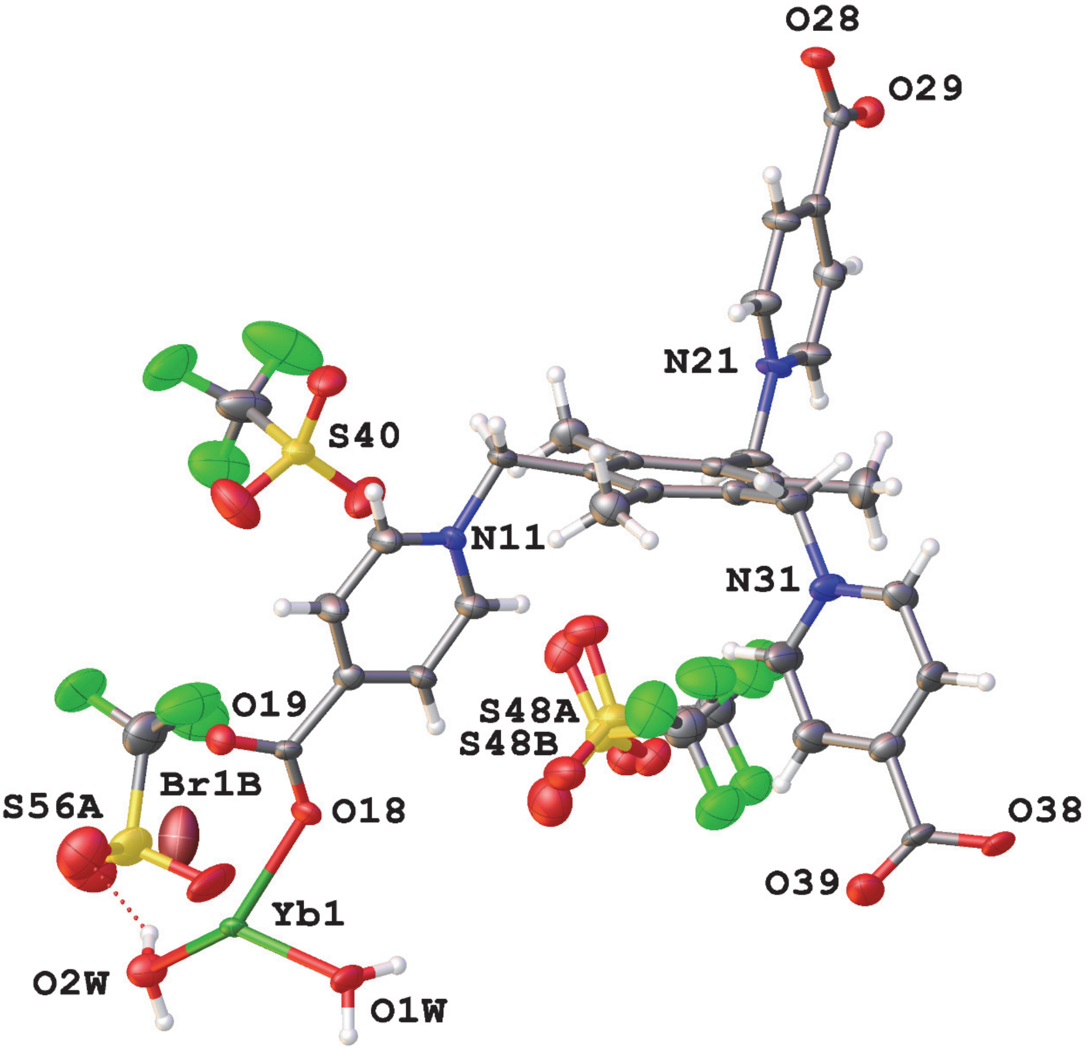

Figure S16. Asymmetric unit contents of **TTTPC Yb(OTf)$_3$**.

S3.5 TTTPC$_2$ Sm$_2$(OTf)$_6$ (CSD ref. 1833446)

The asymmetric unit of **TTTPC$_2$ Sm$_2$(OTf)$_6$** (Fig. S17) contains double the amount of components than the regular **TTTPC Ln(OTf)$_3$** structures, and shares individual characteristics with both **TTTPC Nd(OTf)$_3$** and **TTTPC Yb(OTf)$_3$**. It consists of two ligand molecules, of which one is disordered (N31A, N31B etc. with A:B occupancy of 75 % : 25 %), in *cis-cis* conformation. Two crystallographically independent Sm centers (Sm1 and Sm2) are bound by the ligands and have two or three water molecules in their coordination sphere. Sm1 has three water molecules (O1W, O2W and O3W) with coordination number eight, and it has a distorted bicapped trigonal prismatic geometry. Sm2 has two water molecules (O4W and O5W) with similar coordination number and geometry. Sm1 and Sm2 are bridged by the disordered O38A and O39A. O39B coordinates only to Sm1 and O38B is left hanging free in the water channel. Similarly non-coordinating carboxylate oxygen is O67 whereas O68 is coordinated to Sm2. Six triflate anion positions can be found, of which four are not disordered. First disordered triflate parts have occupancy of 60 % (S1A etc.) and 40 % (S1B etc.) and the parts are slightly staggered with respect to each other. The second disordered triflate exhibited threefold disorder with part occupancies of 65 % (S9A etc.), 25 % (S9B etc.) and additionally a bromide (Br1C) with 10 % occupancy (similar reasoning to **TTTPC Yb(OTf)$_3$**). Twelve diffuse solvent molecules of water were identified and removed with Solvent mask, but a placeholder disordered water was also assigned for some residual electron density (O6W). Overall, this structure did not exhibit any new interactions that have not been issued already in the main text, but was included for the sake of completion, for its structure could be reliably determined. Crystal structure and refinement information are displayed in table S11.

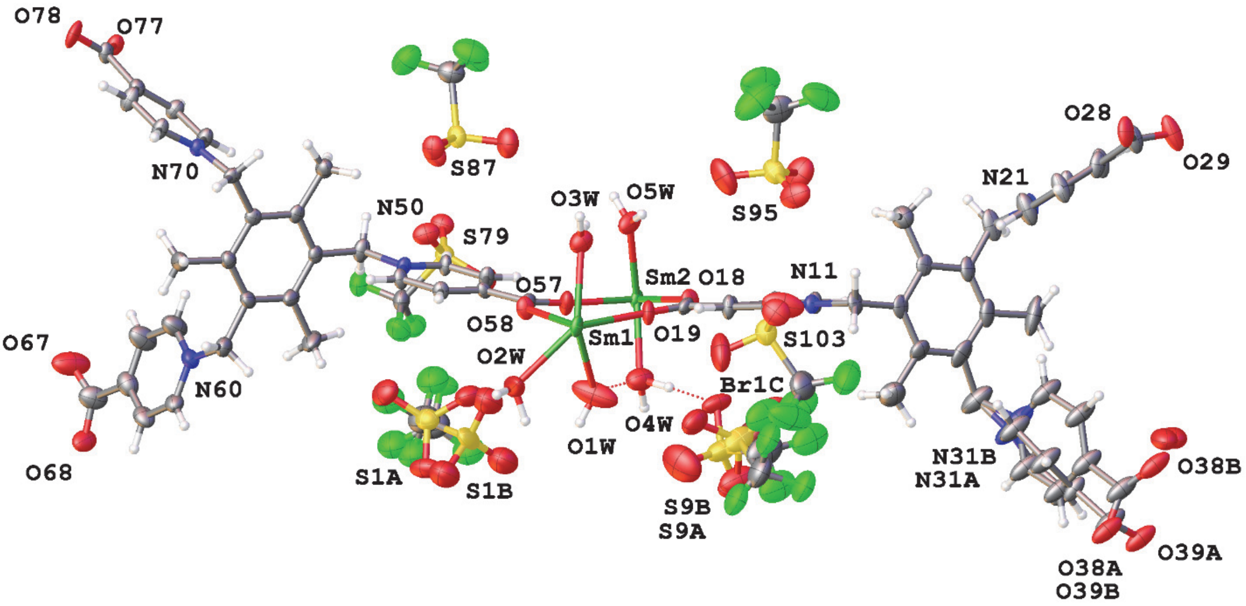

Figure S17. Asymmetric unit contents of **TTTPC$_2$ Sm$_2$(OTf)$_6$**.

Table S11. Crystal structure and refinement data for **TTTPC$_2$ Sm$_2$(OTf)$_6$**

Name	**TTTPC$_2$ Sm$_2$(OTf)$_6$**
Empirical formula	$C_{65.9}H_{86}Br_{0.1}F_{17.7}N_6O_{47.45}S_{5.9}Sm_2$
Formula weight	2555.55
Temperature / K	123.00(10)
Crystal system	triclinic
Space group	*P*-1
a / Å	10.1269(3)
b / Å	14.2176(4)
c / Å	34.2981(6)
α / °	89.1178(19)
β / °	87.111(2)
γ / °	87.308(3)
Volume / Å^3	4926.1(2)
Z	2
ρ_{calc} / g/cm^3	1.723
μ / mm^{-1}	11.237
F(000)	2568
Crystal size / mm^3	0.167 × 0.109 × 0.046
Radiation	CuKα (λ = 1.54184)
2Θ range for data collection / °	6.224 to 136
Index ranges	$-12 \le h \le 12$, $-17 \le k \le 16$, $-41 \le l \le 36$
Reflections collected	29760
Independent reflections	17807 [R_{int} = 0.0610, R_{sigma} = 0.0940]
Data/restraints/parameters	17807/4/1256
Goodness-of-fit on F^2	1.022
Final R indexes [I ≥ 2σ (I)]	R_1 = 0.0694, wR_2 = 0.1760
Final R indexes [all data]	R_1 = 0.0845, wR_2 = 0.1891
Largest diff. peak/hole / e Å^{-3}	1.64/-1.39
CSD reference no.	1833446

S3.6 TTTPC $NdBr_2OAc$ (CSD ref. 1833431) additional images and tables

Table S12. Crystal structure and refinement data for **TTTPC $NdBr_2OAc$**

Name	**TTTPC $NdBr_2OAc$**
Empirical formula	$C_{32}H_{56}Br_2N_3NdO_{21}$
Formula weight	1122.85
Temperature / K	120.01(10)
Crystal system	triclinic
Space group	*P*-1
a / Å	9.1533(9)
b / Å	14.3573(13)
c / Å	18.8779(16)
α / °	107.505(8)
β / °	103.919(8)
γ / °	96.822(8)
Volume / $Å^3$	2247.0(4)
Z	2
ρ_{calc} / g/cm^3	1.66
μ / mm^{-1}	11.59
F(000)	1134
Crystal size / mm^3	0.157 × 0.064 × 0.036
Radiation	CuKα (λ = 1.54184)
2Θ range for data collection / °	6.598 to 135.992
Index ranges	$-11 \le h \le 10$, $-17 \le k \le 15$, $-22 \le l \le 22$
Reflections collected	13462
Independent reflections	8126 [R_{int} = 0.0427, R_{sigma} = 0.0653]
Data/restraints/parameters	8126/0/439
Goodness-of-fit on F^2	1.038
Final R indexes [I ≥ 2σ (I)]	R_1 = 0.0430, wR_2 = 0.1097
Final R indexes [all data]	R_1 = 0.0498, wR_2 = 0.1163
Largest diff. peak/hole / e $Å^{-3}$	1.21/-1.94
CSD reference no.	1833431

Table S13. C-H···Br^- interaction (hydrogen bond) distances, angles and types for **TTTPC $NdBr_2OAc$**

TTTPC NdBr2OAc	Distance / Å	Angle / °	Type
C12-H12···Br1	2.835	134.45	*o-pyr*
C16-H16···Br1	2.721	167.06	*o-pyr*
C9-H9A···Br1	2.730	148.47	CH_3
C22-H22···Br2	2.875	146.54	*o-pyr*
C32-H32···Br2	2.777	151.69	*o-pyr*
C36-H36···Br2	2.799	174.15	*o-pyr*
C9-H9B···Br2	2.972	154.16	CH_3

S3.7 TTTPC $NdBr_2OTf$ (vac) (CSD ref. 1842357) additional images and tables

Table S14. Crystal structure and refinement data for **TTTPC $NdBr_2OTf$ (vac)**

Name	**TTTPC $NdBr_2OTf$ (vac)**
Empirical formula	$C_{31}H_{31}Br_2F_3N_3NdO_{11}S$
Formula weight	1014.71
Temperature / K	120.01(10)
Crystal system	triclinic
Space group	*P*-1
a / Å	9.4141(3)
b / Å	12.0776(3)
c / Å	18.7454(5)
α / °	105.103(2)
β / °	98.057(2)
γ / °	99.489(2)
Volume / Å^3	1991.69(9)
Z	2
ρ_{calc} / g/cm^3	1.692
μ / mm^{-1}	13.409
F(000)	998
Crystal size / mm^3	0.138 × 0.08 × 0.037
Radiation	CuKα (λ = 1.54184)
2Θ range for data collection / °	7.756 to 135.978
Index ranges	$-11 \le h \le 10$, $-10 \le k \le 14$, $-21 \le l \le 22$
Reflections collected	12783
Independent reflections	7241 [R_{int} = 0.0255, R_{sigma} = 0.0382]
Data/restraints/parameters	7241/8/562
Goodness-of-fit on F^2	1.050
Final R indexes [I ≥ 2σ (I)]	R_1 = 0.0367, wR_2 = 0.0944
Final R indexes [all data]	R_1 = 0.0378, wR_2 = 0.0952
Largest diff. peak/hole / e Å^{-3}	1.61/-1.11
CSD reference no.	1842357

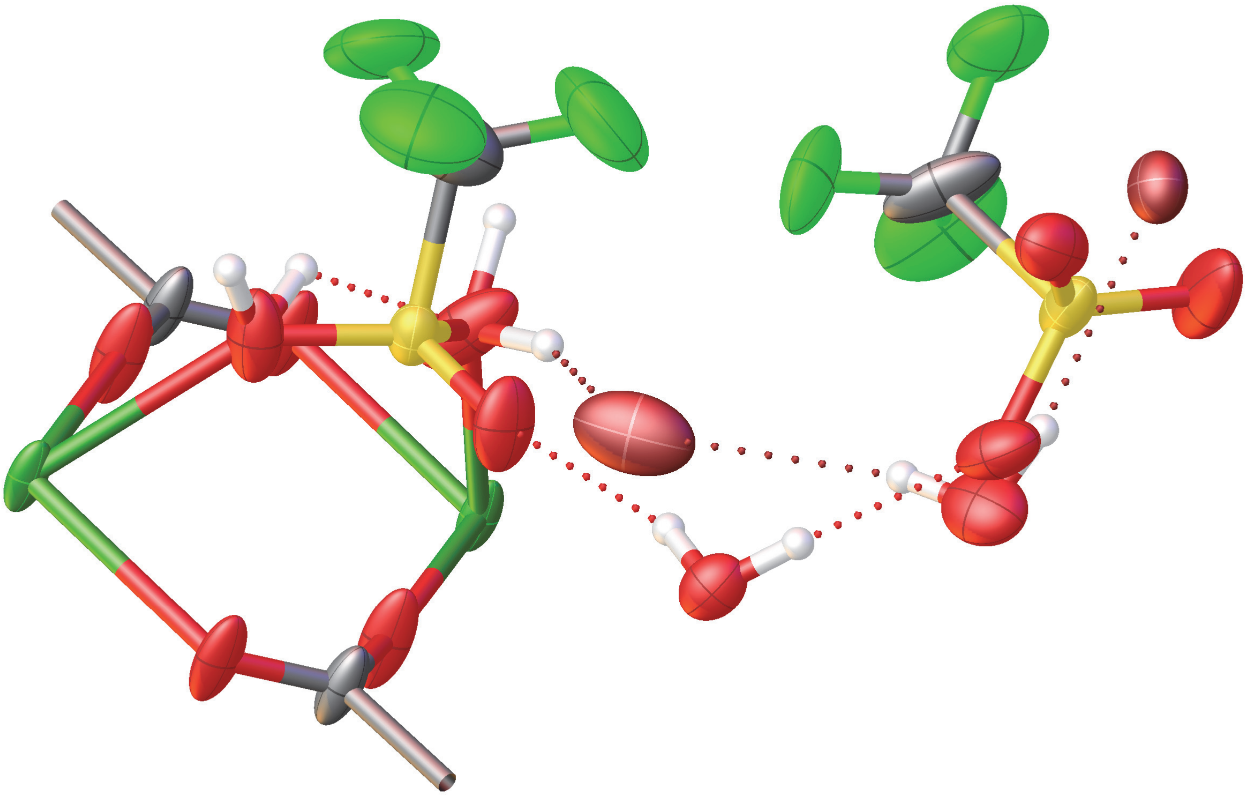

Figure S18. Hydrogen bonded anion assemblies of **TTTPC NdBr$_2$OTf (vac)** inhabiting the same space (substitutional disorder).

Table S15. C-H···Anion interaction (hydrogen bond) distances, angles and types for **TTTPC NdBr$_2$OTf (vac)**

TTTPC NdBr2OTf (vac)	**Distance / Å**	**Angle / °**	**Type**
C23-H23···Br1B	2.881	171.98	*m-pyr*
C26-H26···Br1B	2.803	127.18*	*o-pyr*
C12-H12···Br2B	2.826	174.56	*o-pyr*
C16-H16···Br2B	2.884	146.81	*o-pyr*
C32-H32···Br3	2.905	141.49	*o-pyr*
C36-H36···Br3	2.806	175.03	*o-pyr*
C10-H10B···Br3	2.893	133.98	CH_2
C20-H20A···Br3	3.009	121.11	CH_2
C16-H16···O41A	2.130	142.43	*o-pyr*
C12-H12···O42A	2.237	150.68	*μ-pyr-*CH_2
C10-H10A···O42A	2.416	152.56	*μ-pyr-*CH_2
C8-H8A···O42A	2.490	169.59	CH_3
C22-H22···O43A	2.594	137.55*	*o-pyr*

* Anion acceptor atom exceptionally offset from the pyridinium ring plane, so maybe a borderline interaction

S3.8 TTTPC $NdBr_2OAc$ (dry) (CSD ref. 1894870) additional images and tables

Table S16. Crystal structure and refinement data for **TTTPC $NdBr_2OAc$ (dry)**

Name	**TTTPC $NdBr_2OAc$ (dry)**
Empirical formula	$C_{32}H_{44}Br_2N_3NdO_{15}$
Formula weight	1014.76
Temperature / K	120.01(10)
Crystal system	triclinic
Space group	*P*-1
a / Å	8.7309(9)
b / Å	12.2707(11)
c / Å	19.3079(11)
α / °	106.661(7)
β / °	100.429(7)
γ / °	91.716(8)
Volume / Å^3	1941.6(3)
Z	2
ρ_{calc} / g/cm^3	1.736
μ / mm^{-1}	13.225
F(000)	1014.0
Crystal size / mm^3	0.151 × 0.115 × 0.05
Radiation	CuKα (λ = 1.54184)
2Θ range for data collection / °	7.548 to 135.982
Index ranges	$-10 \leq h \leq 10$, $-14 \leq k \leq 14$, $-17 \leq l \leq 23$
Reflections collected	12498
Independent reflections	7055 [R_{int} = 0.0284, R_{sigma} = 0.0415]
Data/restraints/parameters	7055/0/503
Goodness-of-fit on F^2	1.007
Final R indexes [I ≥ 2σ (I)]	R_1 = 0.0251, wR_2 = 0.0589
Final R indexes [all data]	R_1 = 0.0272, wR_2 = 0.0600
Largest diff. peak/hole / e Å^{-3}	0.72/-0.71
CSD reference no.	1894870

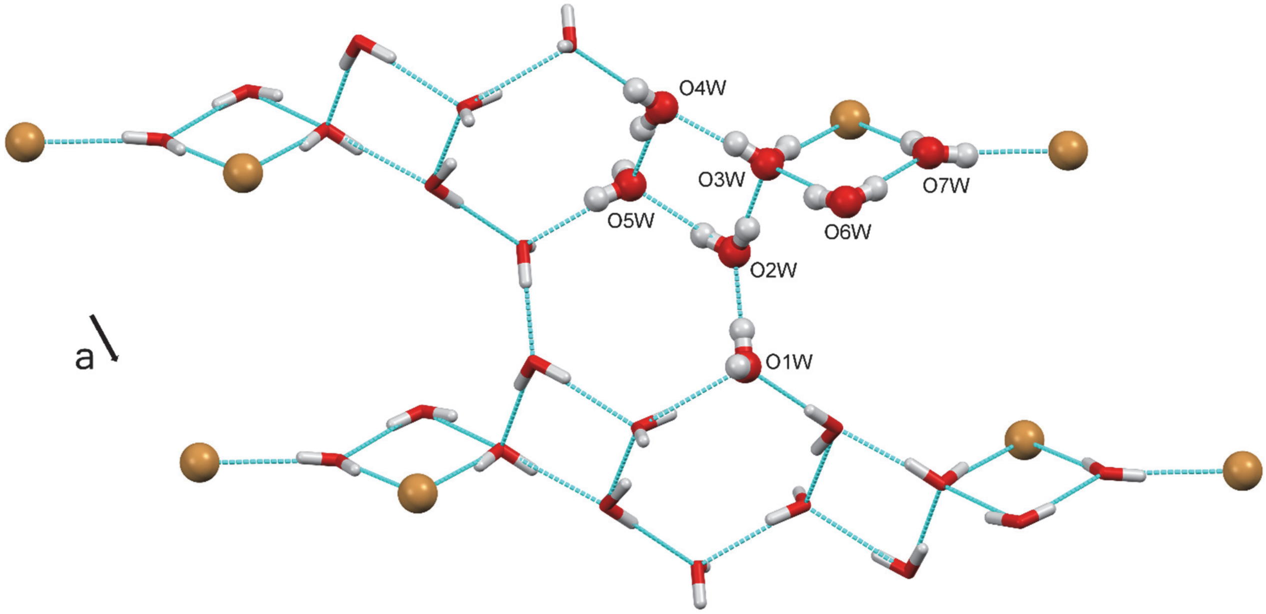

Figure S19. Extended hydrogen bond network between water molecules inhabiting the water channel. Ball-and-stick modelled O1W - O7W are crystallographically independent. Crystallographic *a*-axis direction in the plane of the paper diagonally down (small arrow).

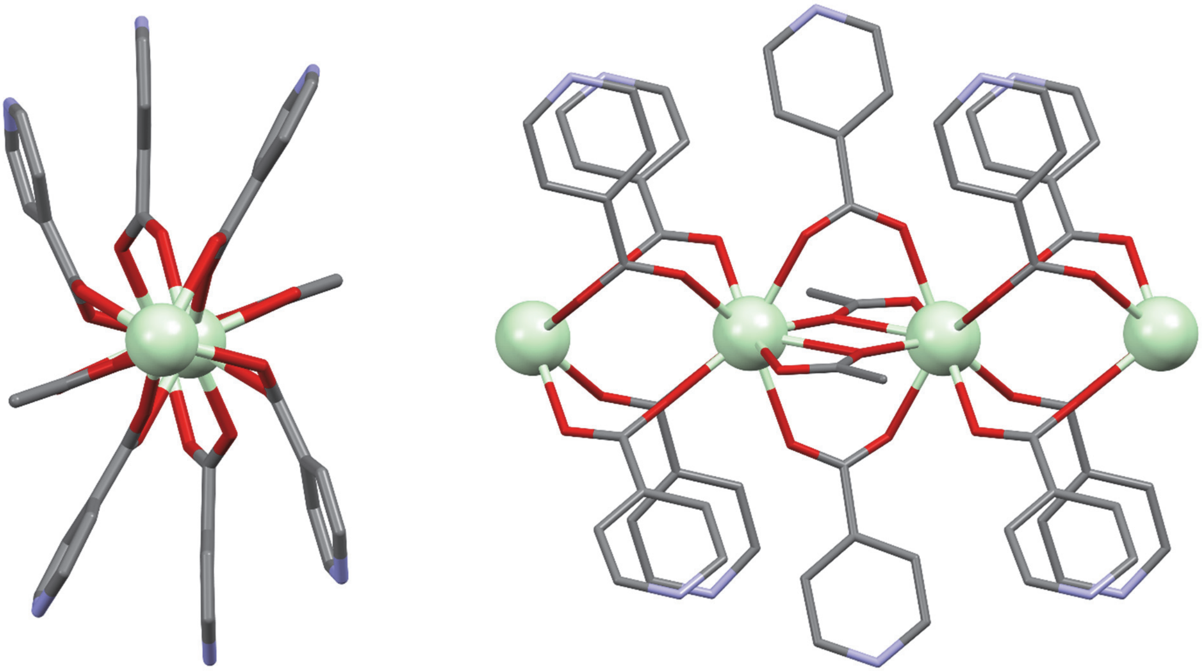

Figure S20. TTTPC ligand orientation ("three-up-three-down", left) and infinite metal chain running along the *a*-axis with restored paddlewheel structures that were disturbed by the water molecules in the fresh structure (for comparison see *e.g.* Fig S27). Hydrogen atoms omitted for clarity.

S3.9 TTTPC Ln$(NO_3)_3$

Wen *et al.*[1] have published the first **TTTPC** Ln-MOF-structure (CSD: ROLZEZ) that is analogous to the ones presented here, with nitrate as a recognized anion. In their structure, PLATON/SQUEEZE was used to handle the solvent, and the crystal was measured in room temperature. Their structure determination concludes that the 3+ charge of the Eu metal is balanced by one nitrate anion and "two terminal hydroxyl groups", obviously referring to the first coordination sphere oxygen atoms interpreted as two hydroxides. Since we do not have the exact data and we have not replicated their experimental procedure (different starting materials and solvents), we are unsure whether their interpretation of the hydroxides is correct or not, but we have a strong doubt. Most likely their structure has contained all three nitrates (or disordered bromides), but due to the measurement made in room temperature, the difficult to pinpoint anions have been overlooked and mistakenly wiped by the SQUEEZE routine, and the charge balance corrected with the hydroxides. Here we report three structures with all nitrates assigned (Table S17).

Table S17. Crystal structure and refinement data for **TTTPC Ln$(NO_3)_3$**

Name	**TTTPC La$(NO_3)_3$**	**TTTPC Nd$(NO_3)_3$**	**TTTPC Y$(NO_3)_3$**
Empirical formula	$C_{30}H_{45}LaN_6O_{24}$	$C_{30}H_{43}N_6NdO_{23}$	$C_{30}H_{41}N_6O_{22}Y$
Formula weight	1012.63	999.94	926.6
Temperature / K	120.01(10)	120.00(10)	120.01(10)
Crystal system	triclinic	triclinic	triclinic
Space group	*P*-1	*P*-1	*P*-1
a / Å	9.6393(4)	9.5948(6)	9.5796(3)
b / Å	12.2016(6)	12.3229(9)	12.0095(7)
c / Å	19.0185(7)	18.8983(13)	18.6284(5)
α / °	105.771(4)	106.033(6)	104.551(4)
β / °	99.826(3)	99.619(6)	98.841(3)
γ / °	99.967(4)	99.928(6)	102.169(4)
Volume / Å^3	2063.50(16)	2060.2(3)	1978.82(16)
Z	2	2	2
ρ_{calc} / g/cm^3	1.63	1.612	1.555
μ / mm^{-1}	8.855	10.441	2.906
F(000)	1032	1018	956
Crystal size / mm^3	0.086 × 0.064 × 0.042	0.215 × 0.169 × 0.078	0.136 × 0.061 × 0.057
Radiation	CuKα (λ = 1.54184)	CuKα (λ = 1.54184)	CuKα (λ = 1.54184)
2Θ range for data collection / °	7.74 to 135.998	7.672 to 135.95	7.878 to 135.998
Index ranges	$-11 \le h \le 11$, $-9 \le k \le 14$, $-22 \le l \le 19$	$-10 \le h \le 11$, $-14 \le k \le 14$, $-22 \le l \le 22$	$-7 \le h \le 11$, $-14 \le k \le 13$, $-22 \le l \le 21$
Reflections collected	12441	13092	11727
Independent reflections	7466 R_{int} = 0.0331 R_{sigma} = 0.0532	7471 R_{int} = 0.0292 R_{sigma} = 0.0408	7185 R_{int} = 0.0283 R_{sigma} = 0.0482
Data/restraints/parameters	7466/12/438	7471/6/549	7185/9/492
Goodness-of-fit on F^2	1.087	1.030	1.109
Final R indexes [I ≥ 2σ (I)]	R_1 = 0.0671, wR_2 = 0.1801	R_1 = 0.0401, wR_2 = 0.1081	R_1 = 0.0551, wR_2 = 0.1496
Final R indexes [all data]	R_1 = 0.0736, wR_2 = 0.1883	R_1 = 0.0415, wR_2 = 0.1098	R_1 = 0.0593, wR_2 = 0.1527
Largest diff. peak/hole / e Å^{-3}	2.68/-2.39	1.80/-1.73	1.86/-0.97

As in the main text, the Nd structure is presented as archetype and it will be discussed in most detail. Lanthanum and yttrium structures bring no significant new insights to the discussion apart from the assurance of the structure similarity. Yttrium is pseudo-lanthanoid and corresponds roughly to the ionic radius of Er, so it represents the heavy lanthanoids reasonably well in this regard.[2]

S3.9.1 TTTPC Nd(NO_3)$_3$ (CSD ref. 1842358)

The asymmetric unit (Fig. S21) consists of a Nd center with two coordinated water molecules (O1W, O2W), a **TTTPC** ligand in *anti* conformation, three more or less disordered nitrate anions and one additional disordered solvent water over three positions (O3WA, O3WB, O3WC). The O3W water oxygen atoms were assigned as placeholders due to residual electron density left from the OLEX[2] Solvent mask, and their occupancies were set to 33 % each. A total of six diffuse water molecules were identified in the unit cell. Nitrates N40 etc. and N44 etc. were found to be slightly disordered so that their oxygen atoms (O42, O43 and O47) had to be split into parts. The third nitrate needed to be assigned over two positions also because of disorder (N48A etc. and N48B etc., 34 % and 66 % occupancies respectively). Nitrates N44 and N48B showed tendencies to form hydrogen bonds with the first coordination sphere water (O1W), and there was also a likely hydrogen bond between O1W-H1WA···O3WA. Additionally, a hydrogen bond between O1W and O2W is likely (O2W-H2WB···O1W, distance O1W-O2W: 2.901 Å). Ligand-anion interactions were found to be analogous to those observed with the structures in the main text with bromides and triflates, namely *o-pyr*, *m-pyr* and *µ-pyr* and *µ-pyr-CH*$_2$ type interactions, with probable charge transfer interactions also present. However, due to uncertainty arising from the disorder, no further analysis of these interactions were made.

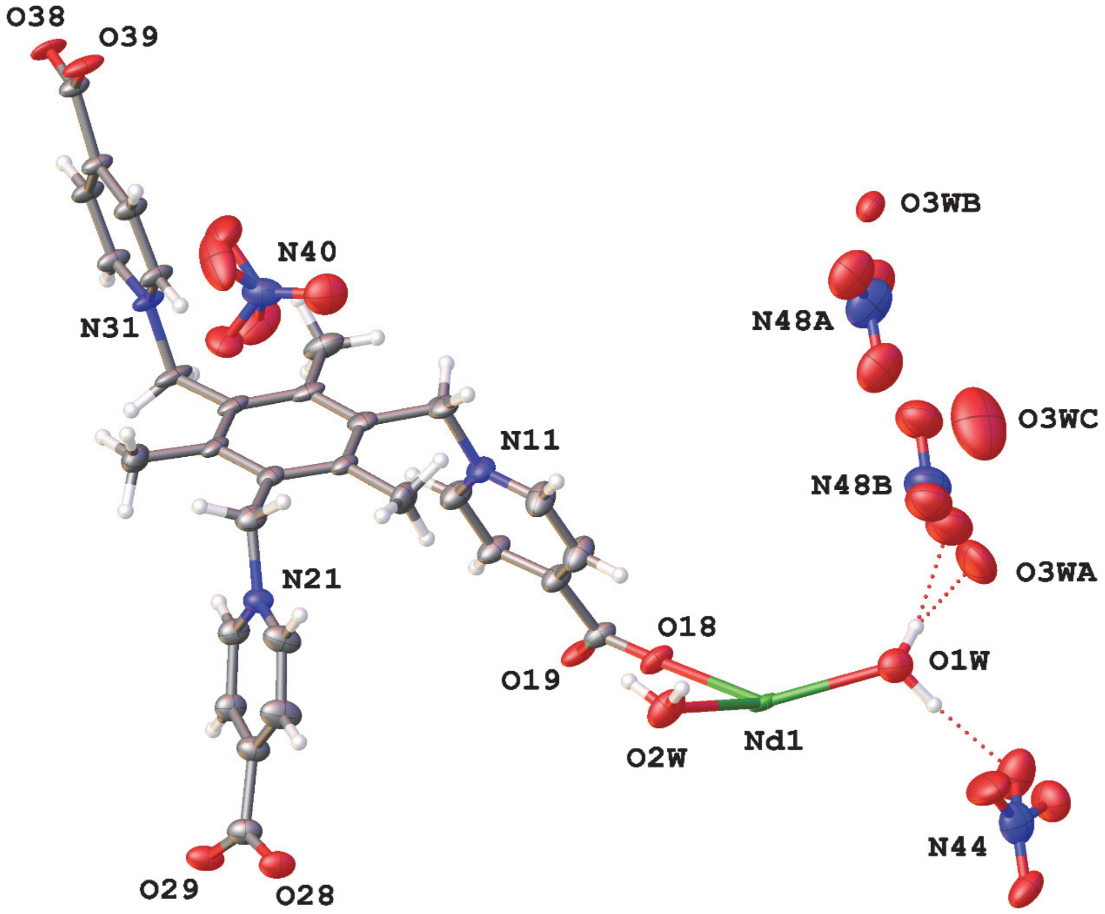

Figure S21. Asymmetric unit contents of **TTTPC Nd(NO_3)$_3$**.

Structure packing and topology follows the **TTTPC NdBr$_3$** and related structures, so no comprehensive explanation is needed to elucidate this structure. Secondary building unit is the same as in Fig. 9a, ligand orientation the same as in Fig. 10a and so on. The water channel is running in the direction of the crystallographic *a*-axis (Fig. S24b).

S3.9.2 TTTPC La(NO$_3$)$_3$ (CSD ref. 1833441)

The asymmetric unit of **TTTPC La(NO$_3$)$_3$** follows the same principles as its Nd counterpart but the three nitrates have been assigned so that they each have full occupancy (Fig. S22). Anion naming and positioning is analogous to the Nd structure as well, so N48 corresponds to N48A, and N48B is not present in this structure (its contribution was probably so small that it could not be resolved from the diffuse electron density of the solvent water). A total of seven water molecules were removed with OLEX^2 Solvent mask. Metal coordination environment is practically the same as with Nd, with 8-coordinate La, as are the packing and supramolecular features (Fig. S24a).

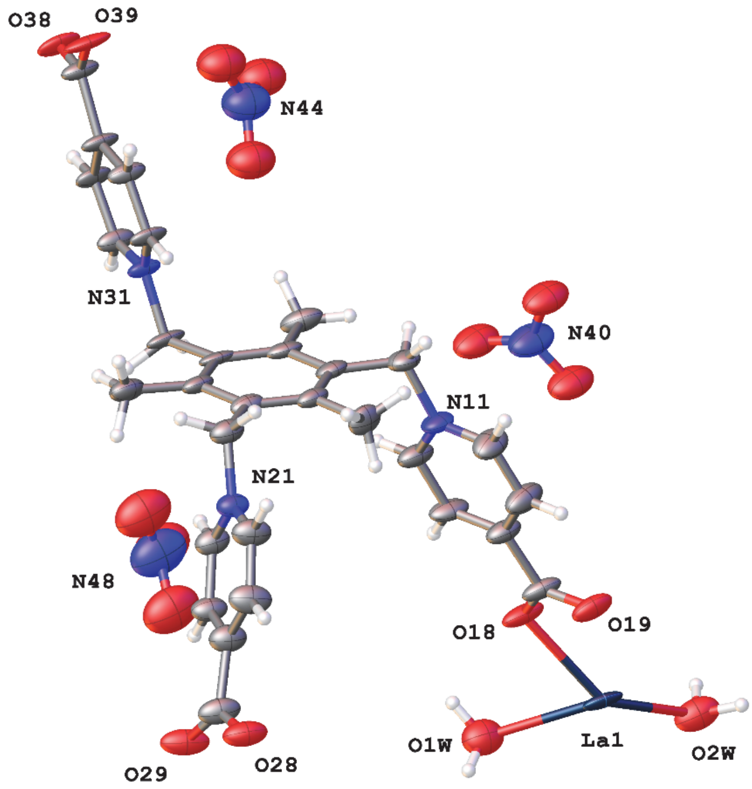

Figure S22. Asymmetric unit contents of **TTTPC La(NO$_3$)$_3$**.

S3.9.3 TTTPC Y(NO$_3$)$_3$ (CSD ref. 1833444)

The asymmetric unit contents of **TTTPC Y(NO$_3$)$_3$** (Fig. S23) are essentially the same as the La counterpart, so no specifically detailed discussion is needed. Labelling of the anions is the opposite regarding N40 etc. and N44 etc. in their respective positions, compared to the La and Nd structures. In this structure, there is an H-bond between O1W and O42. A total of five water molecules were removed with OLEX^2 Solvent mask. Topologically the structure is identical to the previous ones. Only a diminutive shift of the ligand and anion orientations can be seen (Fig. S24c), which probably reflects the slightly larger *γ*-angle of this structure compared to the other relatively uniform parameters (Table S17). This slight difference is most likely due to the metal ionic radius being smaller, for the other components are essentially the same.

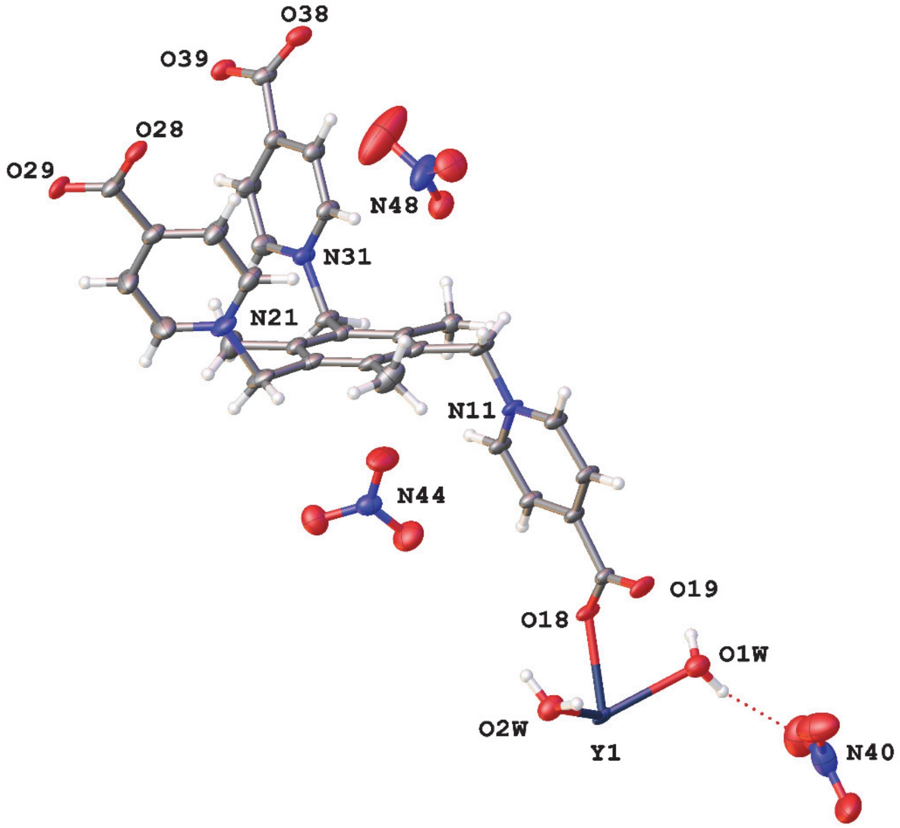

Figure S23. Asymmetric unit contents of **TTTPC Y(NO$_3$)$_3$**.

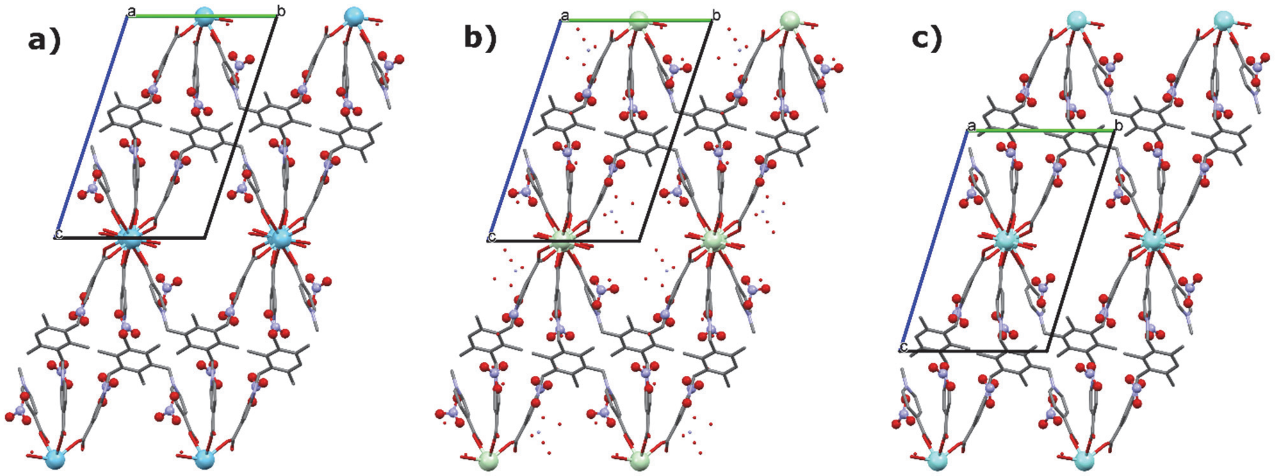

Figure S24. Overview of 2x2 packed **TTTPC Ln(NO$_3$)$_3$** structures along crystallographic *a*-axis (Ln = a) La, b) Nd, c) Y). Hydrogen atoms omitted for clarity.

S3.10 Other supporting figures

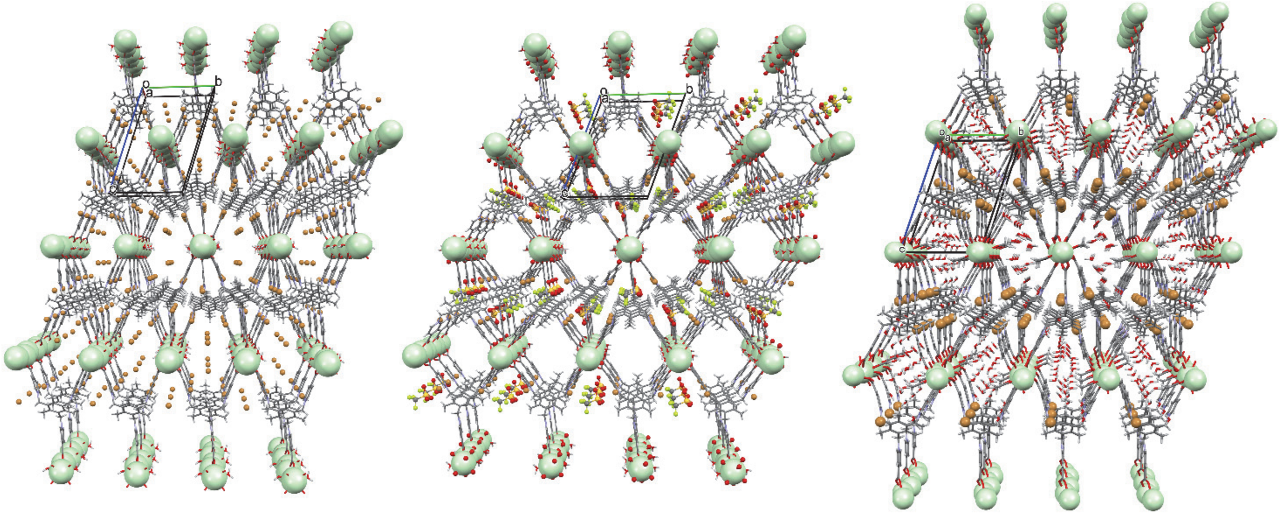

Figure S25. Dimensions of **TTTPC NdBr$_3$** (left), **TTTPC NdBr$_2$OTf** (middle) **TTTPC NdBr$_2$OAc (dry)** and viewed along the *a*-axis with water pores visible, and partially filled with anionic species.

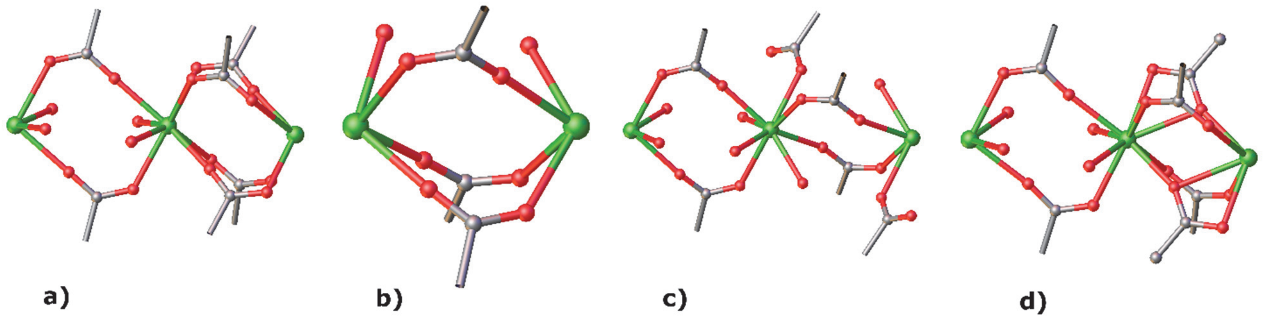

Figure S26. Linear repeating units of metal-ligand rows of a) **TTTPC NdBr$_3$**, b) **TTTPC NdBr(OTf)$_2$**, c) **TTTPC Nd(OTf)$_3$** and d) **TTTPC NdBr$_2$OAc** viewed perpendicular to the water channel direction (hydrogens omitted for clarity).

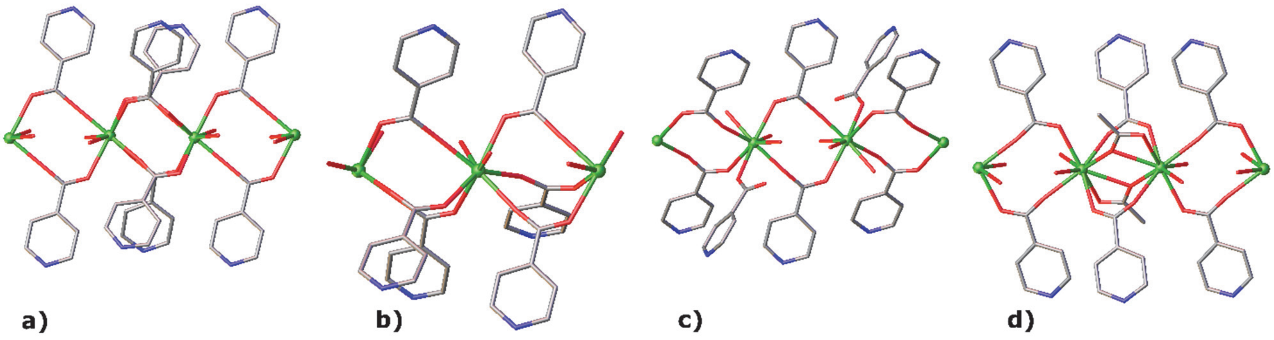

Figure S27. Extended ligand orientations of a) **TTTPC NdBr$_3$**, b) **TTTPC NdBr(OTf)$_2$**, c) **TTTPC Nd(OTf)$_3$** and d) **TTTPC NdBr$_2$OAc** viewed perpendicular to the water channel direction (hydrogens omitted for clarity).

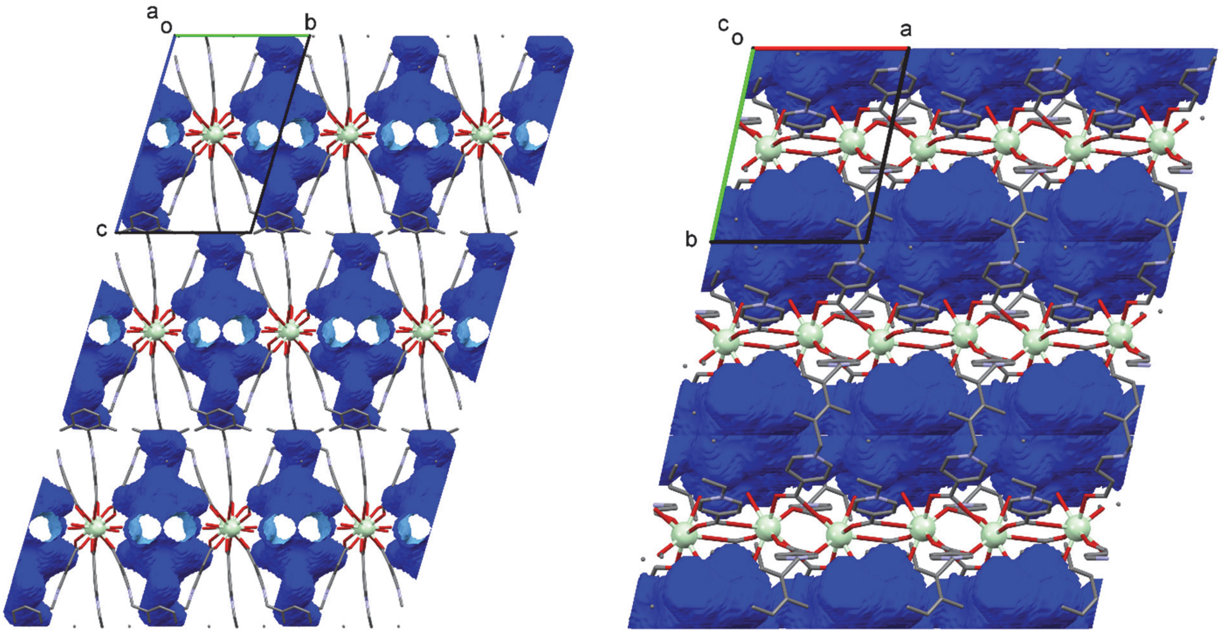

a) b)

Figure S28. Water channels of **TTTPC NdBr$_3$** viewed along crystallographic a) *a*-axis and b) *c*-axis (hydrogens and bromides omitted for clarity, Mercury contact surface mapping with 1.2 Å probe and 0.2 Å grid). Bromides (Br3B) in the water channel partially occlude the channel and choked regions can be seen (compare to topologically identical **TTTPC NdBr$_2$OTf** with no similar anion disorder, Figs. 11a and S30a). The channel is not entirely blocked because of only partial bromide occupancy (60 %).

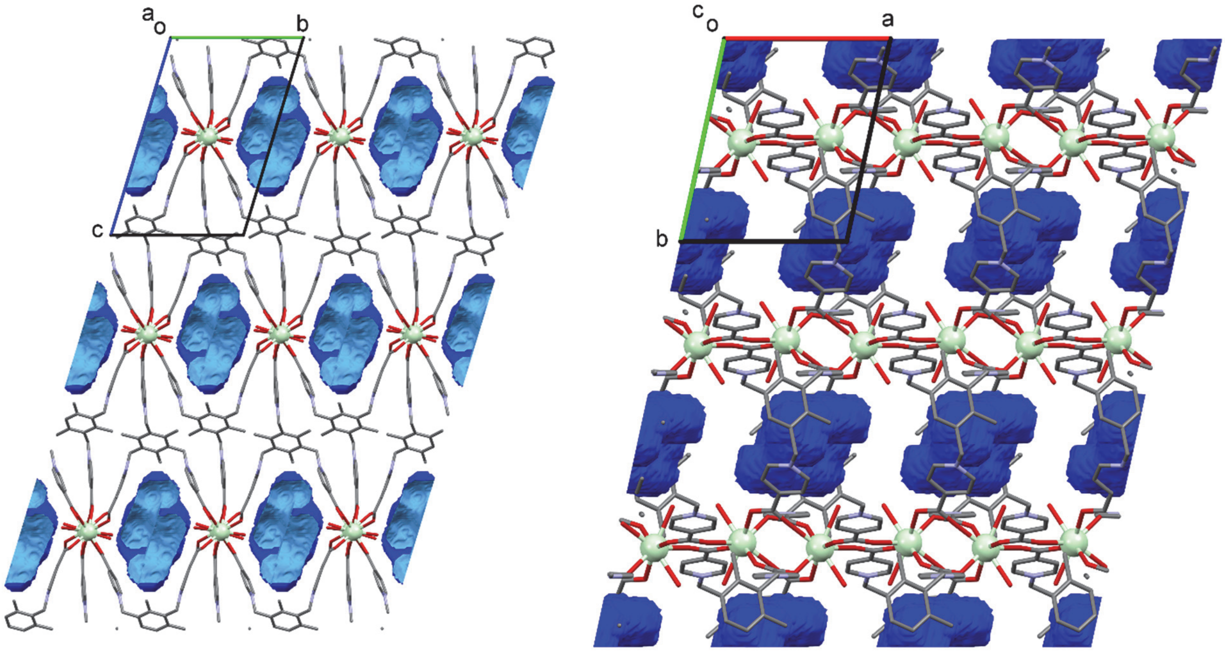

a) b)

Figure S29. Evacuated voids of **TTTPC NdBr$_2$OTf (vac)** viewed along crystallographic a) *a*-axis and b) *c*-axis (hydrogens, anions and non-metal-coordinated water molecules omitted for clarity, Mercury contact surface mapping with 1.2 Å probe and 0.2 Å grid).

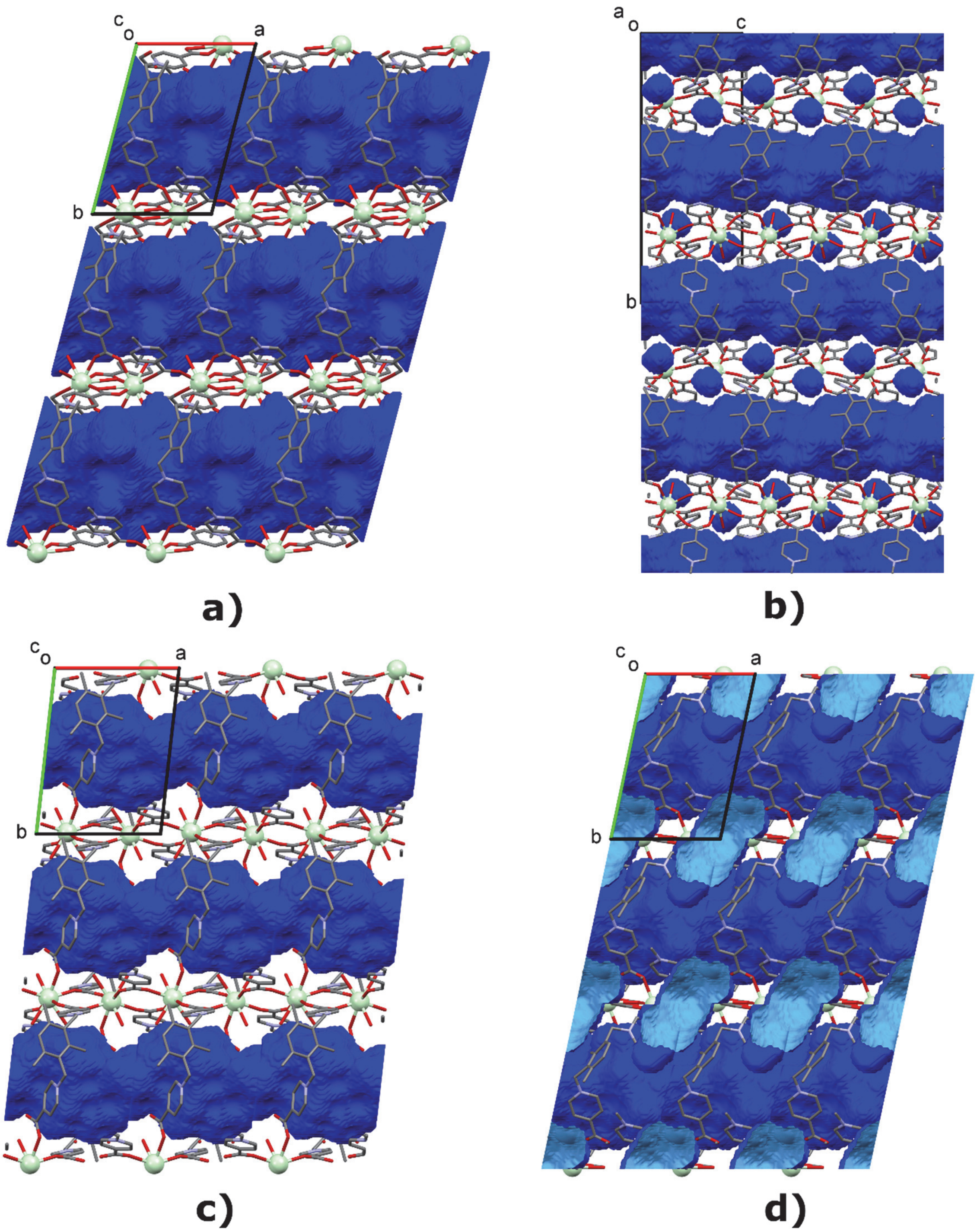

Figure S30. Water channels (side view) of a) **TTTPC NdBr$_2$OTf**, b) **TTTPC NdBr(OTf)$_2$**, c) **TTTPC Nd(OTf)$_3$** and d) **TTTPC NdBr$_2$OAc** (hydrogens, bromides and triflates omitted for clarity, Mercury contact surface mapping with 1.2 Å probe and 0.2 Å grid).

S4 VISUAL DECOMPOSITION STUDIES OF NETWORK SOLIDS

All network solids in the main text were visually inspected in a glass capillary tube using an uncalibrated melting point apparatus. All products exhibited a steady phase for over 280 °C temperatures until a gradual decomposition could be seen starting as an evolution of brown vapor that partially darkened the sample capillary inside the chamber. The products at this point also started to darken, but remained superficially crystalline (larger crystal faces remained visible and reflective). At the temperature of decomposition quoted below, the samples evolved some apparently gaseous products that bubbled and foamed the sample up along the capillary, settling finally into a brown toasted residue. **TTTPC NdBrOTf** mixture, surprisingly, did not end up foaming but gradually dried and burned to a brown residue, and therefore its decomposition temperature could not be recorded. After the measurement, condensed water and some product residue was seen on the walls of the cool capillary tube outside the heating chamber. Decomposition temperatures:

TTTPC $NdBr_3$: 337.9 °C

TTTPC $NdBr_2OTf$: 344.6 °C

TTTPC $NdBr_2OAc$: 332.4 °C

S5 THERMAL ANALYSIS RESULTS OF NETWORK SOLIDS

Thermogravimetric analysis results of all measured network solids show that at the beginning of the run there is a systematic event of solvent loss, as can be expected from the porous crystal structures. In contrast to results reported by Bag *et al.*[3], none of our samples exhibited a stepwise loss of solvent in temperatures significantly over 125 °C. Instead, after the solvent had been removed completely latest at 150 °C temperature, there was a stable phase until approximately 300 °C temperatures were reached. After this temperature, decomposition processes occurred, and the compounds lost most of their weight. The amount of inorganic matter (ash, metal salts) left after heating to 850 °C under nitrogen atmosphere was approximately 40 % or less. In Figure S31, partial thermogravimetric analysis curves of dry **TTTPC $NdBr_3$**, **TTTPC $NdBr_2OTf$**, **TTTPC BrOTf** mixture and **TTTPC $NdBr_2OAc$** are displayed, measured under nitrogen atmosphere. Respectively in Figure S32, the partial curves of evacuated samples can be seen. Individual curves for each compound under different atmospheres can be seen in the following Figs. S33 - S40.

For **TTTPC $NdBr_3$** the solvent loss is complete at approximately 150 °C. The endothermic two-stage process and measured weight loss associated to the presumed complete loss of water for the dry sample is 15.96 % under air and 15.67 % under N_2, which correspond to approximately nine water molecules per one ligand molecule. For the evacuated sample, a similar one-stage endothermic process is seen under N_2 with an associated loss of 7.54 %, corresponding to approximately four molecules of water. Further on, the compound is stable until the temperature of approximately 300 °C is reached, where the decomposition takes place. The measured onset temperatures of this event are 307.3 °C and 300.1 °C for the dry sample under air and N_2 respectively, and for the evacuated sample under N_2, 296.7 °C. Overall, observed amounts of lost solvent are well in line with both crystallographic and elemental analysis results (see next section S6).

For **TTTPC $NdBr_2OTf$** the solvent is similarly completely removed by reaching the temperature of approximately 150 °C. Weight losses for dry samples are 12.07 % under air and 11.62 % under N_2, corresponding to approximately seven water molecules per ligand equivalent. For the evacuated sample under N_2, a 4.10 % loss is seen, corresponding to approximately two water molecules. Decomposition onsets for dry samples are measured 336.2 °C under air and 331.4 °C under N_2. For the evacuated sample, decomposition occurs at onset temperature of 328.9 °C under N_2. Observed solvent losses are in congruence with the obtained single crystal structure, but not as well with elemental analysis results. Powder diffraction also suggests that the bulk material does not consist of only **TTTPC $NdBr_2OTf$** but is a mixture similar to the following sample.

For the synthesized sample mixture (see section 2.3.3 in the main text) consisting of **TTTPC Nd(OTf)$_3$**, **NdBr$_2$OTf** and **NdBr(OTf)$_2$** (NdBrOTfMix for short), relatively similar thermogravimetric analysis curves were obtained as for the **TTTPC NdBr$_2$OTf**, with solvent losses of 10.76 % under air and 10.70 % under N_2 (complete at 150 °C) and decomposition processes beginning at onset temperatures of 338.4 °C and 326.1 °C respectively. For the evacuated sample under N_2, a solvent loss of 3.67 % was observed in completion at 160 °C, followed by the decomposition at onset temperature of 328.6 °C. The solvent losses are similarly, approximately seven molecules for dry samples, and two molecules for the evacuated sample. The mixture nature and characteristics similar to the previous sample are agreeably confirmed with powder diffraction and elemental analysis results.

Lastly, for **TTTPC NdBr$_2$OAc** the solvent loss is complete already by reaching 90 - 100 °C, deviating from the other compounds distinctly. The measured weight losses of 11.87 % under air and 11.73 % under N_2 with dry samples and 1.83 % with the evacuated sample correspond to approximately seven water molecules and one molecule of water respectively. Decomposition processes occur at onset temperatures of 312.6 °C under air and 318.8 °C under N_2 for the dry samples, and 318.0 °C for the evacuated sample under N_2. Here, only a minute discrepancy with elemental analysis results is observed with the evacuated sample, and as crystallography suggests, the water loss of the dry sample **TTTPC NdBr$_2$OAc (dry)** is spot on.

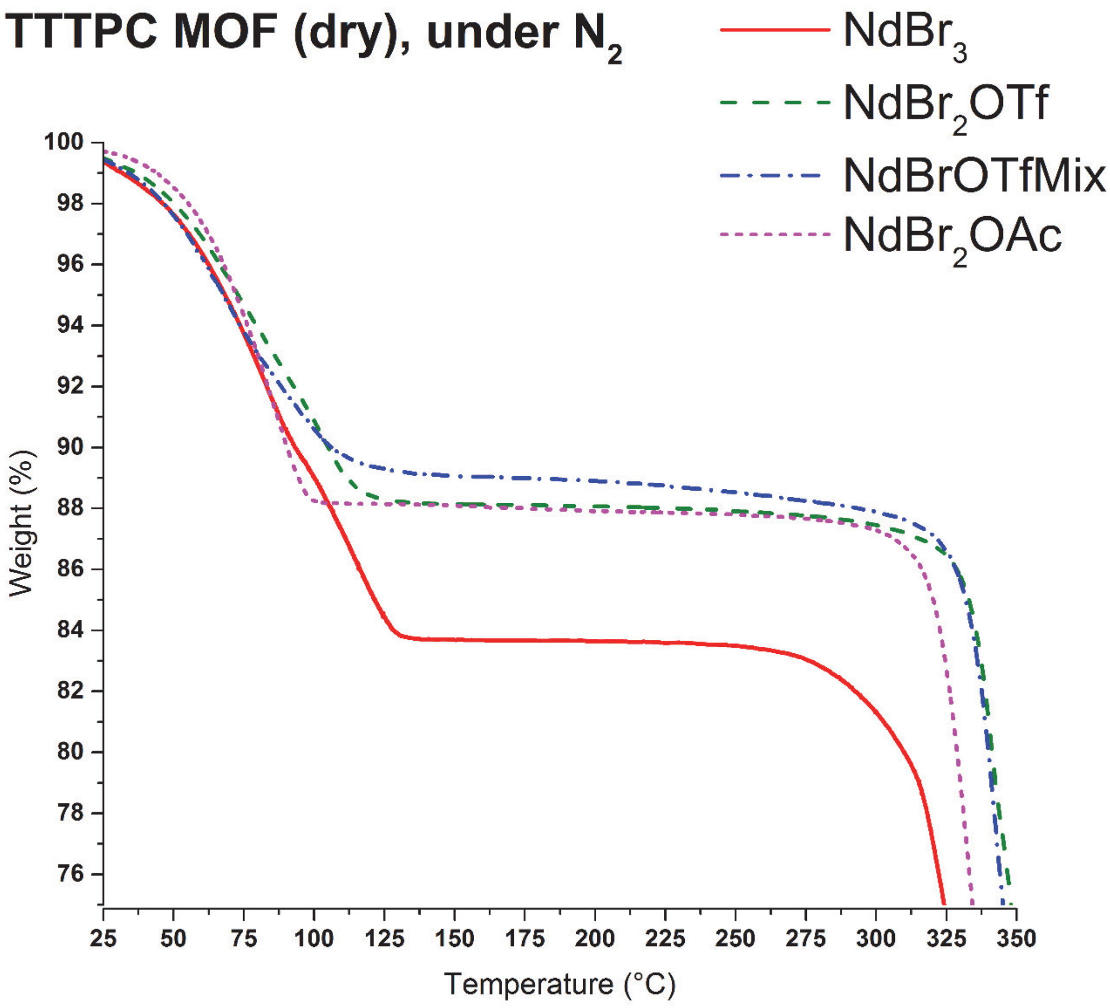

Figure S31. A portion of thermogravimetric analysis curves of dry, un-evacuated TTTPC network solids (**TTTPC NdBr$_3$** red, solid; **TTTPC NdBr$_2$OTf** green, dashed; **TTTPC BrOTf** mixture blue, dash-dot; **TTTPC NdBr$_2$OAc** magenta, short dash).

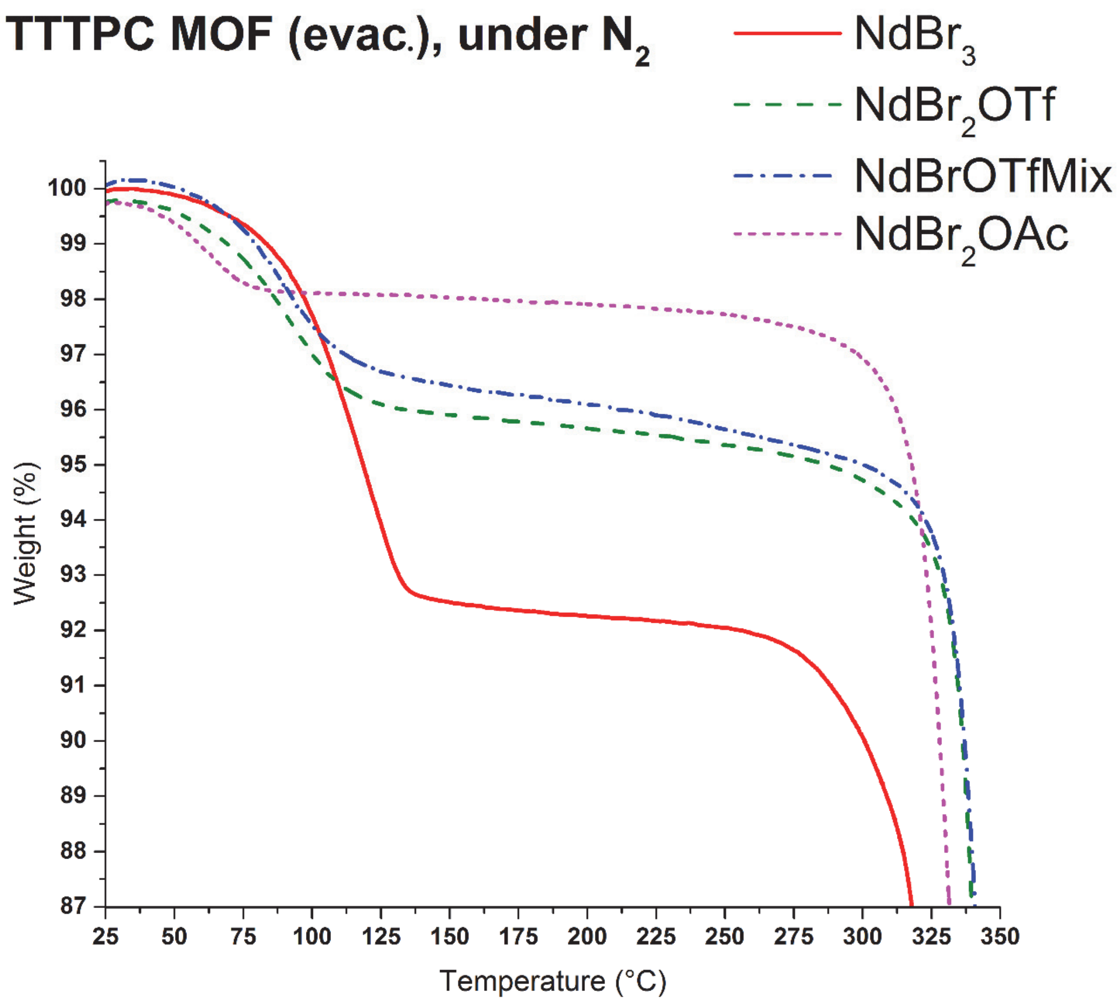

Figure S32. A portion of thermogravimetric analysis curves of evacuated TTTPC network solids (legend as in Fig. S31).

S5.1 TTTPC NdBr$_3$

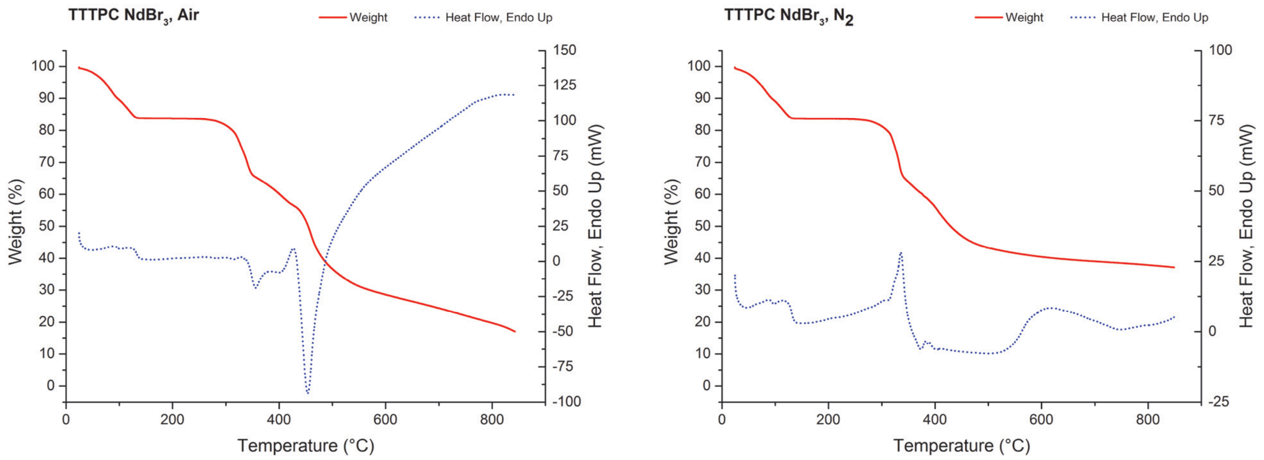

Figure S33. Thermal analysis curves of **TTTPC NdBr$_3$** under air (left) and nitrogen (right) atmospheres.

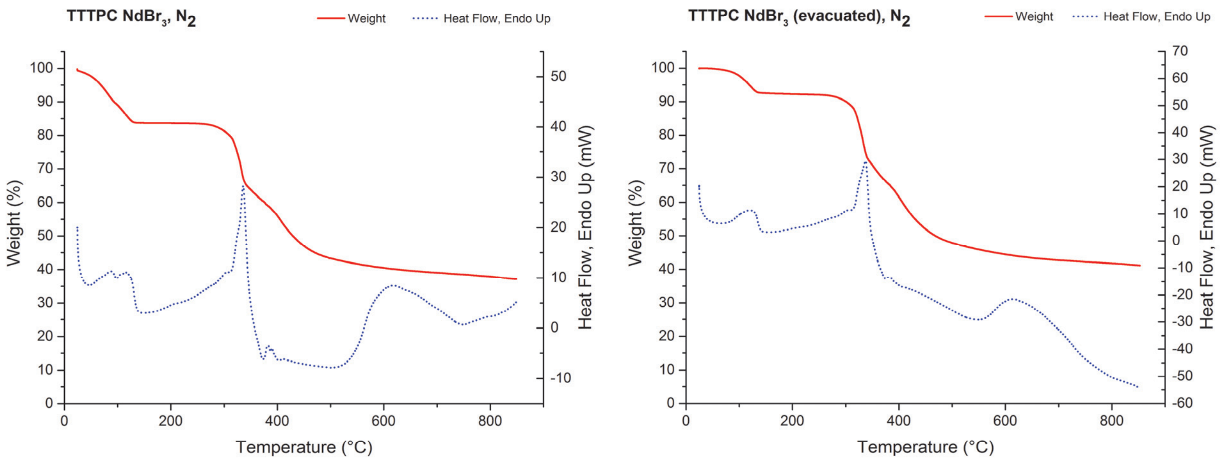

Figure S34. Thermal analysis curves of **TTTPC NdBr$_3$** under nitrogen atmosphere from fresh sample dried in a desiccator (left) and sample subjected to 1 x 10^{-6} bar vacuum (right).

S5.2 TTTPC NdBr$_2$OTf

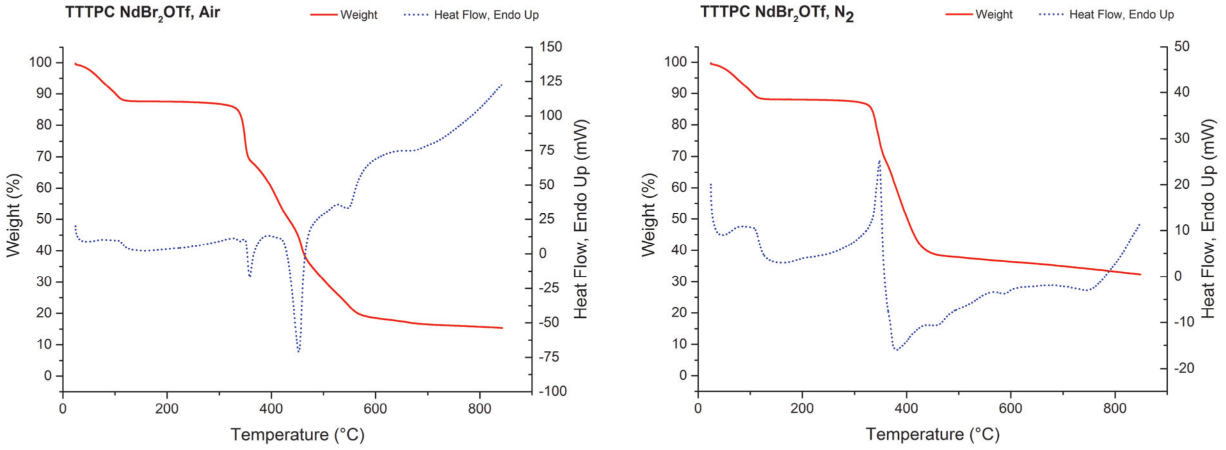

Figure S35. Thermal analysis curves of **TTTPC NdBr$_2$OTf** under air (left) and nitrogen (right) atmospheres.

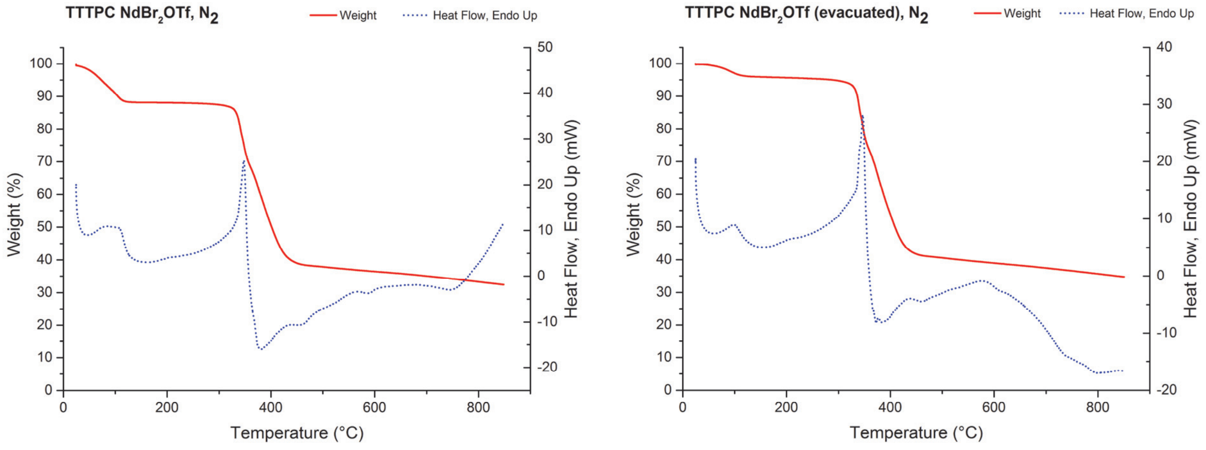

Figure S36. Thermal analysis curves of **TTTPC NdBr$_2$OTf** under nitrogen atmosphere from fresh sample dried in a desiccator (left) and sample subjected to 1 x 10^{-6} bar vacuum (right).

S5.3 TTTPC NdBrOTfMix

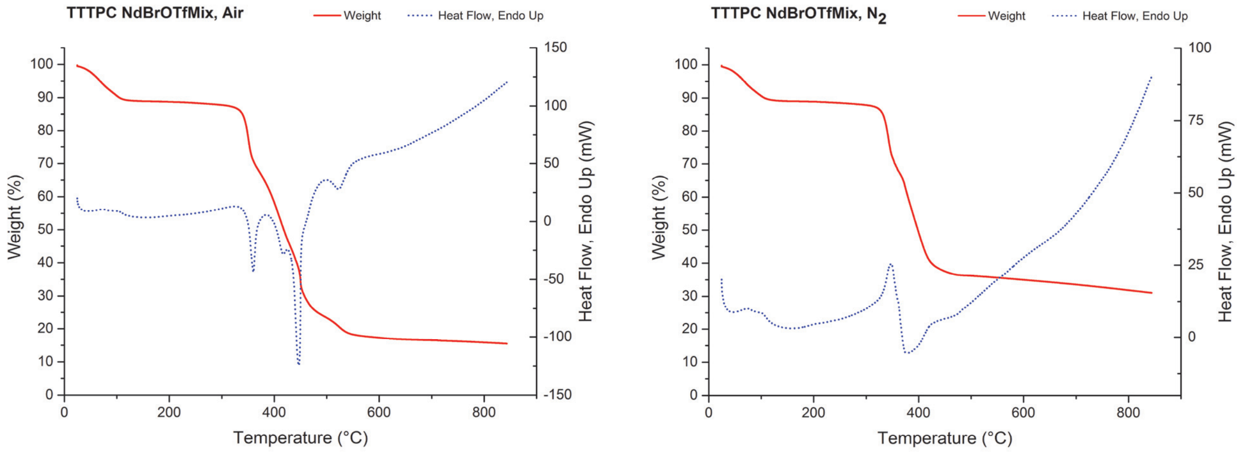

Figure S37. Thermal analysis curves of **TTTPC NdBrOTf** mixture under air (left) and nitrogen (right) atmospheres.

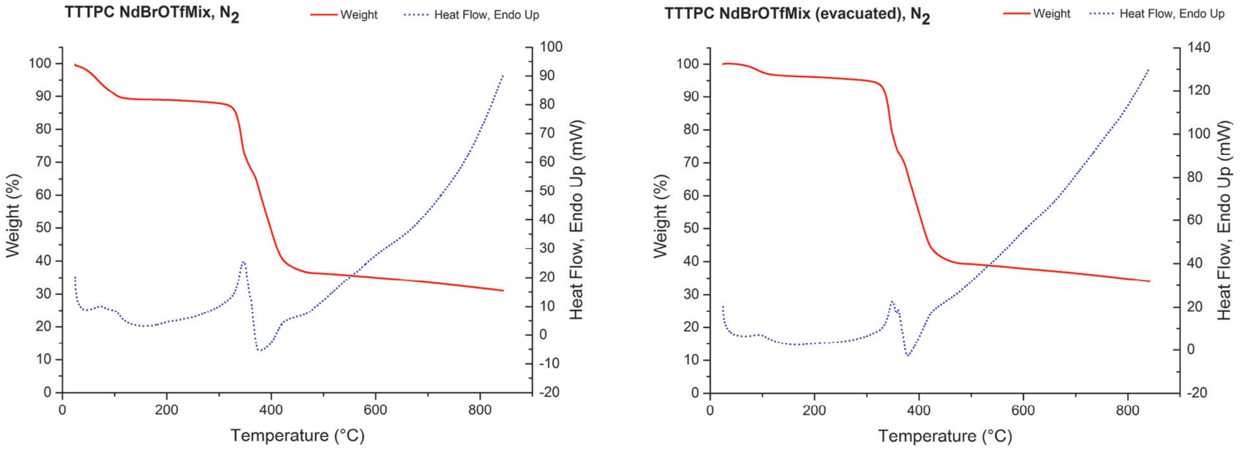

Figure S38. Thermal analysis curves of **TTTPC NdBrOTf** mixture under nitrogen atmosphere from fresh sample dried in a desiccator (left) and sample subjected to 1 x 10^{-6} bar vacuum (right).

S5.4 TTTPC $NdBr_2OAc$

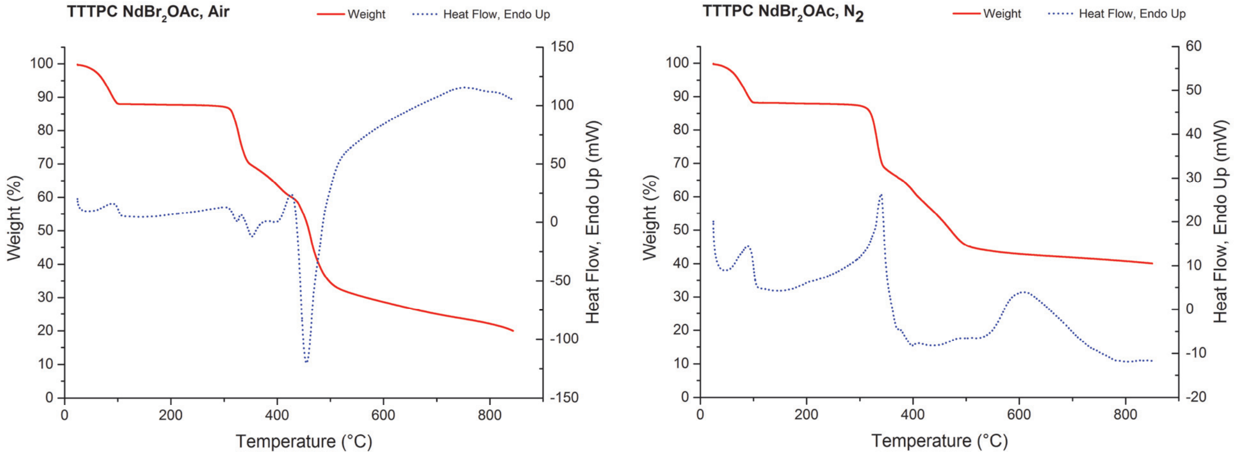

Figure S39. Thermal analysis curves of **TTTPC $NdBr_2OAc$** under air (left) and nitrogen (right) atmospheres.

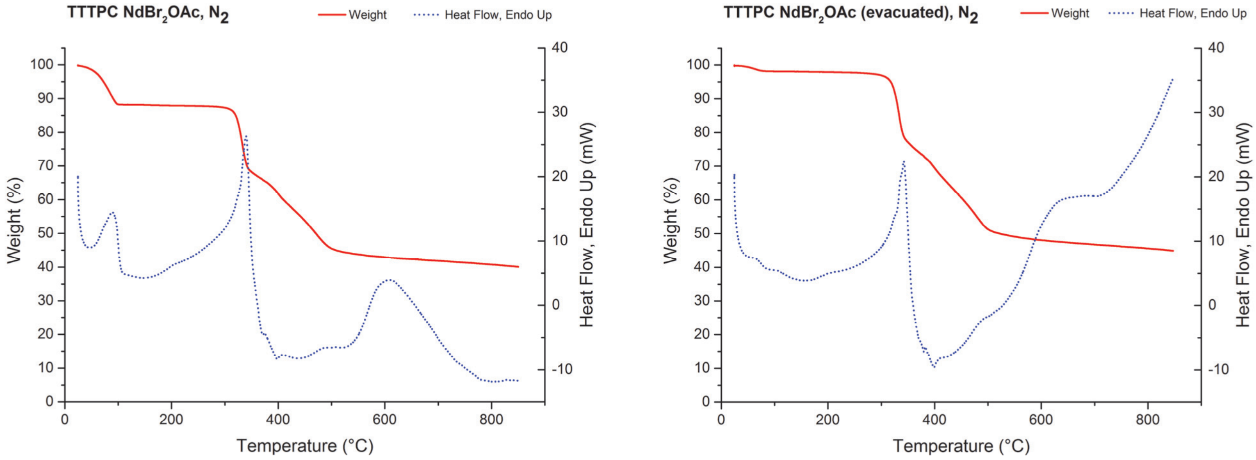

Figure S40. Thermal analysis curves of **TTTPC NdBr$_2$OAc** under nitrogen atmosphere from fresh sample dried in a desiccator (left) and sample subjected to 1 x 10^{-6} bar vacuum (right).

S6 ELEMENTAL ANALYSIS RESULTS OF NETWORK SOLIDS

All network solid samples were evacuated for 3 days in 1x10^{-6} bar pressure for 3 days prior to the CHN analysis. Neodymium containing products were initially pink or purple in color, but after evacuation their colors had faded to colorless, or in the case of the tribromide, to permanent pale yellow color. Different light source (natural or fluorescent) didn't change the outlook of the evacuated products.

Tribromide and dibromide-acetate systems were most congruent with the results from thermogravimetric analyses, but the mixed bromide-triflate systems were somewhat anomalous. This is most likely due to the samples being non-homogeneous, and containing more than one species of compounds, as is stated in the main text. The results from both **TTTPC NdBr$_2$OTf** and **TTTPC NdBrOTfMix** samples are overall closer to the **TTTPC NdBr$_2$OTf** compound ideally, if the amount of water is adjusted to four equivalents. If the water content is adjusted to the expected two equivalents, an ideal composition close to **TTTPC NdBr(OTf)$_2$** must be had, to better reflect the obtained experimental values.

In the following calculations, TTTPC, $C_{30}H_{27}N_3O_6$

S6.1 TTTPC NdBr$_3$

Found (%): C, 36.34; H 3.64; N 4.57.
Calculated compound composition of TTTPC$_1$Nd$_1$Br$_3$(H$_2$O)$_{4.5}$ requires (%): C 36.38; H 3.66; N 4.24.

S6.2 TTTPC NdBr$_2$OTf

Found (%): C 35.66; H 3.32; N 4.12.
Calculated compound composition of TTTPC$_1$Nd$_1$Br$_2$(OTf)$_1$(H$_2$O)$_4$ requires (%): C 35.44; H3.36; N 4.00.
Calculated compound composition of TTTPC$_1$Nd$_1$Br$_1$(OTf)$_2$(H$_2$O)$_2$ requires (%): C 35.46; H2.88; N 3.88.

S6.3 TTTPC NdBrOTfMix

Found (%): C 35.30; H 3.25; N 3.97.
Calculated compound composition of TTTPC$_1$Nd$_1$Br$_2$(OTf)$_1$(H$_2$O)$_4$ requires (%): C 35.44; H3.36; N 4.00.
Calculated compound composition of TTTPC$_1$Nd$_1$Br$_1$(OTf)$_2$(H$_2$O)$_2$ requires (%): C 35.46; H2.88; N 3.88.

S6.4 TTTPC NdBr$_2$OAc

Found (%): C 41.53; H 3.72; N 4.58.
Calculated compound composition of TTTPC$_1$Nd$_1$Br$_2$(OAc)$_1$(H$_2$O)$_2$ requires (%): C 41.57; H 3.71; N 4.54.

S7 IR SPECTRA OF NETWORK SOLIDS

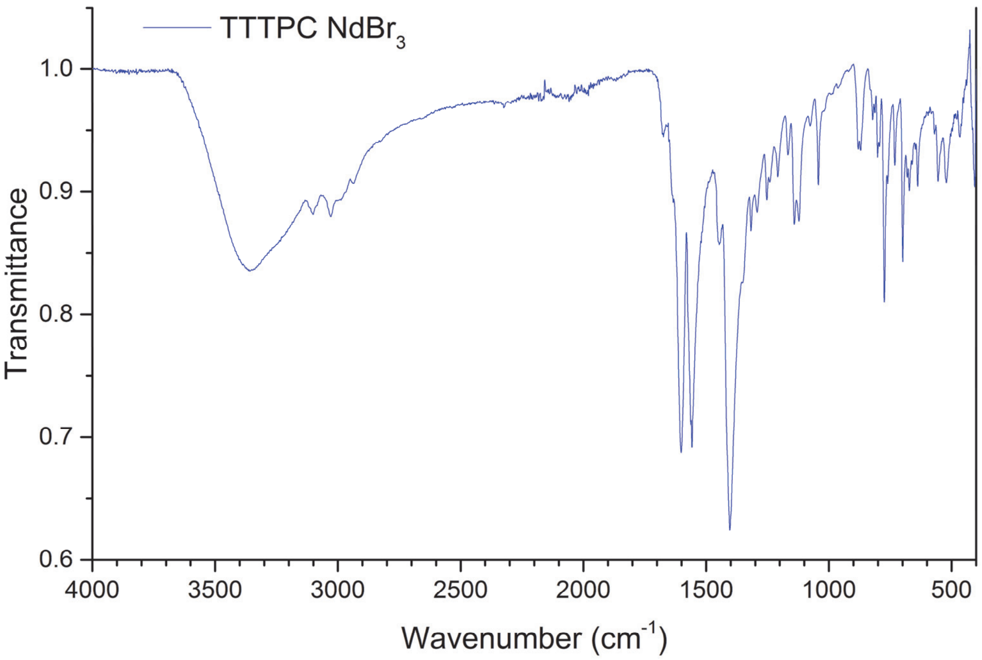

Figure S41. FT-IR spectrum of **TTTPC NdBr$_3$**. Peaks at cm^{-1}: 405.97;465.94;521.13;555.39;638.21;672.19;680.39;699.01;731.40;760.24;774.00;801.47;870.53;880.39; 1042.65;1121.76;1140.82;1166.80;1208.00;1252.68;1291.98;1317.29;1403.44;1446.62;1557.73;1601.67; 1673.93;3029.01;3100.93;3358.23.

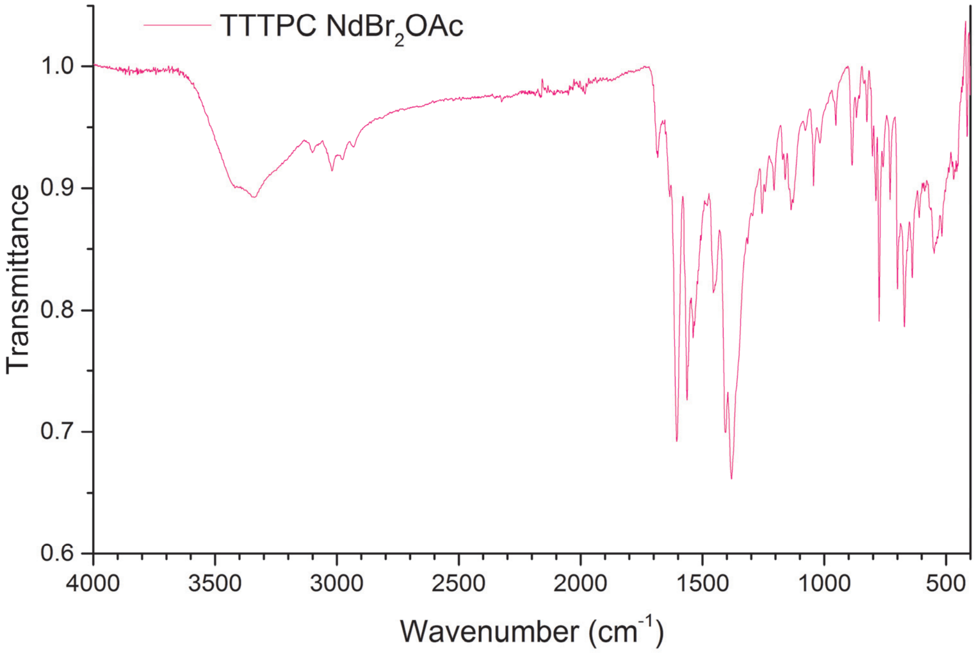

Figure S42. FT-IR spectrum of **TTTPC NdBr$_2$OAc**. Peaks at cm^{-1}: 413.42;455.75;468.99;517.39;548.76;587.82;610.27;638.95;670.99;699.59;729.84;758.59;774.85;788.08; 802.25;825.11;867.97;885.93;952.62;1018.01;1044.06;1077.83;1136.14;1160.60;1206:02;1242.57;1255.45; 1380.82;1404.58;1455.08;1538.11;1563.17;1605.25;1634.36;1683.26;2933.61;2977.68;3020.29;3100.51; 3340.13.

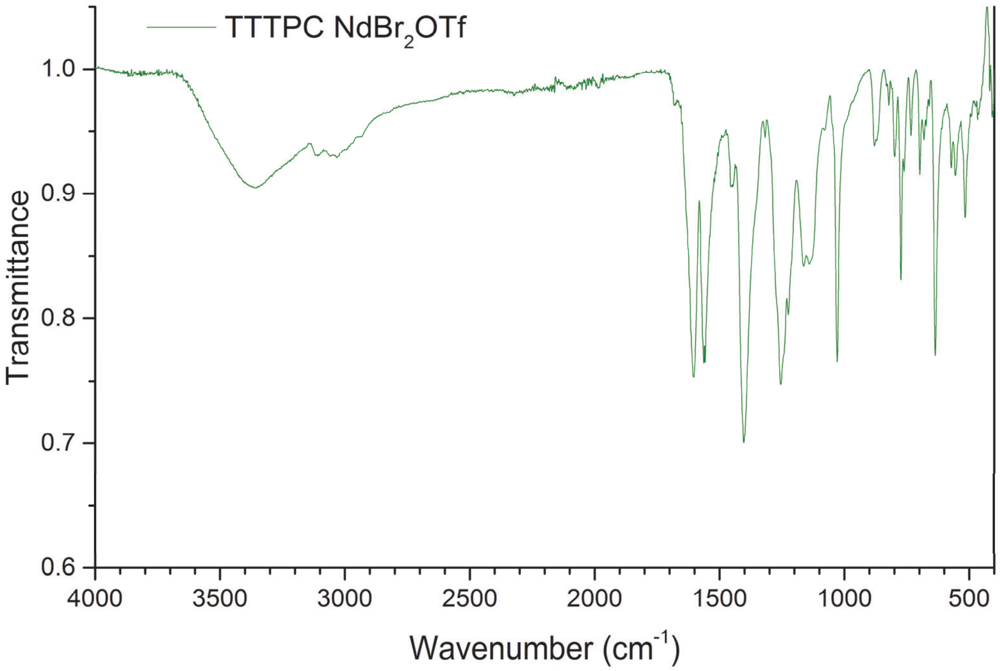

Figure S43. FT-IR spectrum of **TTTPC NdBr$_2$OTf**. Peaks at cm^{-1}: 407.99;466.82;516.47;556.19;571.93;636.15;681.34;697.94;733.07;760.61;773.59;798.76;821.90;879.43; 1028.40;1140.27;1162.83;1224.75;1254.92;1317.46;1403.02;1450.91;1557.74;1563.02;1602.73;3032.50; 3108.17;3354.35.

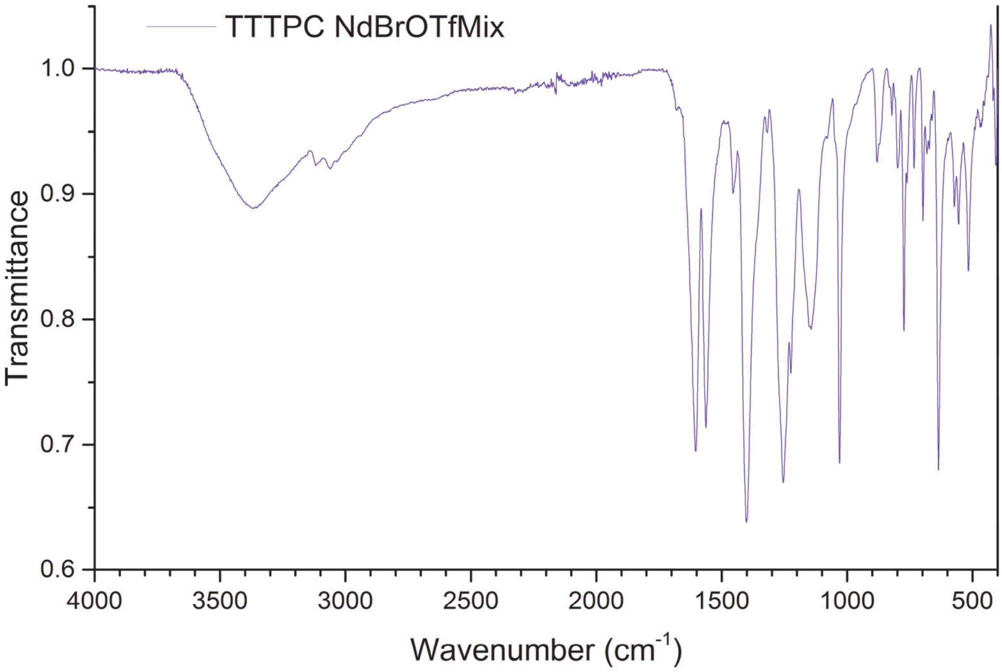

Figure S44. FT-IR spectrum of **TTTPC NdBrOTfMix**. Peaks at cm^{-1}: 407.14;469.43;516.41;555.29;572.52;635.81;672.36;682.16;697.67;733.16;761.25;773.57;798.70;821.64; 880.75;1030.29;1143.46;1224.40;1254.83;1317.98;1401.65;1454.94;1562.98;1603.84;3059.50;3118.53; 3371.22.

Both **TTTPC NdBr$_2$OTf** and **NdBrOTfMix** spectra are very similar, differing only in minute details (*eg*. peaks at 1140 - 1150 cm^{-1}).

S8 X-RAY POWDER DIFFRACTION PATTERNS OF NETWORK SOLIDS AND DISCUSSION

The powder diffraction pattern of **TTTPC $NdBr_3$** (Fig. S45) is well in line with the simulated pattern suggesting phase purity in the bulk product. Some minor peak shifts can be attributed to the unit cell dimension changes during drying and thermal expansion of the sample, because of different measurement conditions (measured powder sample dry @ RT, simulated single crystal sample @ 120 K). However, these shifts are not as prominent as observed with other samples discussed below, that lose more water when dry. Peak intensity discrepancies between the measured and simulated pattern can likely be attributed to preferred orientation effects in the prepared sample.

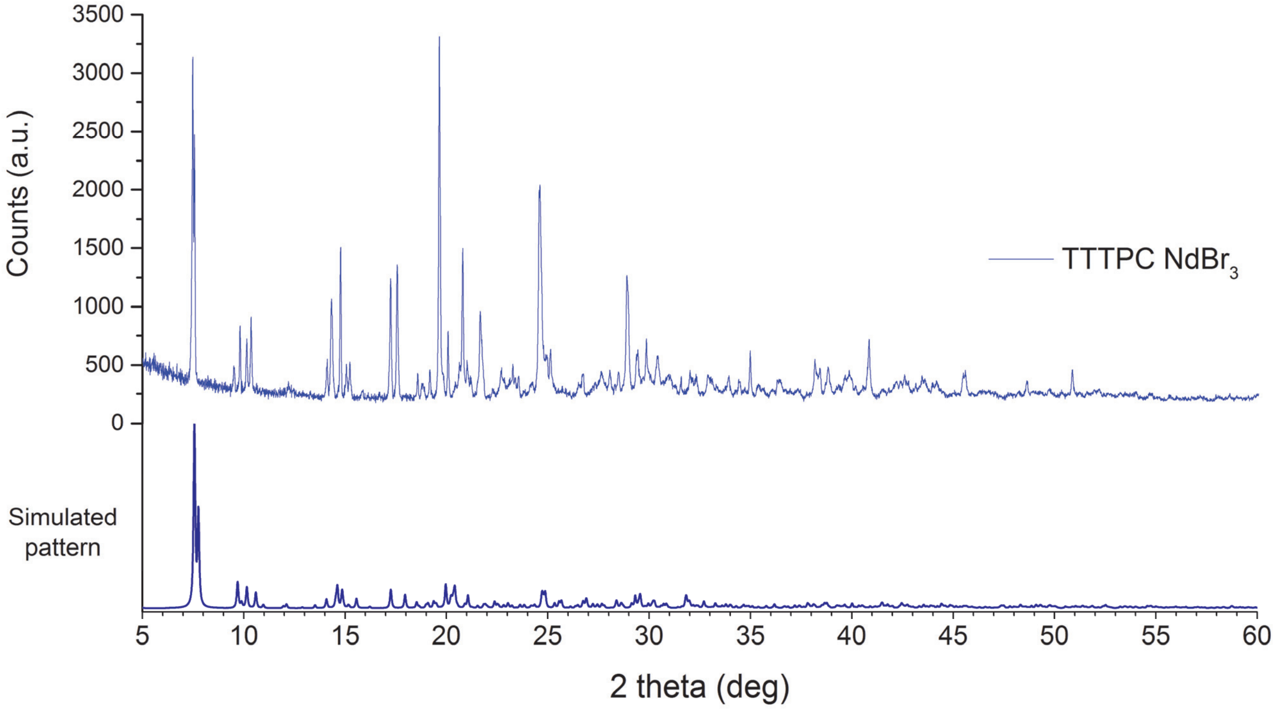

Figure S45. Measured and simulated powder diffraction patterns of **TTTPC $NdBr_3$**.

The two relatable samples, **TTTPC $NdBr_2OTf$** and **TTTPC NdBrOTfMix** can be confirmed without hesitation as mixtures of products, for the powder patterns contain separate identifiable peaks from the simulated patterns of individual components (Figs. S46 and S47). A prominent peak shift towards higher angle in the measured pattern is related to unit cell dimension changes from the fresh sample to dry, especially in the *b* direction, *e.g.* the first visible large peak belongs to the reflections corresponding to the (010) and (01-1) planes in the case of **TTTPC $NdBr_2OTf$** and **TTTPC $Nd(OTf)_3$**. The underlying pattern of monoclinic **TTTPC $NdBr(OTf)_2$** seems rather unaffected by this phenomenon probably due to the different topology and crystal system, so that the observable low angle peaks are visible where they are expected. The dynamic nature of these triclinic systems is thus an observable trait. Due to unoptimized conditions and for it was not the original intention of this work, further attempts to obtain single phase samples and quantize the aforementioned phenomena were not conducted.

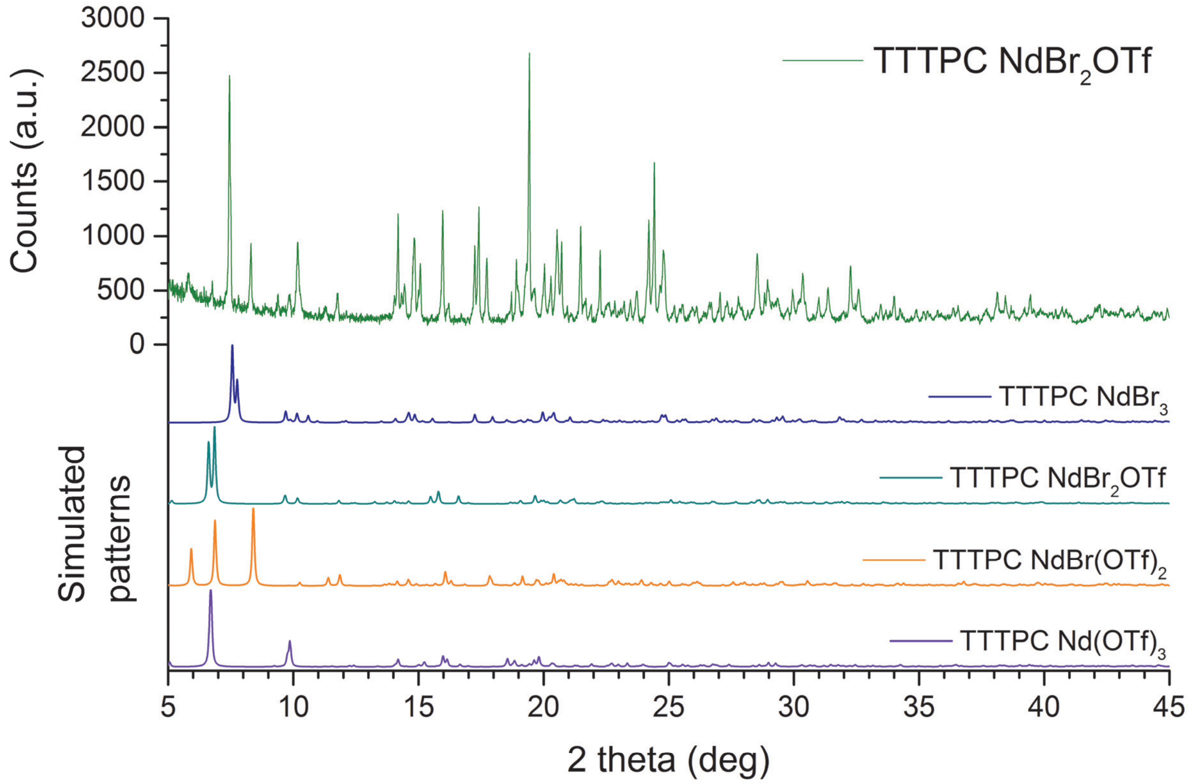

Figure S46. Measured powder diffraction pattern of **TTTPC NdBr₂OTf** bulk sample with simulated patterns of the Br/OTf series for comparisons. The un-optimized bulk sample as described above is a mixture of products.

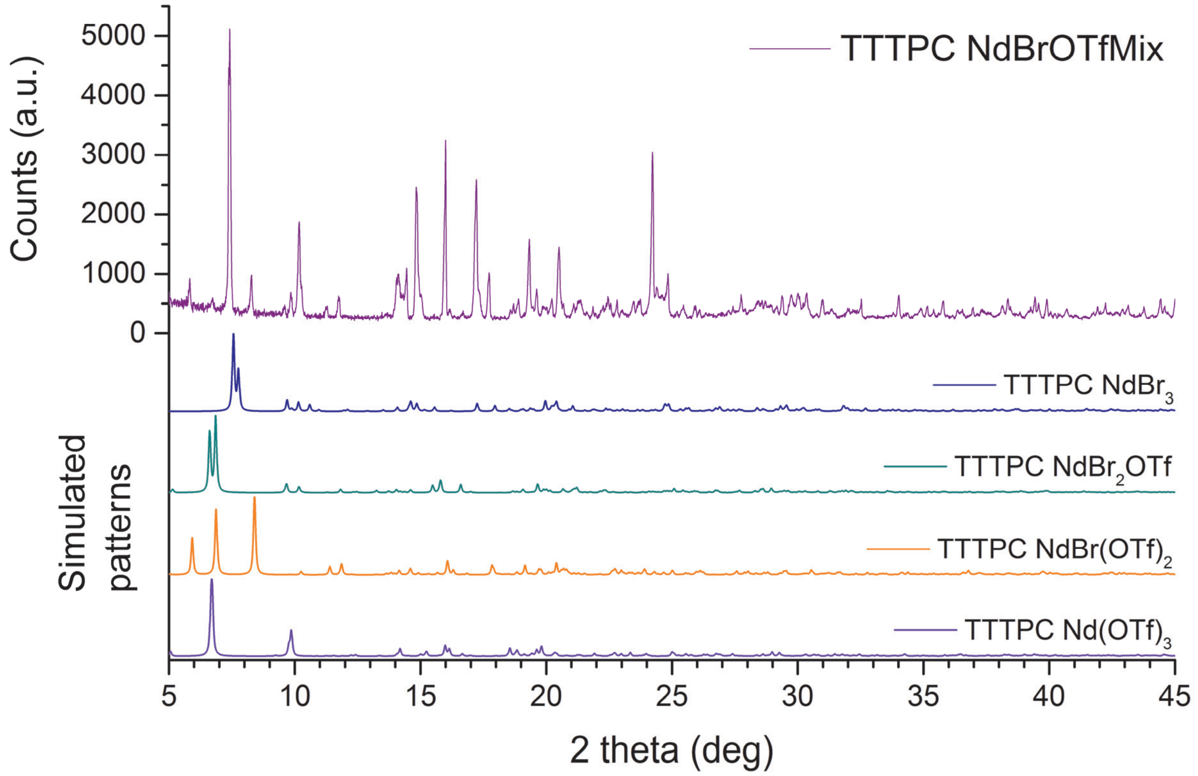

Figure S47. Measured powder diffraction pattern of **TTTPC NdBrOTfMix** bulk sample with simulated patterns of the Br/OTf series for comparisons. The un-optimized bulk sample is also a mixture of products, and differs from **TTTPC NdBr2OTf** by having some stronger peaks.

TTTPC $NdBr_2OAc$ displays an interesting characteristic between the fresh and dry structure, that the two structures are not identical. Instead, as single crystal data (sections 3.1 and 3.3 in the main text) show, the fresh 2D polymer crystal structure changes, resulting in the dry structure that resembles other 3D network solids with ligand connectivity and anion distribution, but with no water in the coordination sphere of the metal. This phenomenon has been recorded using powder diffraction as a series of six minute scans taken from a sample in ambient conditions (Figure S48). The first run displays a pattern that represents the **TTTPC $NdBr_2OAc$** structure in its pure form, and a gradual change in this pattern is obvious as the measurement progresses in run 2, where a transitional pattern can be seen forming from overlapping reflections originating from the structure of **TTTPC $NdBr_2OAc$ (dry)**. Notable are the rapid disappearances and shifts of peaks at 2Θ positions of 6.82°, 12.35°, 18.79° and 25.50° that are the strongest peaks in the initial pattern. In run 3, the final pattern is already visible, and ultimately there is little to no change between runs 4 and 5. In the resulting pattern, new strong peaks *e.g.* at positions of 7.65°, 14.50°, 17.25°, 17.75° and 24.66° are not visible in the initial pattern.

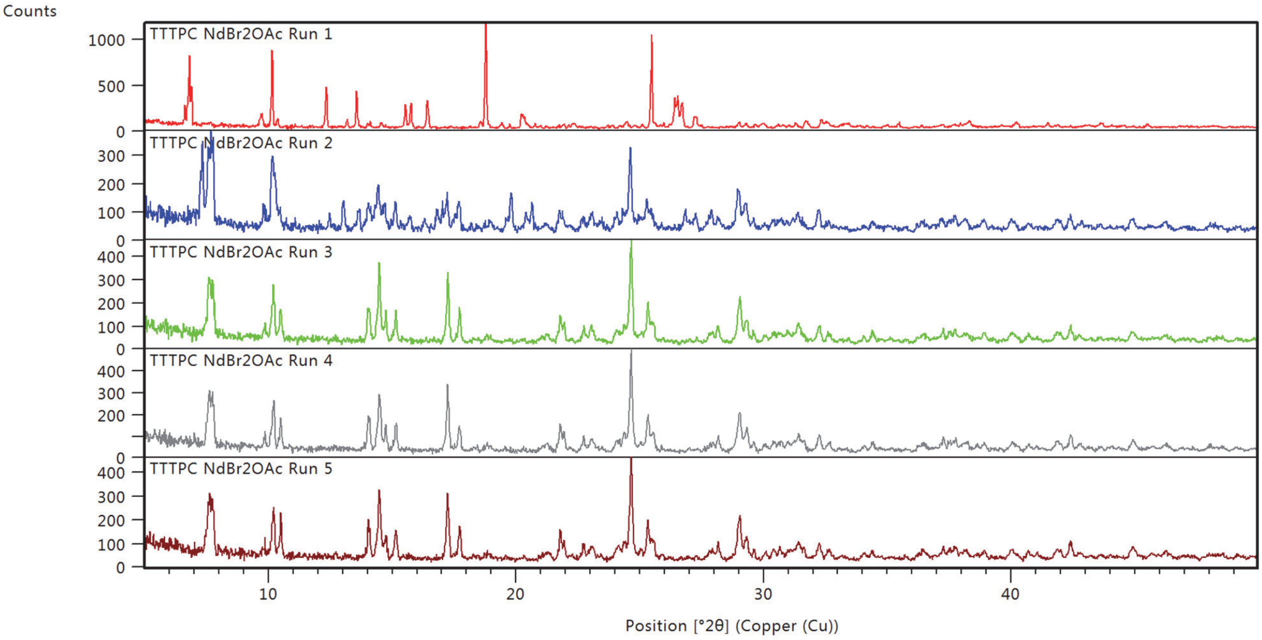

Figure S48. Powder diffraction patterns taken repeatedly from a single sample of fresh **TTTPC $NdBr_2OAc$**, that can be seen transforming to **TTTPC $NdBr_2OAc$ (dry)**.

The transformation from one crystal structure to another was recorded also using a Kapton sealed sample of **TTTPC $NdBr_2OAc$** that was left standing for 24 h in its intact sample holder. Diffraction patterns of the initial state and end state can be seen in Figures S49 and S50 with simulated patterns for comparison from single crystal structures of the fresh and dry structures. Intensity of some peaks is greatly exaggerated compared to the simulated pattern most likely because of orientation effects, for the sample was prepared quickly without homogenization to capture the fresh pattern, and the rod-like crystals were most likely aligned in an ordered manner. The measured and simulated patterns match reasonably well, although some peak positions are slightly out of place due to temperature effects, as discussed above. It is also justified to assume this phenomenon to be a single phase transformation, for no significant peaks are identical in both initial and end state patterns, suggesting a true single crystal to single crystal transformation of the bulk material. Isolating a single crystal and drying it in a controlled environment would be the next step to confirm this result, but that was unfortunately beyond this work.

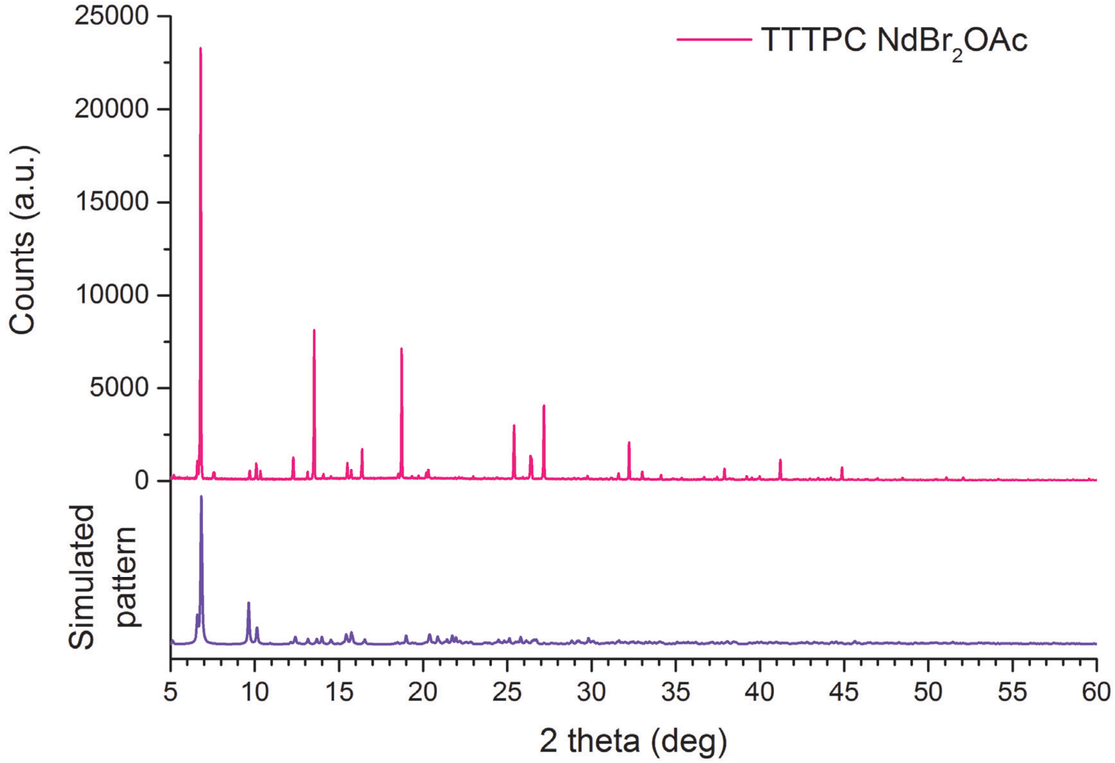

Fig. S49. Measured and simulated initial state powder diffraction patterns of fresh **TTTPC NdBr$_2$OAc.**

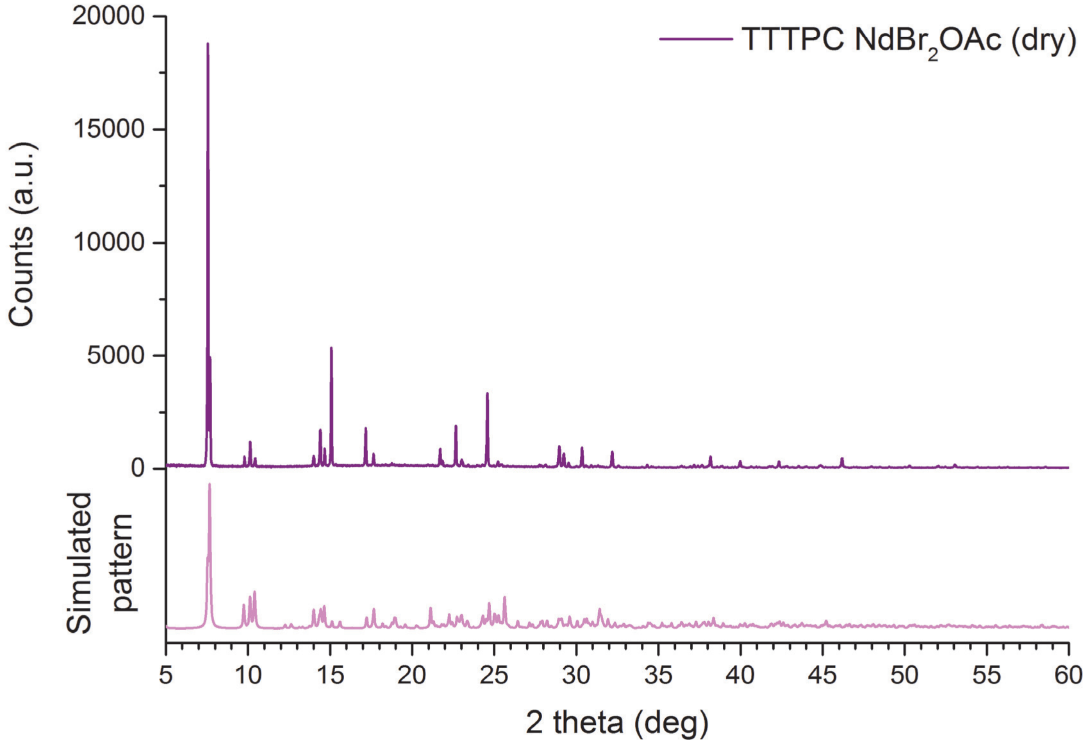

Fig. S50. Measured and simulated end state powder diffraction patterns of **TTTPC NdBr$_2$OAc (dry)**.

S9 SEM IMAGING AND EDX ANALYSES OF NETWORK SOLIDS AND DISCUSSION

Scanning electron microscopy (SEM) images were acquired to ascertain bulk material consistency in terms of crystallinity, resistance to evacuation process and following state of possible erosion, as well as to examine overall crystal morphology. Samples had to be gold coated to prevent excessive particle charge build-up and ejection to the microscope chamber, but despite the coating, most of the sample particles were still clearly shaking and moving during the measurements under the electron beam.

TTTPC $NdBr_3$ displayed the most severe crystal degradation (Fig. S51) and the bulk material had very few large crystals left intact, as most of them had been reduced to a fine microcrystalline powder instead. Crystal morphology could not be well examined for the crystals were not properly defined, but they were overall rather irregular in shape. This habit was noticed also when searching for a suitable crystal for single crystal experiments, as firstly a good clear well-faceted crystal was rather difficult to find, and secondly upon keeping the crystals for extended periods outside mother liquor, some of them could be seen degrading even under oil within a time period of a few hours. **TTTPC $NdBr_2OTf$** and **TTTPC NdBrOTfMix** were generally much more intact with clearly visible crystal faces among the bulk, but with obvious eroded material in the midst of the intact crystals as well. Block-like crystals were identified that were presumably **TTTPC $NdBr_2OTf$** and/or **TTTPC $Nd(OTf)_3$**, but plate-like crystals (presumably **TTTPC $NdBr(OTf)_2$**) were seen as well (Figs. S52 - S55). Even after evacuation, solid crystals well suitable for possible single crystal experiments in the size range of 50-200 µm could be seen. Overall bulk material morphology was similar in both of these samples. **TTTPC $NdBr_2OAc$** bulk (Fig. S56) was consistently reduced to crystalline particles that were mostly irregular, but some clearly plate-like and not too large (most less than 100 µm). A large number of crystals displayed visible cracks that were most likely the result of drying under vacuum. However, crystal faces could still be observed, and the material was not as finely divided as **TTTPC $NdBr_3$** bulk.

EDX spectra of the four main samples were measured from different selected crystals based on their outlook. Table S18 summarizes the obtained elemental analysis results and Fig. S57 the respective crystals. Analysis results are somewhat inconclusive, for none of the crystals compared well to their theoretical elemental analysis compositions calculated from the single crystal structures. Generally, carbon content is approximately 10-20 % lower than expected in all samples and neodymium content varies erratically, even though it should be fairly constant (considering all systems have the same ligand-to-metal ratio). Similar uncertainties can be found from other elemental results, as well, and thus the results should be considered semiquantitative at most, for no standardization was used. Most expected elements were, however, fairly reliably detected (or lacked detection) from samples of expected composition.

Table S18. Elemental analysis results from EDX. Results are normalized weight percentages (w-%) to a total of 100 w-%, with a fixed hydrogen content of 3 w-% (*) estimated from single crystal structures. Not detected (n.d.) elements account for 0 w-% in the calculation.

Sample	**$NdBr_3$**	**$NdBr_2OTf$**	**$NdBr_2OTf$**	**NdBrOTfMix**	**NdBrOTfMix**	**NdBrOTfMix**	**$NdBr_2OAc$**
Crystal (Fig. S57)	irregular (a)	plate (b)	irregular (c)	block (d)	plate (e)	prism (f)	plate (g)
C	17.09	20.54	22.86	21.00	19.17	16.15	25.39
N	6.50	n.d.	10.55	5.60	4.92	5.15	5.03
O	8.23	15.34	20.53	13.51	14.08	9.78	13.12
F	n.d.	17.64	21.09	12.81	22.05	9.15	n.d.
S	n.d.	6.58	2.01	4.34	5.96	5.16	n.d.
Br	41.97	15.73	13.82	19.85	14.10	28.86	22.89
Nd	23.21	21.17	6.13	19.89	16.72	22.76	30.57
H (*)	3.00	3.00	3.00	3.00	3.00	3.00	3.00

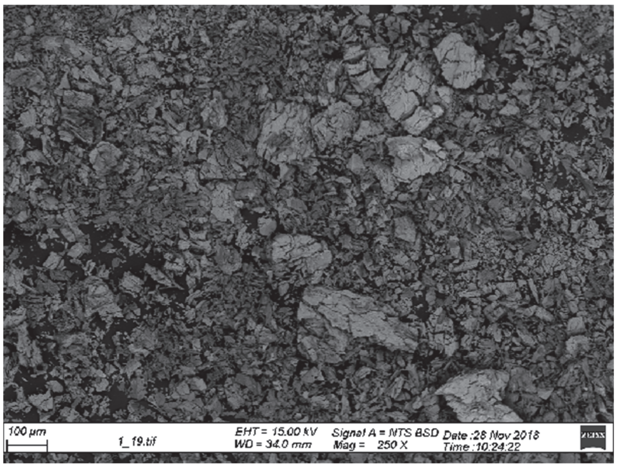

Figure S51. SEM image of **TTTPC NdBr$_3$** bulk material.

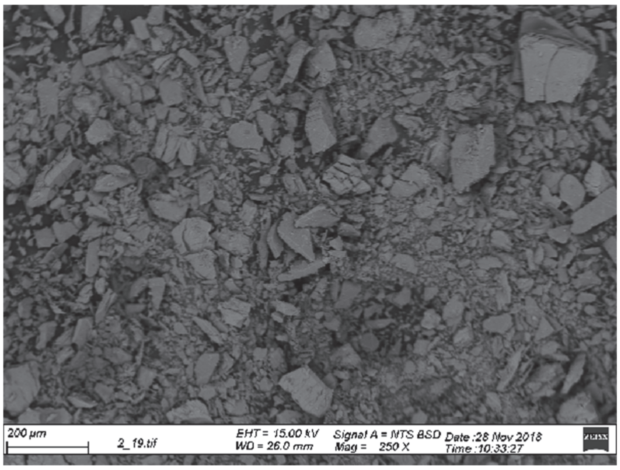

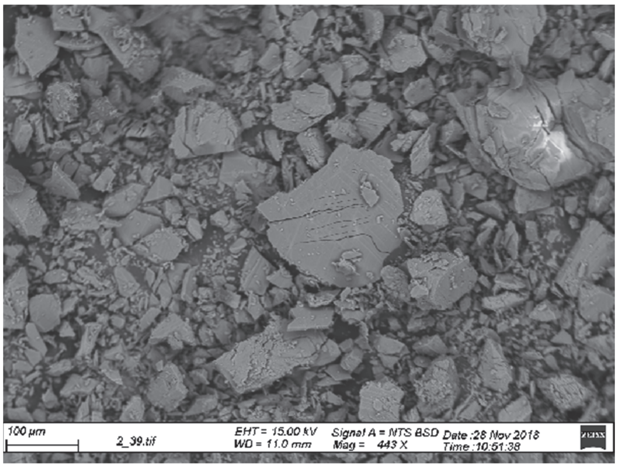

Figure S52 (left). SEM image of **TTTPC NdBr$_2$OTf** bulk material.

Figure S53 (right). Close-up SEM image of **TTTPC NdBr$_2$OTf** bulk material, showing the platelike crystal (most likely corresponding to **TTTPC NdBr(OTf)$_2$** structure) in the middle, with visible damage (parallel cracks) induced by the EDX measurement (see Fig. S57 b).

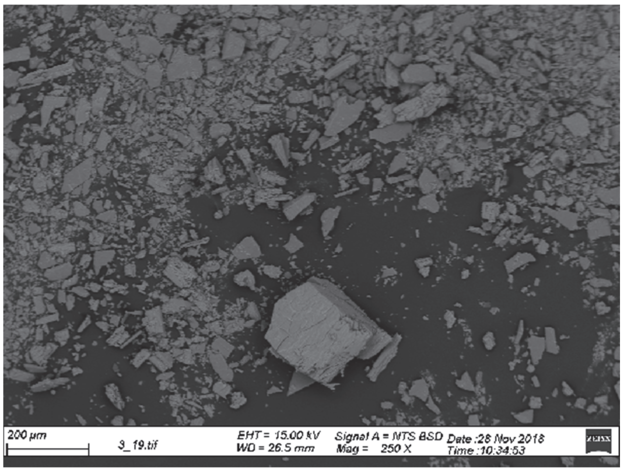

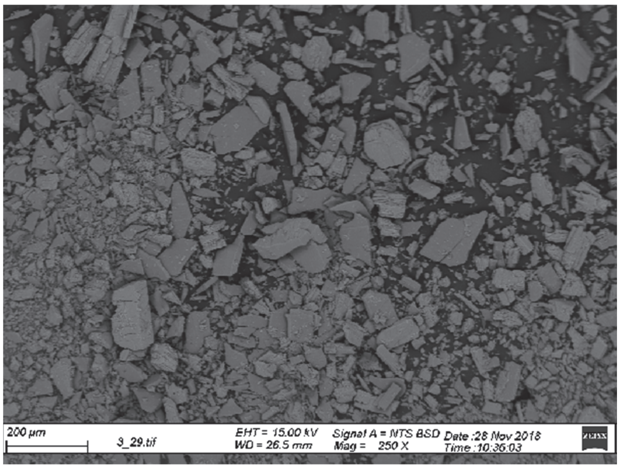

Figure S54 (left). SEM image of **TTTPC NdBrOTfMix** bulk material.

Figure S55 (right). SEM image of **TTTPC NdBrOTfMix** bulk material from a different sample region.

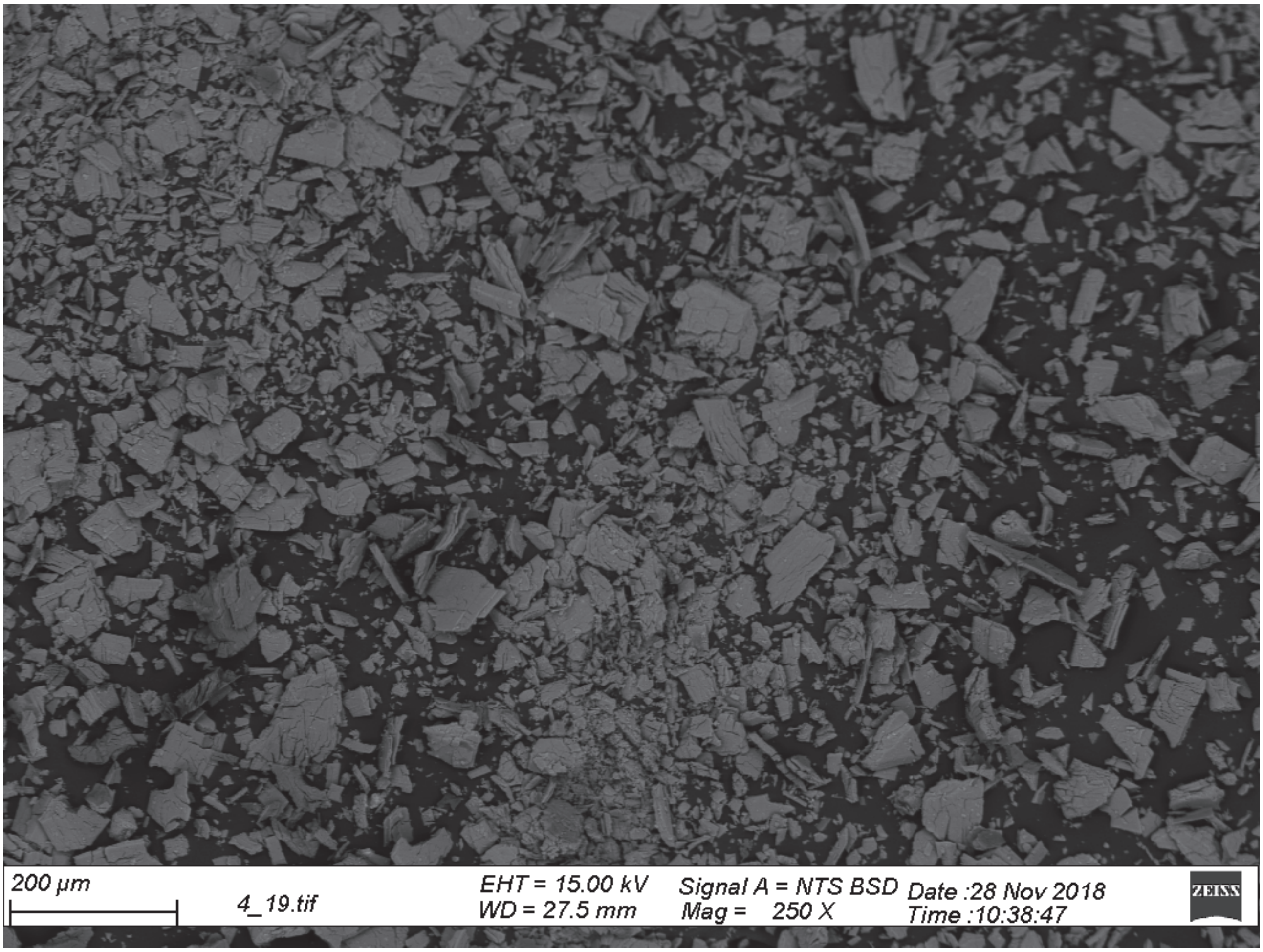

Figure S56. SEM image of **TTTPC NdBr$_2$OAc** bulk material.

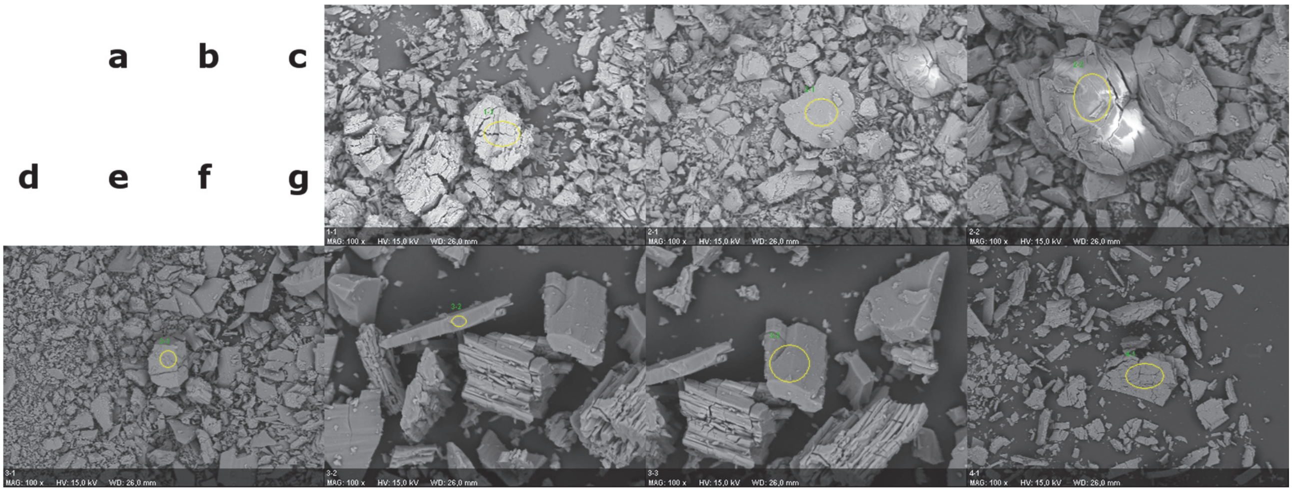

Figure S57. EDX measurement points (yellow dashed circle) in crystal samples. Refer to table S18 for sample information.

S10 SOLID STATE UV-VIS SPECTRA OF NETWORK SOLIDS AND DISCUSSION

Characteristic hypersensitive absorption peaks of Nd ion are at approximately 521, 578, and 806 nm positions.[4] According to Lambert *et al.*[5], four major peaks can be found in the wavelength region of 500-900 nm that are at approximately 531, 589, 749 and 809 nm positions (depending on the literature cited). The profile of these peaks changes upon the chemical environment of the ion, and they can be analyzed closely to extract structural information from compounds containing the metal in a certain coordination symmetry etc. However, this was beyond the scope of this paper, and only qualitative analysis was pursued in this regard.

Both desiccator dried and evacuated samples' solid state absorption spectra (Fig. S58) were measured and compared to each other in order to further elucidate the properties of Nd coordination networks presented in the main text. Organic ligand absorption was found beginning from approximately 400 nm and extending below the lower measurement limit. Roll-off of the absorption band was more prominent with the samples that had been evacuated, and especially with **TTTPC $NdBr_2OAc$**. Absorbance band edge was also in this case seen migrating from over 400 nm to below that. **TTTPC $NdBr_2OTf$** and **TTTPC NdBrOTfMix** spectra were very similar in both dry and evacuated samples with no apparent features to distinguish one from another without closer inspection. This is reasonable, for the samples are chemically very similar, and both are mixtures in nature, as have been discussed. **TTTPC $NdBr_3$**, Br-OTf mixtures and **TTTPC $NdBr_2OAc$** spectra were found generally very similar, but aforementioned neodymium peak shapes are slightly different between different species. Some distinguishable features were *e.g.* peak shoulders at 578 nm and different overlapping partial peak positions and intensities at 749 nm positions.

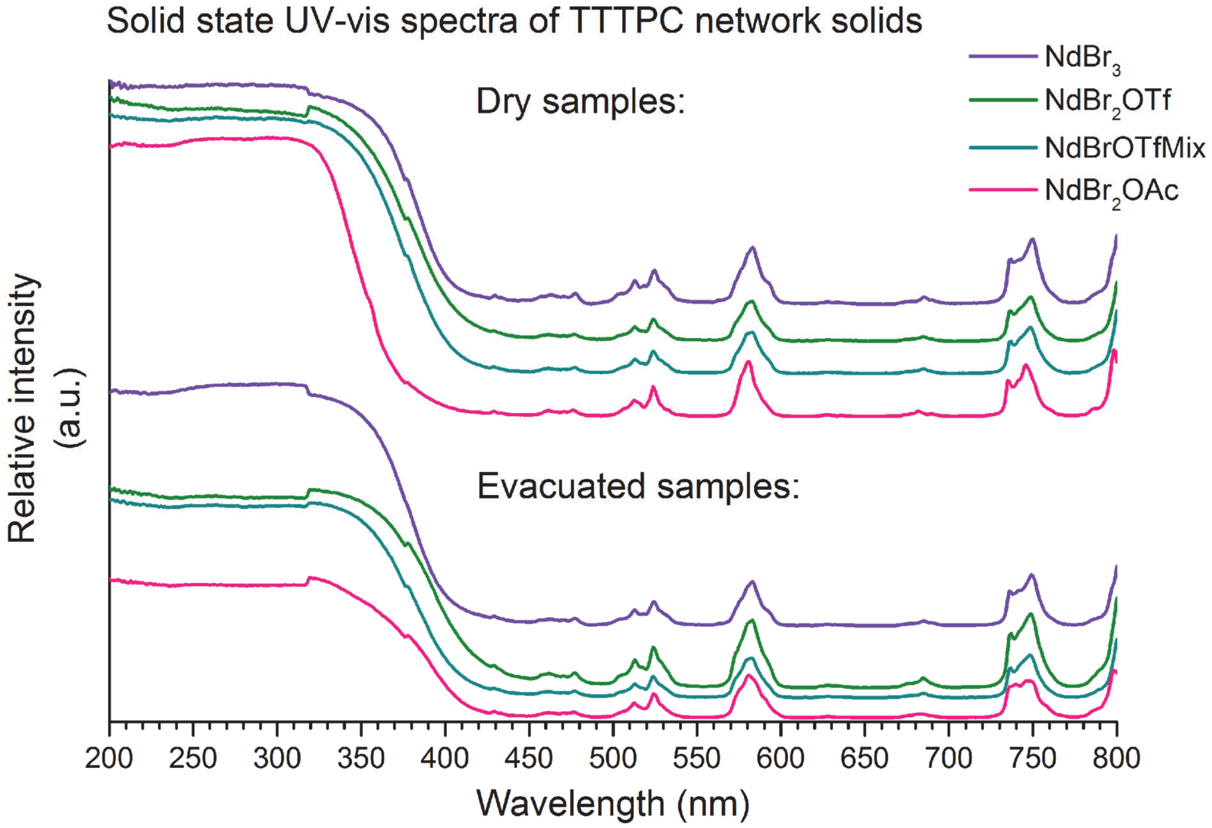

Figure S58. Solid state UV-vis spectra of TTTPC network solids measured from desiccator dry samples and evacuated samples. Anomalous discontinuations of the spectra at approximately 325 nm and 380 nm positions arise from equipment limitations, which originate from lamp and filter change procedures, respectively.

S11 BET SURFACE AREA ANALYSIS RESULTS AND DISCUSSION

Previously, Bag *et al.* had conducted adsorption studies[3] on the network solids that predate this work, and their method was to first activate the pores by removing their contents with overcritical CO_2 flush procedure, followed by active surface area measurements. We had access to Brunauer, Emmet and Teller (BET) surface area analysis equipment, but we had no overcritical CO_2 at our disposal. Our samples were thus prepared for measurements only by degassing *in vacuo*. Two samples, **TTTPC $NdBr_3$** and **TTTPC $NdBr_2OAc$**, were selected for this measurement only, because of their phase purity confirmed by other methods in this work. Bromide-triflate samples were deliberately left out because of limited measurement resources and because their results could not be easily assessed to a single component of the mixture of products. Previous BET surface area results by Bag *et al.* for structurally similar compounds made with La and Yb were 54 and 34 m^2/g, respectively. Our results differ from these values, by being an order of magnitude smaller.

Measured BET surface areas:

TTTPC $NdBr_3$:	1.4001 ± 0.0122 m^2/g
TTTPC $NdBr_2OAc$:	1.5178 ± 0.0373 m^2/g

These results suggest that either the water channels have not been evacuated properly, or they have been obstructed by the anionic species in the channel after water removal (as suggested by the single crystal evidence of **TTTPC $NdBr_2OTf$ (vac)**). Thermogravimetric analysis results of **TTTPC $NdBr_3$** imply that the former explanation is viable, whereas with **TTTPC $NdBr_2OAc$** the evacuation process should eliminate almost all water content, and therefore the latter explanation may be more proper. Nevertheless, the channel obstruction by collapsing bromides may be possible with **TTTPC $NdBr_3$** also. Further work is thus needed to make these types of structures economical for practical gas adsorption applications.

S12 CHARACTERIZATION RESULTS OF $H_{2.5}$TTTPC

S12.1 NMR and CHN characterization of $H_{2.5}$TTTPC ethyl ester

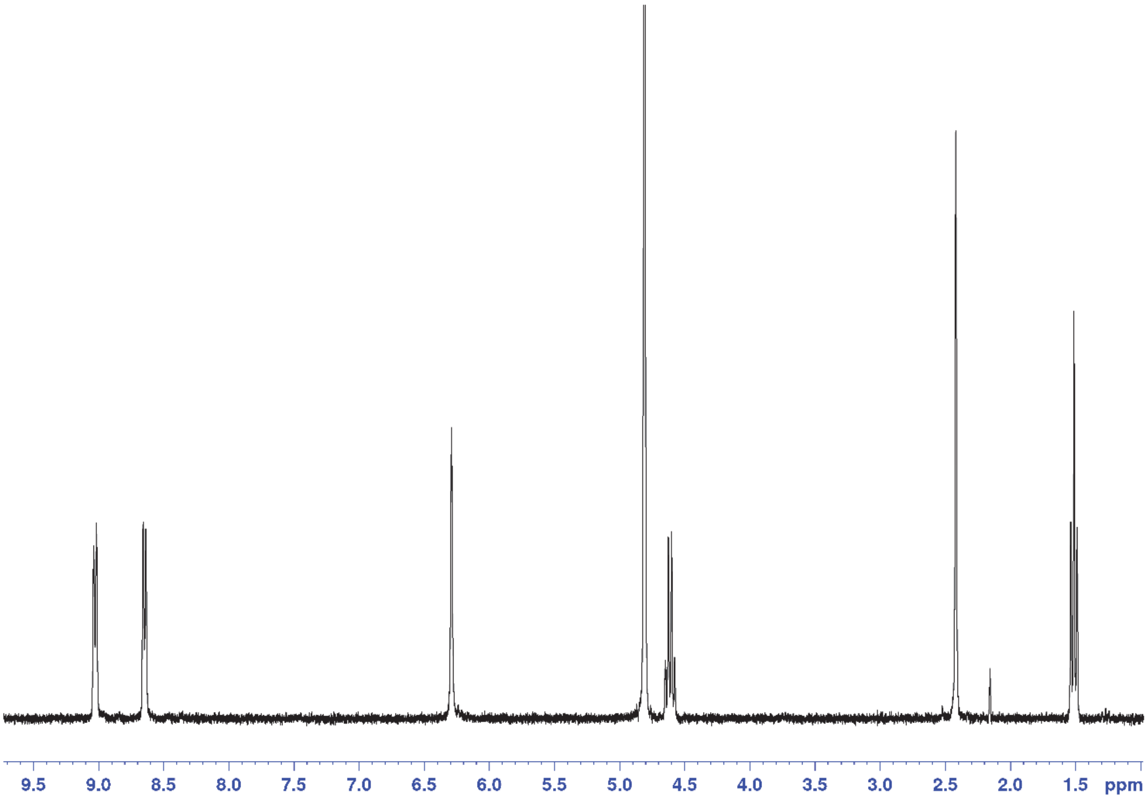

Figure S59. 300 MHz ^{1}H NMR spectrum of **$H_{2.5}$TTTPC** ethyl ester measured in D_2O. Very small acetonitrile impurity is seen at δ 2.1 ppm.

^{1}H NMR (300 MHz, D_2O, calib. residual H_2O @ δ 4.81): δ 1.508 (3H, t, -CH_2*CH_3*), 2.420 (3H, s, -CH_3), 4.613 (2H, q, -*CH_2*CH_3), 6.291 (2H, s, -CH_2-), 8.648 (2H, m, C3/C5), 9.027 (2H, m, C2/C6).

Elemental analysis, found (%): C 49.70; H 4.89; N 5.07.

Expected CHN from dry compound requires $C_{36}H_{42}Br_3N_3O_6$ (%): C 50.72; H 4.97; N 4.93. Experimental result falls short of carbon. The sample may have been moist, for the ester was readily water soluble and somewhat hygroscopic. Expected CHN with one equivalent of water, $C_{36}H_{44}Br_3N_3O_7$ (%): C 49.67; H 5.10; N 4.83.

S12.2 NMR and CHN characterization of $H_{2.5}$TTTPC

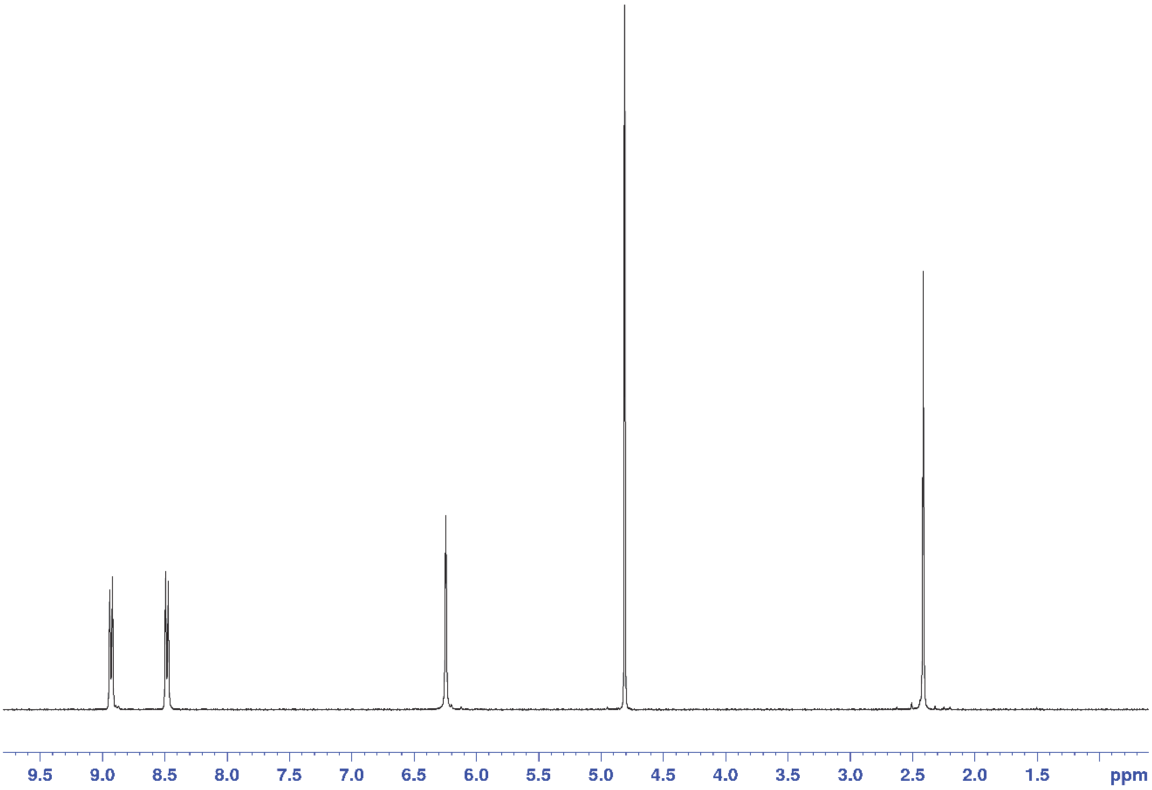

Figure S60. 300 MHz ^{1}H NMR spectrum of **$H_{2.5}$TTTPC** measured in D_2O.

^{1}H NMR (300 MHz, D_2O, calib. residual H_2O @ δ 4.81): δ 2.414 (3H, s, $-CH_3$), 6.245 (2H, s, $-CH_2-$), 8.483 (2H, m), 8.931 (2H, m).

Elemental analysis, found (%): C 46.68; H 4.39; N 5.43.

Expected $H_5TTTPC_2Br_5(H_2O)_4$, $C_{60}H_{67}Br_5N_6O_{16}$ (see section S2, Scheme 2 in the main text and crystal structure later) requires (%): C 47.17; H 4.42; N 5.50. With an additional water equivalent (moisture), expected $H_5TTTPC_2Br_5(H_2O)_5$, $C_{60}H_{69}Br_5N_6O_{17}$ requires (%): C 46.62; H 4.50; N 5.44. The expectation with moisture is very much in line with the experimental result, but the ideal crystal structure expectation is also not too far away.

S12.3 Crystallography of $H_{2.5}$TTTPC (CSD ref. 1833433)

$H_{2.5}$TTTPC crystallizes in the triclinic crystal system in space group *P*-1 (#2). Asymmetric unit (Fig. S61) consists of one ligand molecule in *syn* conformation, two water molecules and two bromides in regular crystallographic positions. The third bromide resides on crystallographical special position of (½,1,0), in the middle of a unit cell edge. This special position indicates that a single whole bromide is shared between four adjacent unit cells, and concordantly, one total bromide is situated over a single unit cell on four opposite edges. Since the space group has inversion symmetry, only one half of a bromide is crystallographically independent (Br1), and thus the total number of bromides in the asymmetric unit is two and a half. This raises the question of charge balance, for there is the ligand with three quaternary positively charged nitrogen atoms and three carboxylate groups. It follows that two and a half carboxylates must be protonated to result in a neutral overall charge. Measuring C-O bond distances and from the electron density map, two of these carboxylates are trivial to assess. Oxygen atoms O19 and O29 are protonated, and they initiate a typical hydrogen bond motif to the adjacent water molecules (O1W and O2W) continuing onwards to the bromides Br2 and Br3. The "one half" of a proton is in the third carboxylate, but there is also severe disorder present. This is because between the two carboxylate moieties, there is a hydrogen bond involving a total of one proton (H38A), the carboxylic acid-carboxylate dimer is not planar, and it is free to rotate over all the unit cells in the whole crystal in juxtaposed positions (Scheme S1), displaying an averaged region of electron density of a total of two oxygen atoms in the asymmetric unit. This disorder was modeled in six positions (O38A, O39A, O38B, O39B, O38C and O39C) for it was not meaningful to model the disorder further, even though some residual electron density was left in this region. H38A was found from the electron density map as a very weak peak between the carboxylate groups and was assigned in an unoptimized position with a crystallographic occupancy of ½. Crystal data and refinement parameters are displayed in Table S18. Packing and supramolecular properties have been reported by Kong and Wu.[6]

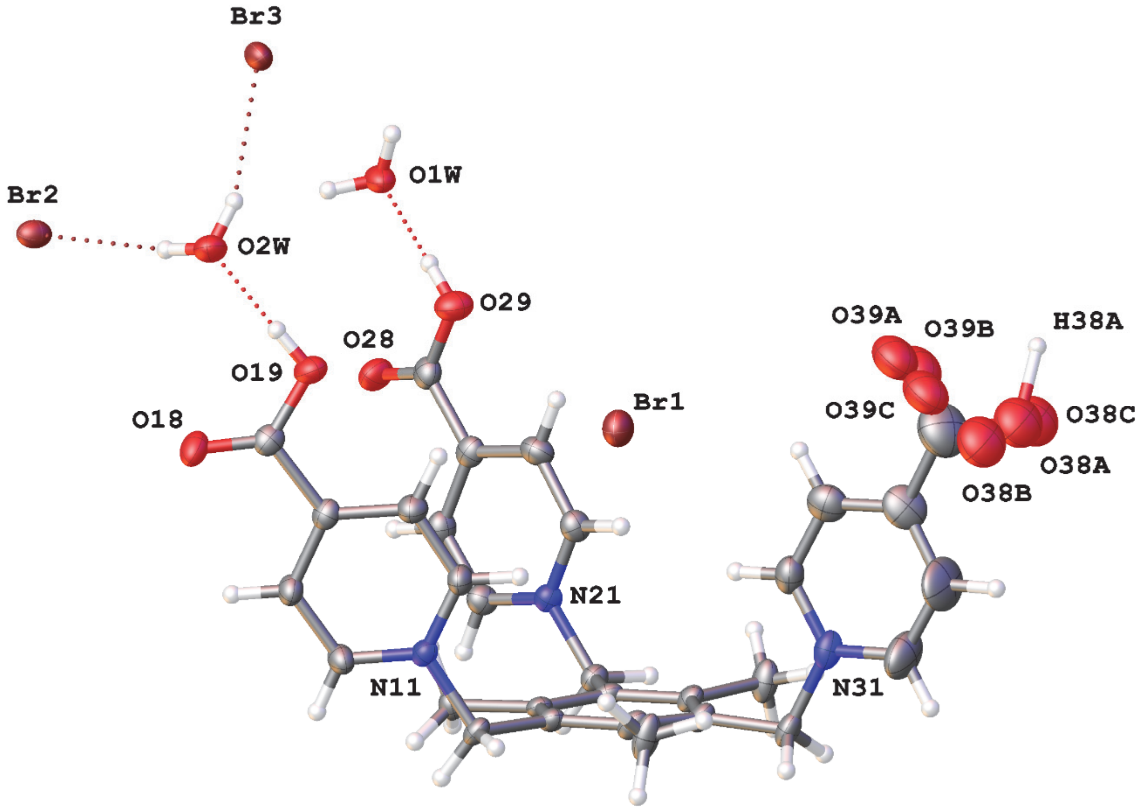

Figure S61. Asymmetric unit contents of **$H_{2.5}$TTTPC**.

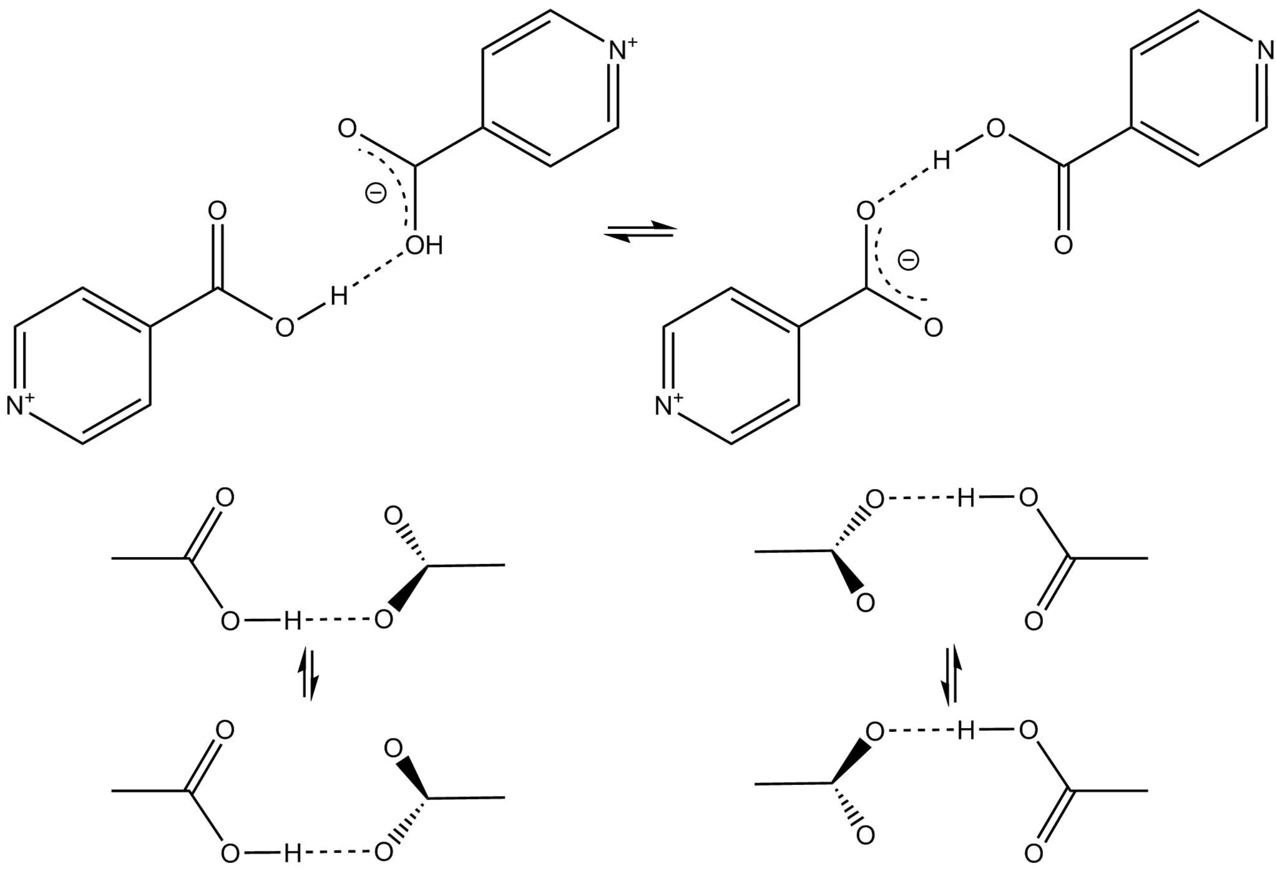

Scheme S1. Hydrogen bonding of carboxylic acid and carboxylate moieties with examples of bond permutations and carboxylate torsions between different unit cells in the bulk crystal.

Table S18. Crystal structure and refinement data for **$H_{2.5}$TTTPC.**

Name	**$H_{2.5}$TTTPC**
Empirical formula	$C_{60}H_{67}Br_5N_6O_{16}$
Formula weight	1527.74
Temperature / K	123.01(10)
Crystal system	triclinic
Space group	*P*-1
a / Å	11.1828(6)
b / Å	13.1617(5)
c / Å	13.3823(7)
α / °	103.662(4)
β / °	114.054(5)
γ / °	106.336(4)
Volume / Å^3	1581.63(14)
Z	1
ρ_{calc} / g/cm^3	1.604
μ / mm^{-1}	3.248
F(000)	772
Crystal size / mm^3	0.39 × 0.131 × 0.074
Radiation	MoKα (λ = 0.71073)
2Θ range for data collection / °	3.518 to 51.994
Index ranges	$-13 \leq h \leq 13$, $-14 \leq k \leq 16$, $-14 \leq l \leq 16$
Reflections collected	11112
Independent reflections	6149 [R_{int} = 0.0263, R_{sigma} = 0.0471]
Data/restraints/parameters	6149/47/420
Goodness-of-fit on F^2	1.026
Final R indexes [I ≥ 2σ (I)]	R_1 = 0.0402, wR_2 = 0.0866
Final R indexes [all data]	R_1 = 0.0539, wR_2 = 0.0941
Largest diff. peak/hole / e Å^{-3}	1.12/-0.86
CSD reference no.	1833433

S12.4 Previously reported crystal structure, CSD ref. ENIVUT

Kong and Wu[3] have previously published a single crystal structure of the **TTTPC** ligand in its protonated tribromide form, namely the structure ENIVUT in the Cambridge Structural Database. We followed their synthetic pathway to obtain the similar product and collected the data from a single crystal of our own and had similar results to theirs. However, we refer to our compound as **$H_{2.5}$TTTPC** because it has only has the said number of total acidic protons with respect to our crystallographic data. There is clearly a discrepancy here between the structures, and we believe our structure to be the properly reported one.

The most striking difference is that the ENIVUT structure has three reported bromides in its asymmetric unit, although one of the bromides resides on a special position of (½,0,½) in the middle of one of the unit cell faces. This bromide is thus shared with an adjacent unit cell and should be counted as one half with same reasoning as stated in our structure before. We first considered the possibility that their structure is truly a tribromide and whole different compound from ours, but there is no crystallographic basis supporting that conclusion we can think of. What is more, is the striking similarity between these structures, if overlaid or examined side by side. We noticed that their structure drawn from the database contains no assigned carboxylic acid protons nor hydrogen atoms of the water molecules. Also there seems to be no disorder present in the critical carboxylate connecting with another in a dimeric fashion. We have obtained the crystal structure of **$H_{2.5}$TTTPC** several times from different occasions, not just this one we report here, and every time the disorder has been present. Because in our structure there is indeed the modelled disorder, it is difficult to measure the distances between dimeric oxygens, but when comparing the carboxylate carbon atom distances, they are essentially the same (3.659 Å in ENIVUT and 3.699 Å in ours). There is also a similar offset of the pyridinium rings of the dimers, and in ENIVUT the carboxylate is oddly crooked to the side towards the opposing moiety. The overall packing and hydrogen bonding network of ENIVUT is no different from our structure. All in all, we have a reason to believe the chemical contents of the structure have been interpreted erroneously. There is also a strong indication of possibly poor quality data associated with ENIVUT, if we look at crystallographic and refinement indicators reported by Kong and Wu. For example, their reported R_{int} and R_1 values are much poorer than what we have reported (R_{int} = 0.1083 and R_1 = 0.1209 in ENIVUT, and R_{int} = 0.0263 and R_1 = 0.0402 in our structure). There is also a possibility that the crystal they have had has been a twin, and the quality of the data is thus not so great to begin with, so there may have been difficulties in proper structure determination. Additionally, they have measured the data in room temperature, and while the thermal ellipsoid figures they have presented look reasonably good, upon closer inspection they have presented them with only 25 % thermal ellipsoids. With 50 % ellipsoid probability, the disorder in the carboxylate would most likely be more prevalent, but since we do not possess the original data, we cannot tell.

S12.5 Thermal analysis of $H_{2.5}$TTTPC

In the thermogravimetric analysis of **$H_{2.5}$TTTPC** ligand, the first weight loss of the product can be seen starting from below 100 °C and proceeding until the temperature of approximately 170 °C is reached. This weight loss is associated with an endotherm, typical for a loss of solvent. Weight loss of 4.80 % under air and 4.85 % under N_2 atmosphere equals the loss of approximately two water molecules per one ligand molecule (theoretical loss 4.72 %). When the ligand is heated further, a second endotherm associated to a weight loss occurs starting at onset temperatures of 228.4 °C under air and 225.7 °C under N_2, indicating the beginning of a decomposition reaction similar to the network solids. The event seamlessly proceeds to a more prominent decomposition process associated first with a small endotherm followed by a large exotherm in air (most likely burning) and two small endotherms under N_2. The sample is burned completely without remaining ash under air, but under nitrogen atmosphere, a carbonization process results in a vitreous charred residue of 13.05 % weight at the end of measurement. Thermal analysis curves are displayed in the following Fig. S62.

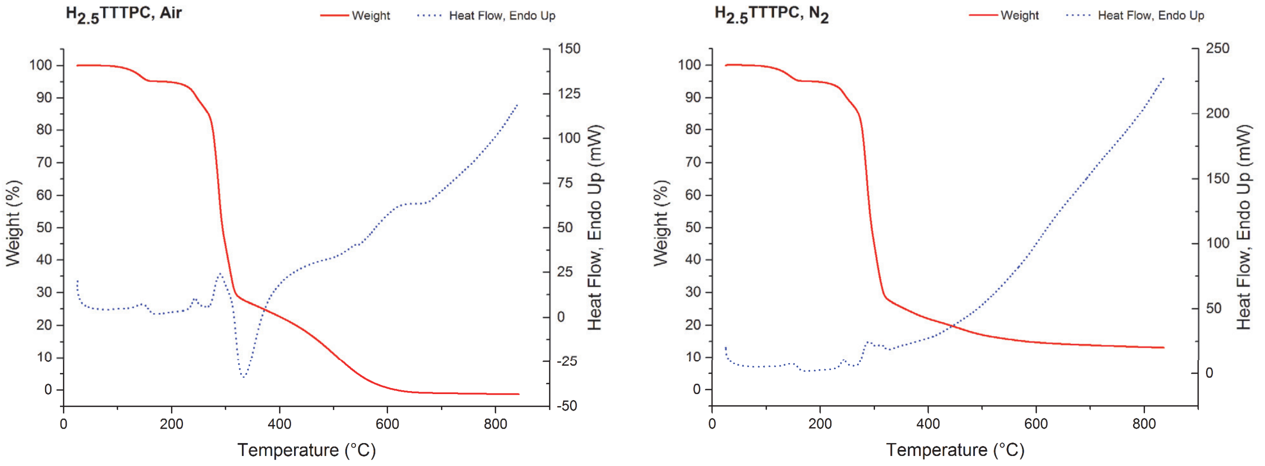

Figure S62. Thermal analysis curves of **H2.5TTTPC** under air (left) and nitrogen (right) atmospheres.

REFERENCES

1. R.-M. Wen, S.-D. Han, G.-J. Ren, Z. Chang, Y.-W. Li and X.-H. Bu, *Dalton Trans.*, 2015, **44**, 10914.
2. C. Gupta, N. Krishnamurthy, *Extractive Metallurgy of Rare Earths,* CRC Press, Boca Raton, Florida, 2005.
3. P. Bag, X.-S. Wang and R. Cao, *Dalton Trans.*, 2015, **44**, 11954.
4. J.-C.G. Bünzli and S.V. Eliseeva, in *Lanthanide Luminescence. Springer Series on Fluorescence (Methods and Applications),* ed. P. Hänninen and H. Härmä, Springer, Berlin, Heidelberg, 1st Edition, 2010, Chapter 1, 1-45.
5. H. Lambert, B. Claux, C. Sharrad, P. Soucek and R. Malmbeck, *Procedia Chemistry*, 2016, **21**, 409.
6. G.-Q. Kong and C.-D. Wu, *Cryst. Growth Des.*, 2010, **10**, 4590.